Cold Ions and their Applications for Quantum Computing and Frequency Standards

- Trapping Ions
- Cooling Ions
- Superposition and Entanglement
- Quantum computer: basics, gates, algorithms, future challenges
- Ion clocks: from Ramsey spectroscopy to quantum techniques

Ferdinand Schmidt-Kaler
Institute for Quantum Information Processing
www.quantenbit.de

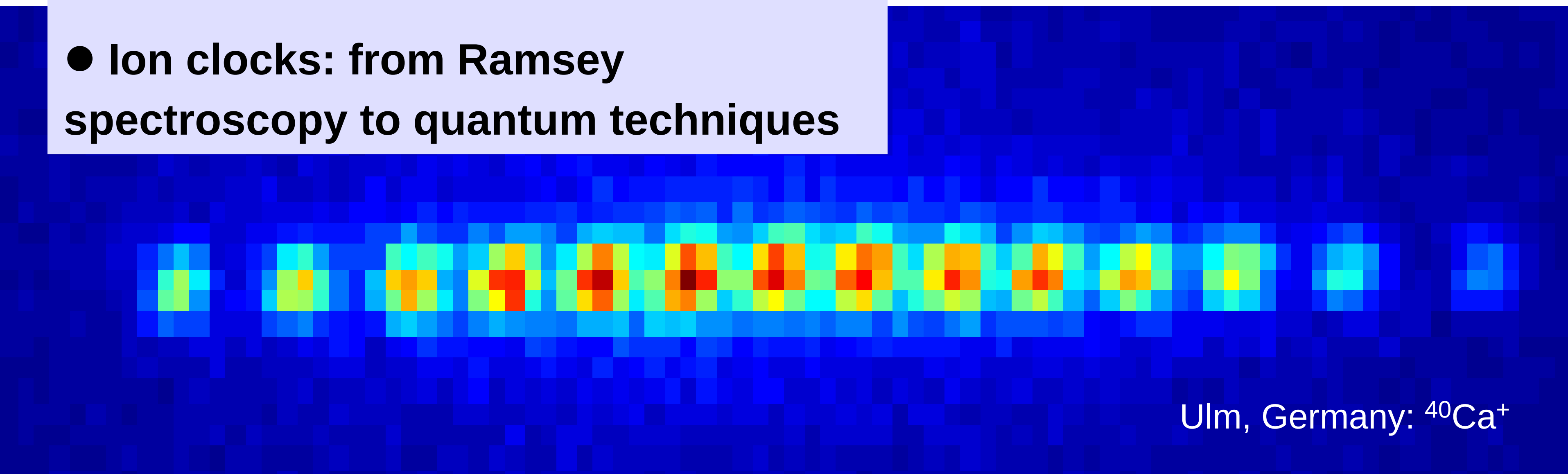

Ion Gallery

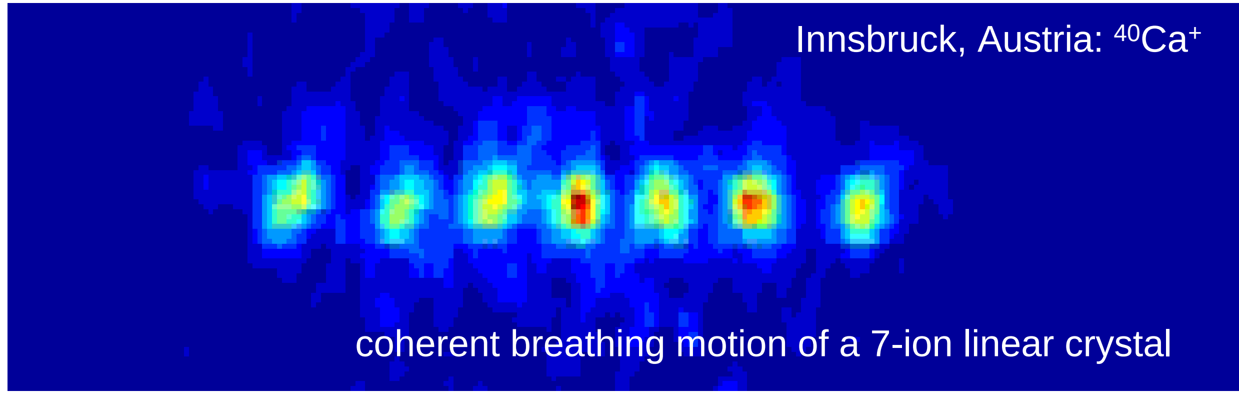

Innsbruck, Austria: $^{40}Ca^+$

coherent breathing motion of a 7-ion linear crystal

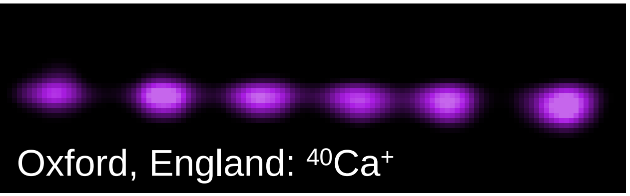

Oxford, England: $^{40}Ca^+$

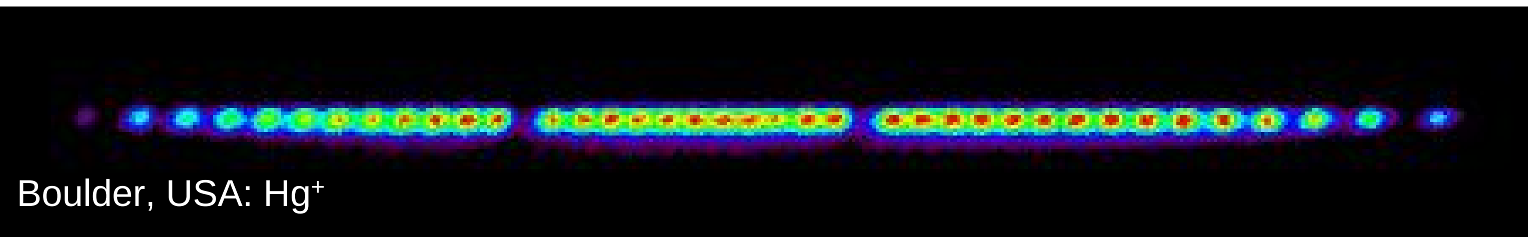

Boulder, USA: Hg^+

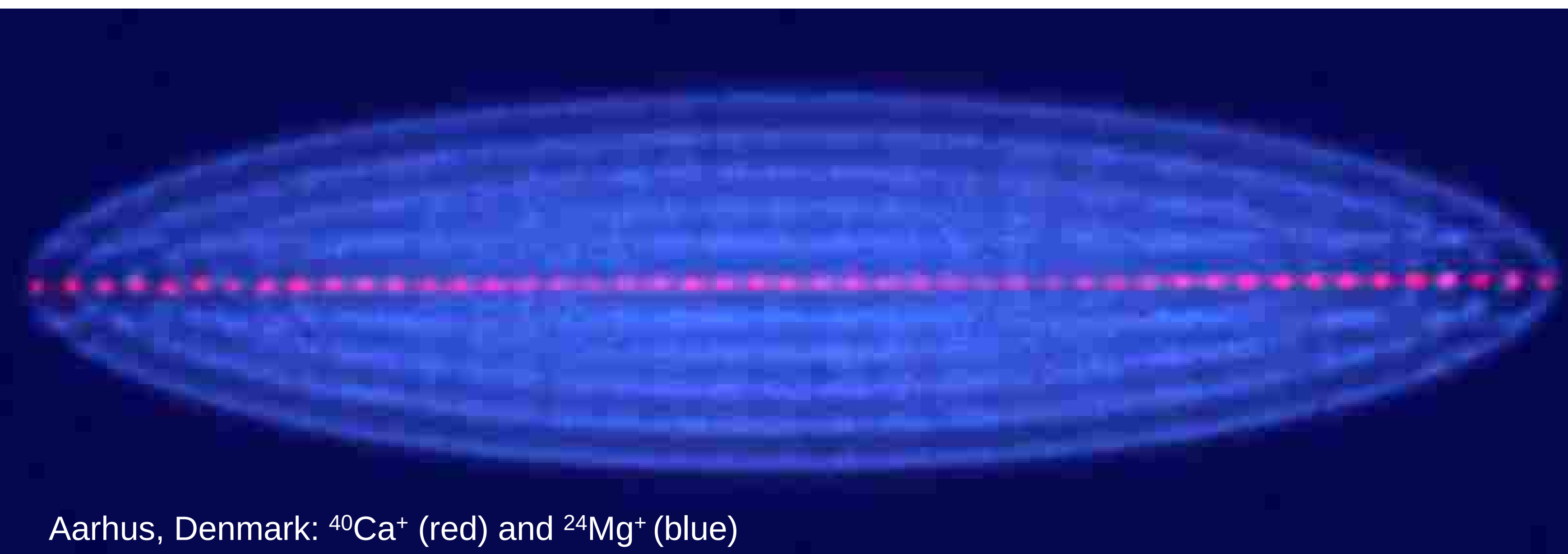

Aarhus, Denmark: $^{40}Ca^+$ (red) and $^{24}Mg^+$ (blue)

Why using ions?

- Ions in Paul traps were the first sample with which laser cooling was demonstrated and quite some Nobel prizes involve laser cooling…

- A single laser cooled ion still represents one of the best understood objects for fundamental investigations of the interaction between matter and radiation

- Experiments with single ions spurred the development of similar methods with neutral atoms

- Particular advantages of ions are that they are
  - confined to a very small spatial region ($\delta x < \lambda$)
  - controlled and measured at will for experimental times of days

- Ideal test ground for fundamental quantum optical experiments

- Further applications for
  - precision measurements
  - cavity QED
  - optical clocks
  - quantum computing
  - thermodynamics with small systems
  - quantum phase transitions

Outline of the talks:

I) Trapping of single ions

Paul trap in 3D
Linear Paul trap

specialized traps:
segmented linear trap
planar segmented trap

Eigenmodes of a linear ion crystal
Stability of a linear crystal
Micromotion

Modern segmented micro Paul trap

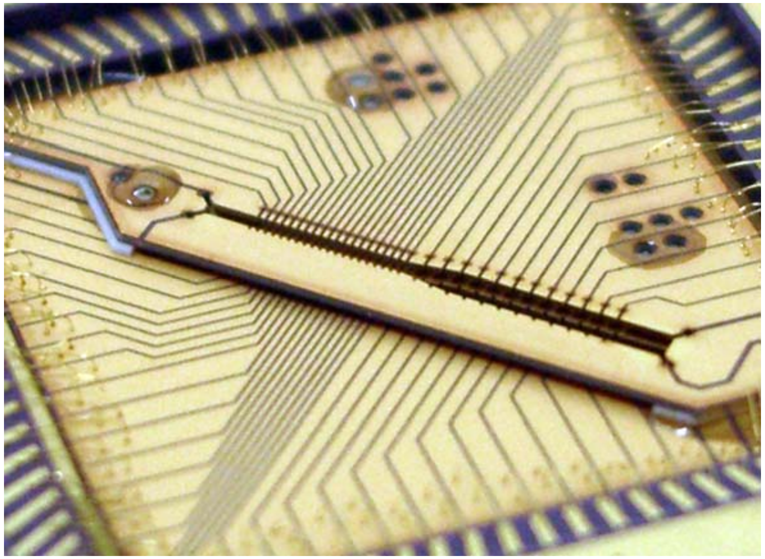

Traditional Paul trap

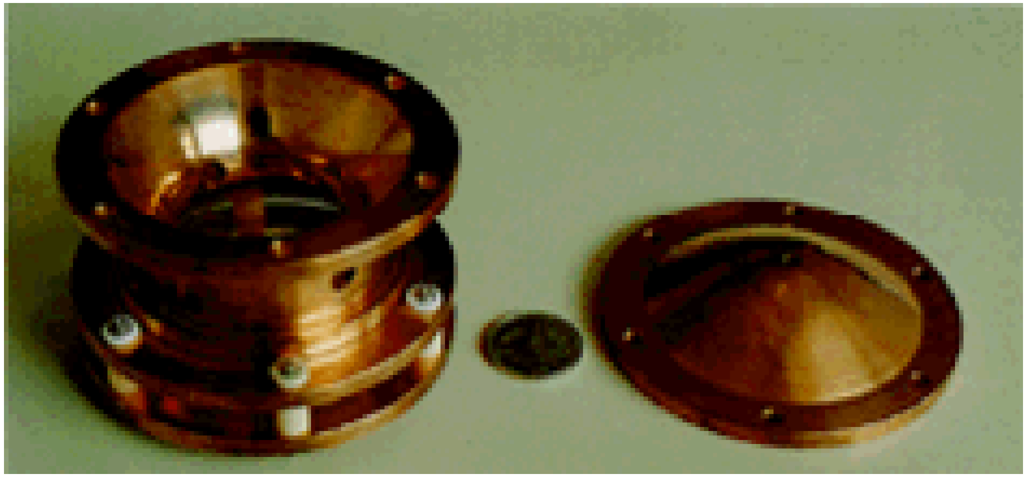

II) Laser cooling

Laser-ion interaction
- Lamb Dicke parameter
- Strong and weak confinement regime

Rate equation model
Cooling rate and cooling limit
Doppler cooling of ions

Dopper recooling measurements
to determine heating rates and
to optimize the transport of ions

Resolved sideband spectroscopy

Temperature measurement techniques
- Sideband Rabi oscillations
- Red / blue sideband ratio
- Carrier Rabi oscillations

Resolved sideband cooling
- Quadrupole transition
- Optimizing the cooling rate
- Raman transition

Heating rate
Coherence of vibrational superposition states

Cooling in multi-level systems
- Dark resonances
- EIT cooling

Reaching the ground state of vibration

III) Quantum computing with trapped ions

Quantum computation, basic description and single qubit gates,
Cirac-Zoller two qubit gate operation, other two qubit gates
long lived Bell states
GHZ- and W-states
Deutsch algorithm
Teleportation with ions

Quantum algorithms

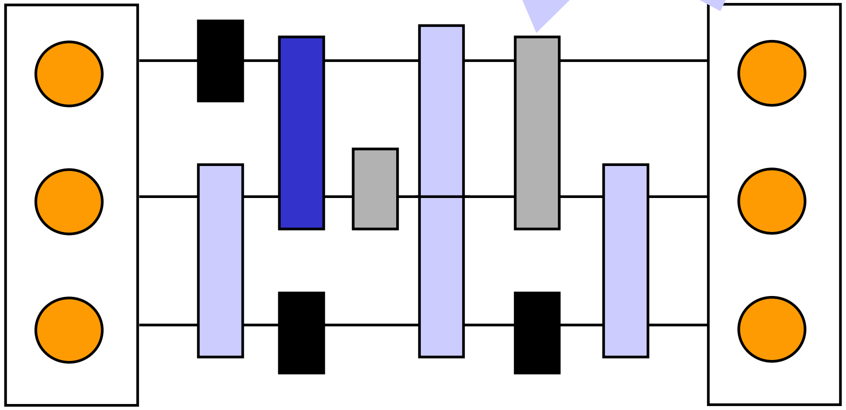

IV) Precision measurements

Absolute frequency measurements, optical comb generator
Hg^+ absolute frequency measurement
Modern clocks using quantum processing:
entangled Be^+ ions
Quadrupole shift precision measuremer
Al^+ absolute frequency measurement
Ions in space testing General and special relativity

frequency uncertainty
7.2 10^{-17}

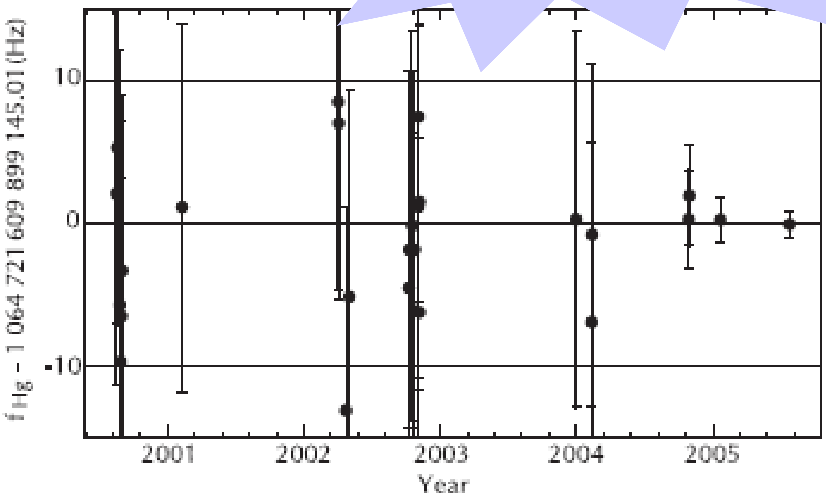

V) Biography

Cold Ions and their Applications for Quantum Computing and Frequency Standards

- **Trapping Ions**
- Cooling Ions
- Superposition and Entanglement
- Quantum computer: basics, gates, algorithms, future challenges
- Ion clocks: from Ramsey spectroscopy to quantum techniques

- Paul trap in 3D
- Linear Paul trap
- Specialized traps:
  Segmented linear trap
  Planar segmented trap

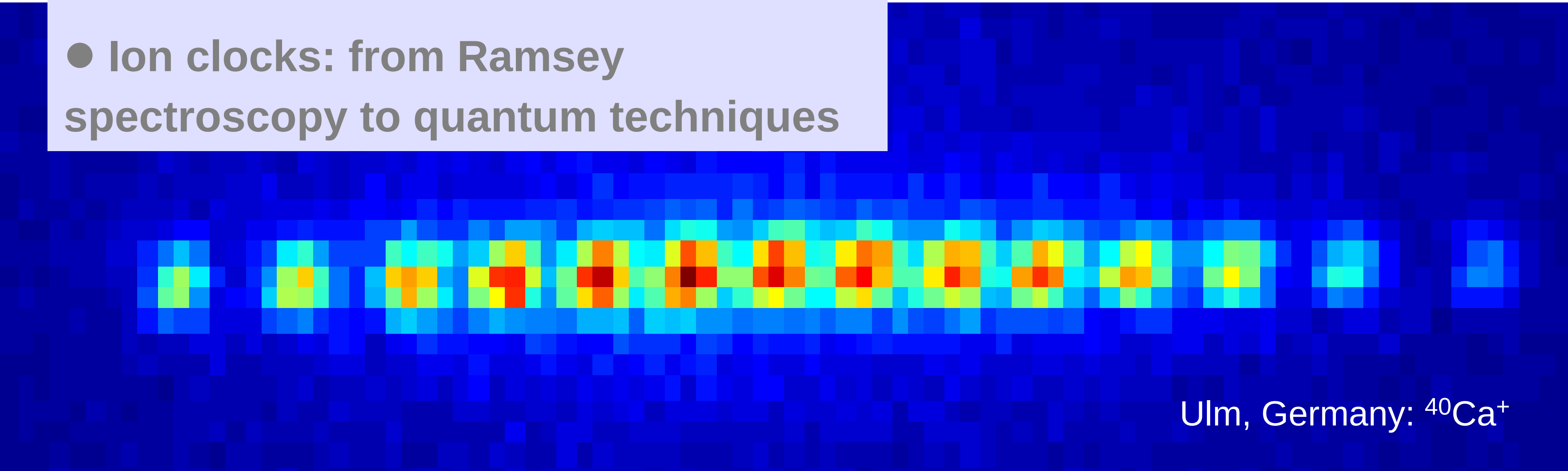

Ulm, Germany: $^{40}Ca^{+}$

Paul trap

G. Werth

Fig. 6 quadrupole trap from Mainz

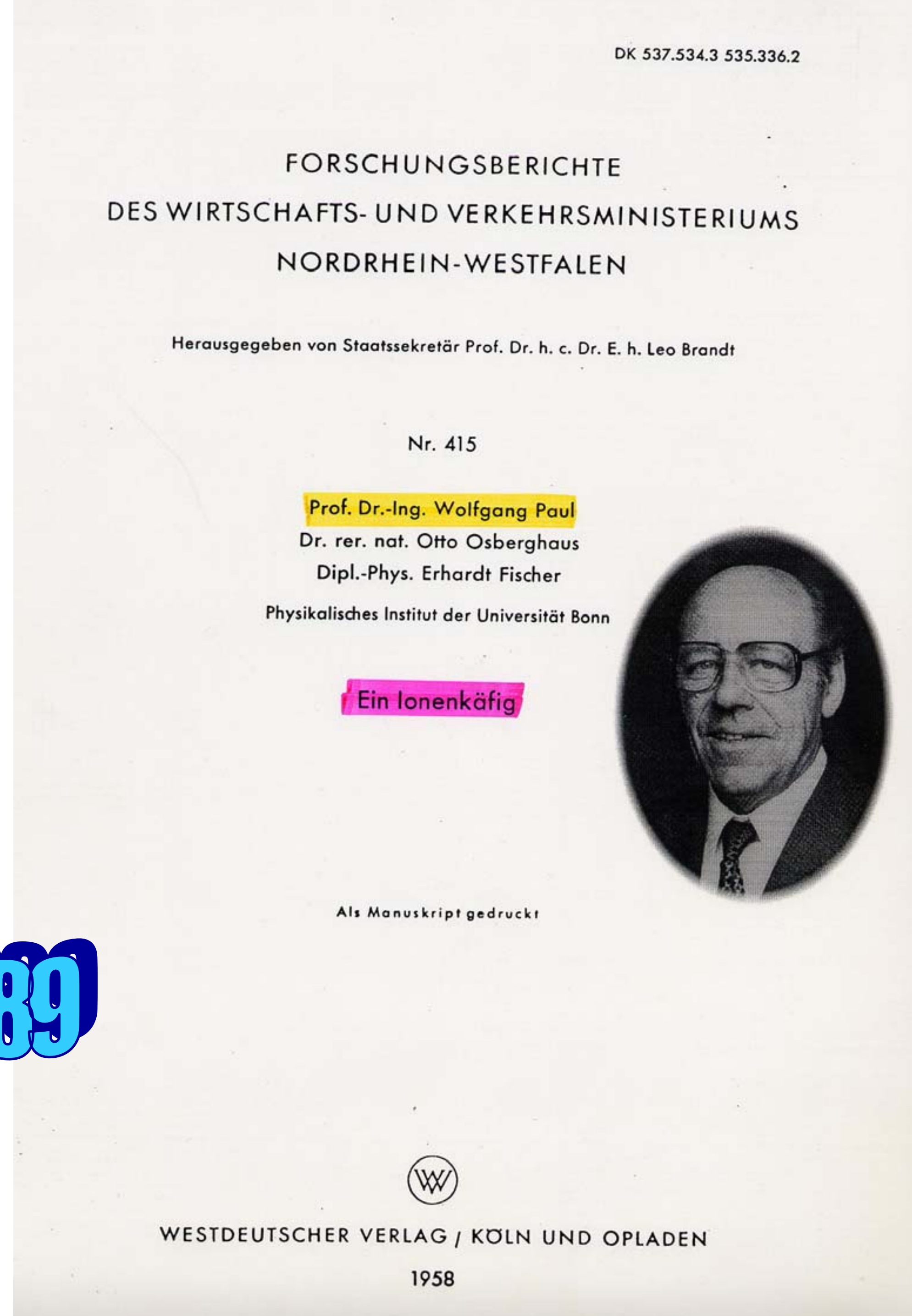

DK 537.534.3 535.336.2

FORSCHUNGSBERICHTE
DES WIRTSCHAFTS- UND VERKEHRSMINISTERIUMS
NORDRHEIN-WESTFALEN

Herausgegeben von Staatssekretär Prof. Dr. h. c. Dr. E. h. Leo Brandt

Nr. 415

Prof. Dr.-Ing. Wolfgang Paul
Dr. rer. nat. Otto Osberghaus
Dipl.-Phys. Erhardt Fischer
Physikalisches Institut der Universität Bonn

Ein Ionenkäfig

Als Manuskript gedruckt

WESTDEUTSCHER VERLAG / KÖLN UND OPLADEN
1958

Nobel prize 1989

Paul trap

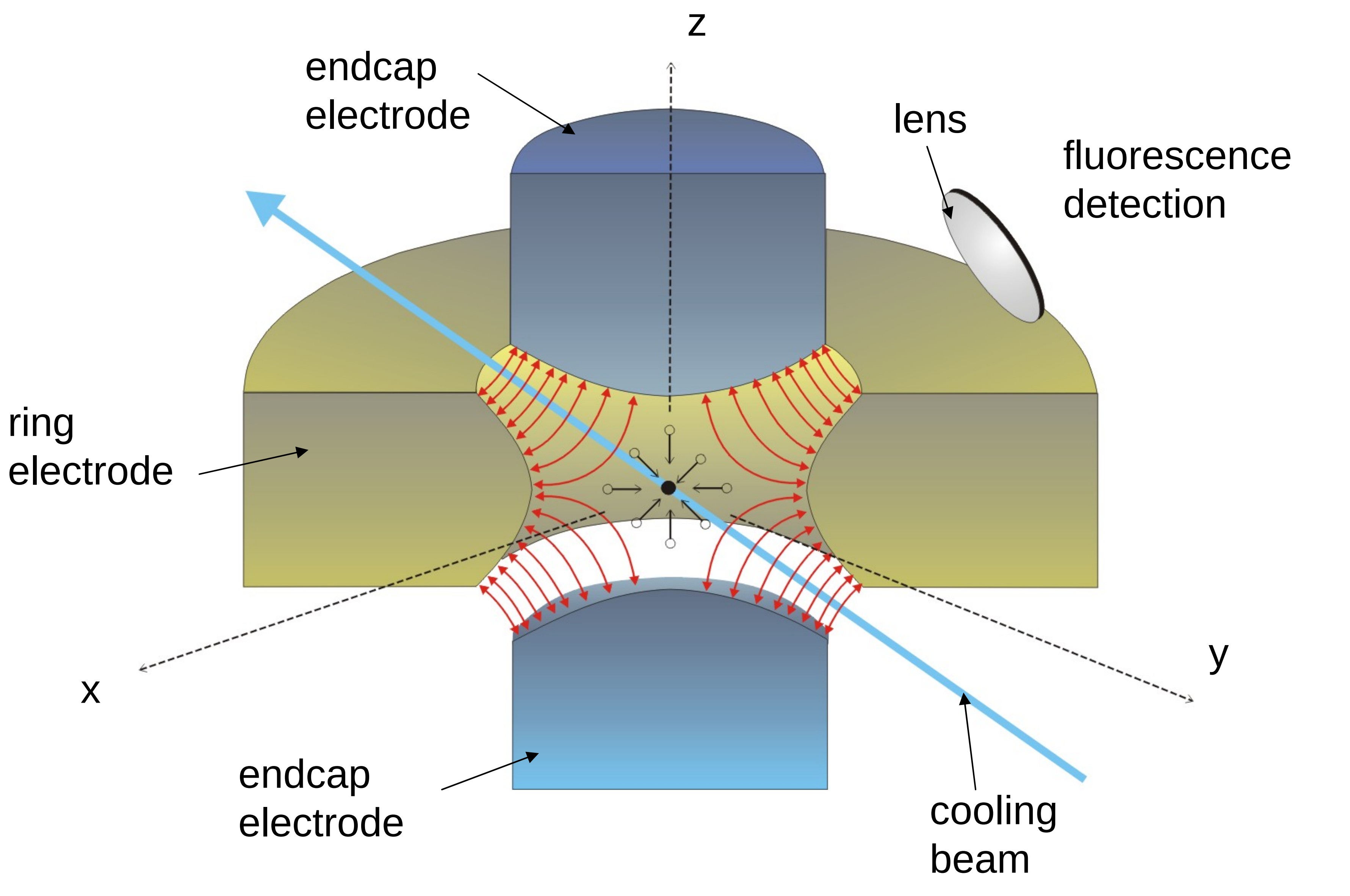
z
endcap electrode
lens
fluorescence detection
ring electrode
x
y
endcap electrode
cooling beam

Binding in three dimensions

Electrical quadrupole potential $\Phi(\vec{r}) = \Phi_0 \cdot \sum \alpha_i (r_i/\tilde{r})^2, \quad i = x, y, z$

trap size: $\tilde{r}$

Binding force for charge *Q* $\vec{F}(\vec{r}) = Q\vec{E}(\vec{r}) = -Q\vec{\nabla}\Phi$

leads to a harmonic binding: $\vec{F}(\vec{r}) \sim \vec{r}$

Ion confinement requires a focusing force in 3 dimensions, but

Laplace equation requires $\vec{\nabla}^2\Phi = (\partial^2/\partial x^2 + \partial^2/\partial y^2 + \partial^2/\partial z^2)\Phi = 0$

such that at least one of the coefficients α_i is negative,
e.g. binding in x- and y-direction but anti-binding in z-direction !

no static trapping in 3 dimensions

Dynamical trapping: Paul‘s idea

time depending potential $$\Phi(\overrightarrow{r},t) = \Phi_0(t)\cdot(x^2+y^2-2z^2)$$

with $$\Phi_0(t) = (U + V cos(\Omega_{RF} t))/\tilde{r}^2$$

leads to the equation of motion for a particle with charge *Q* and mass *m*

$$\ddot{r}_i + \frac{2\alpha_i Q}{m r_0^2}\ \frac{U+V cos(\Omega_{RF} t)}{\tilde{r}^2}\ r_i = 0,\ \alpha_{x,y} = 1, \alpha_z = 2,$$

takes the standard form of the *Mathieu* equation

(linear differential equ. with time depending cofficients)

$$\boxed{\frac{d^2u}{d\tau^2} + (a + 2\ q\ cos(2\tau))u = 0}$$

with substitutions

$$a_z = -2a_r = -\frac{8QU}{m\tilde{r}^2\Omega_{RF}^2} \qquad q_z = -2q_r = -\frac{4QV}{m\tilde{r}^2\Omega_{RF}^2}$$

radial and axial trap radius $\tilde{r}^2 = r_0^2 + 2z_0^2$ $\qquad \tau = \frac{1}{2}\Omega_{RF} t$

Regions of stability

time-periodic diff. equation leads to Floquet Ansatz

$$x(\tau) = Ae^{+i\mu\tau}\,\phi(\tau) + Be^{-i\mu\tau}\,\phi(\tau), \qquad \phi(\tau) = \phi(\tau+\pi) = \sum c_n e^{2in\tau}$$

If the exponent μ is purely real, the motion is bound,
if μ has some imaginary part x is exponantially growing and the motion is unstable.

The parameters *a* and *q* determine if the motion is stable or not.
Find solution analytically (complicated) or numerically:

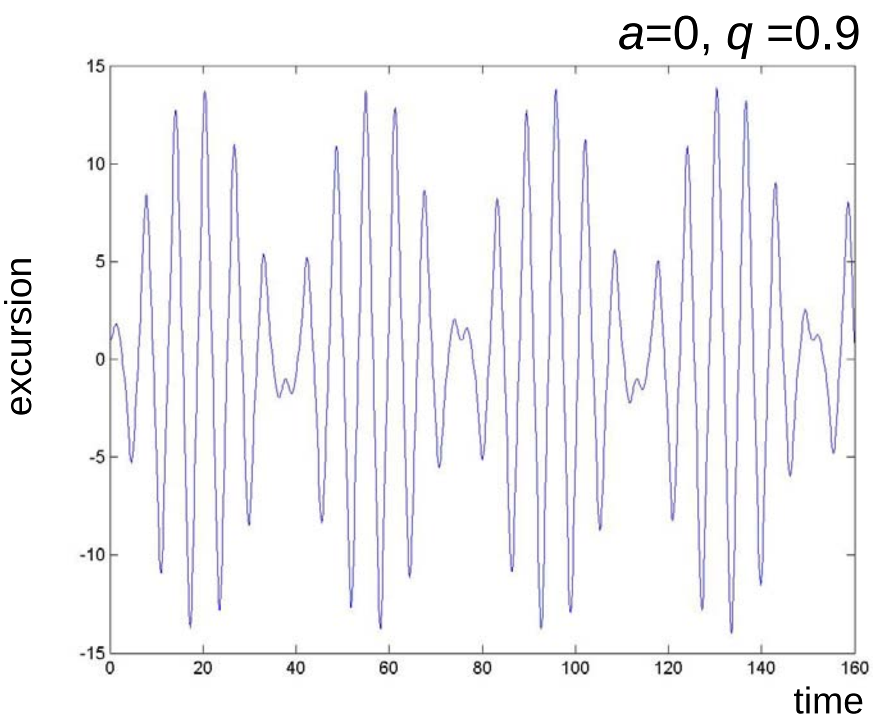

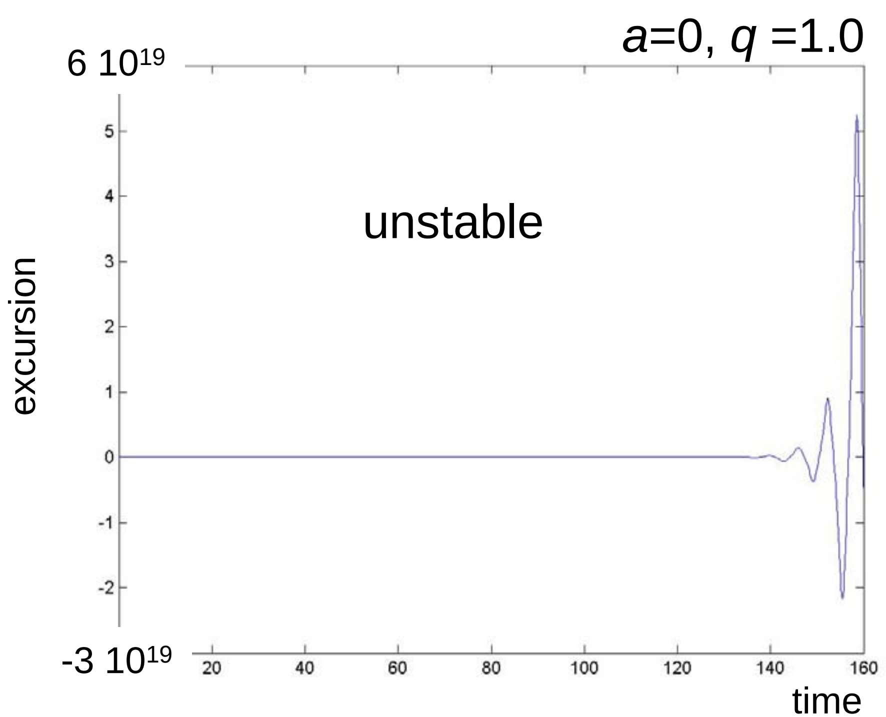

Two oscillation frequencies

slow frequency: Harmonic secular motion, frequency ω increases with increasing q

fast frequency: Micromotion with frequency Ω
Ion is shaken with the RF drive frequency (disappears at trap center)

1D-solution of Mathieu equation

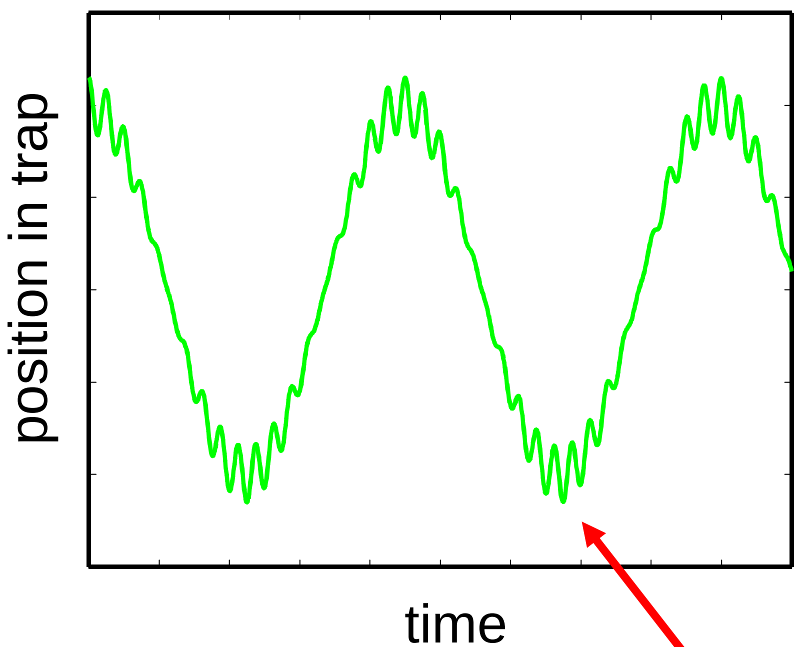

single Aluminium dust particle in trap

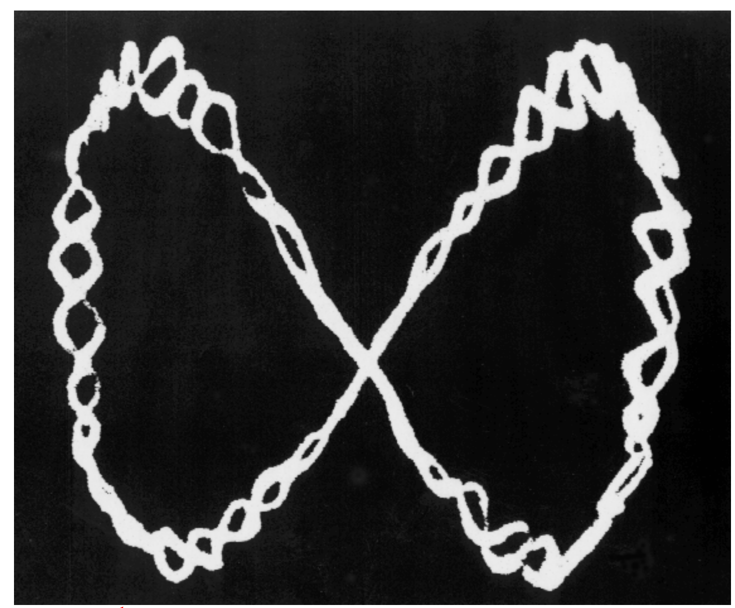

Lissajous figure

micromotion

3-Dim. Paul trap stability diagram

for a << q << 1 exist approximate solutions

$$r_i(t) = r_1^0 cos(\omega_1 t + \phi_i)(1 + \frac{q_i}{2} cos(\Omega_{RF} t))$$

$$\omega_i = \beta_i \frac{\Omega_{RF}}{2}$$

$$\beta_i = \sqrt{a_i + \frac{q_i}{2}}$$

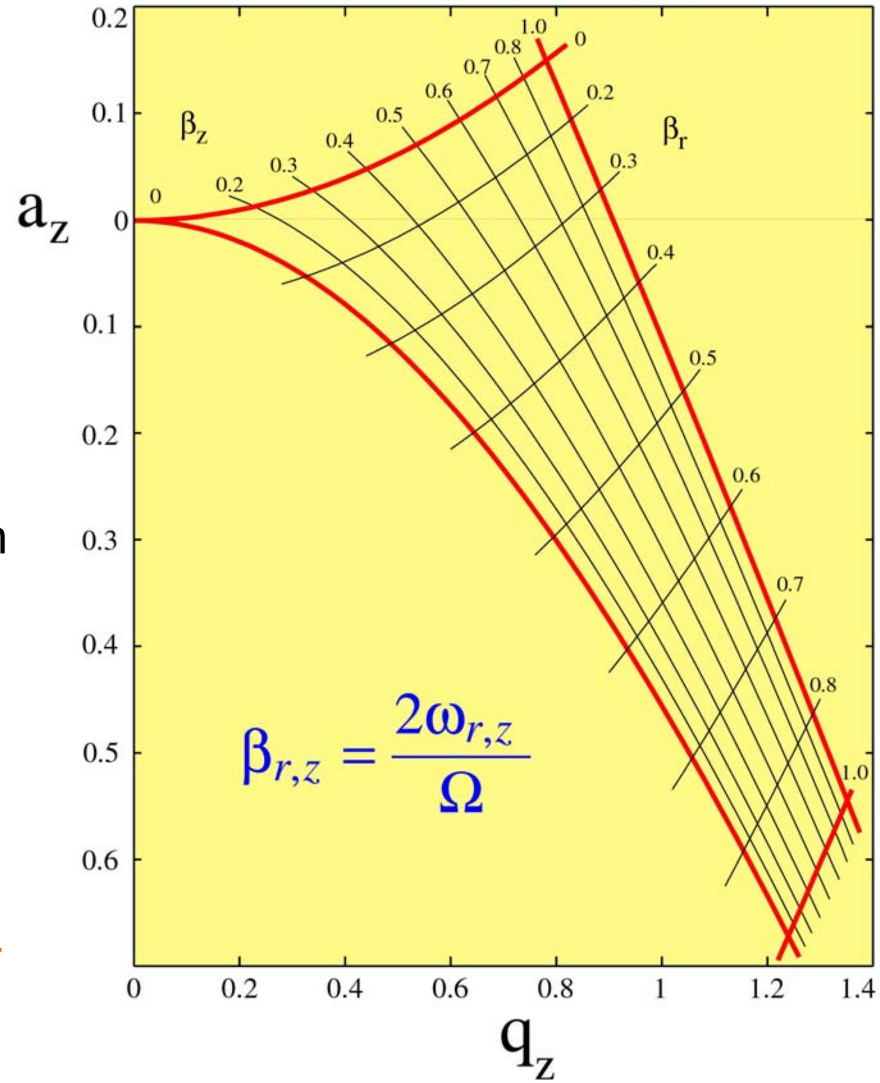

The 3D harmonic motion with frequency W_i can be interpreted as being caused by a pseudo-potential Ψ

$$Q\Psi = \frac{1}{2} \sum m\omega_i^2 r_i^2, \quad i = x, y, z$$

→ leads to a quantized harmonic oscillator

Real 3-Dim. Paul traps

ideal 3-Dim. Paul trap with equi-potental surfaces formed by copper electrodes

G. Werth

quadrupole trap from Mainz

ideal surfaces:

$$r^2 - 2z^2 = \pm\, r_0^2$$

endcap electrodes at distance

$$r_0/z_0 = \sqrt{2}$$

but non-ideal surfaces do trap also well:

A. Mundt, Innsbruck

Real 3-Dim. Paul traps

non-ideal surfaces

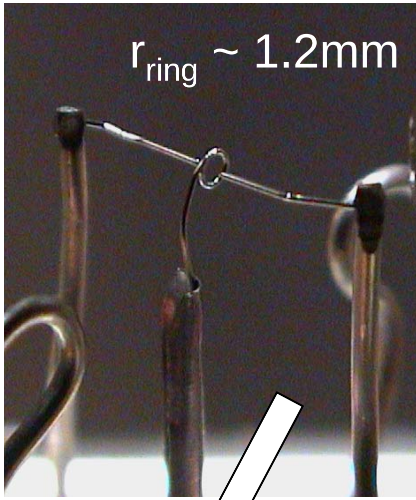

ideal 3 dim. Paul trap with equi-potental surfaces formed by copper electrodes

Fig. 6 quadrupole trap from Mainz

numerical calculation of equipotental lines

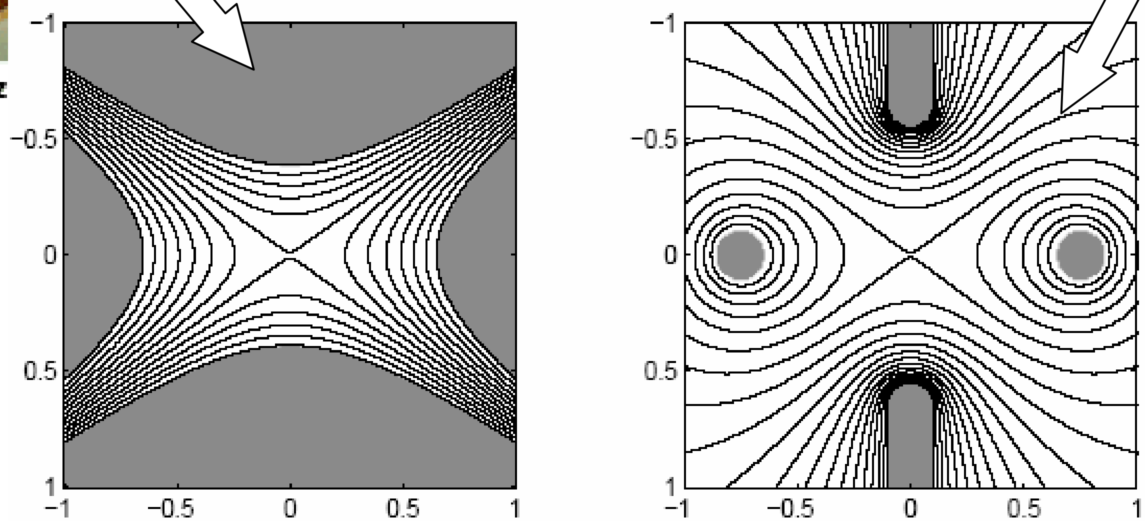

similar potential near the center

Equipotential lines of a quadrupole potential (left plot) and an approximate quadrupole potential (right). Both potentials have a cylindrical symmetry. The horizontal axis corresponds to the radial direction, the vertical axis is the symmetry axis. The electrode structure shown in the right plot is the one used for the experiments if length is measured in millimeters. It is composed of a ring electrode and two cylindrical electrodes with hemispheric endcaps.

Real 3-Dim. Paul traps

Paul trap: wire ring + endcaps

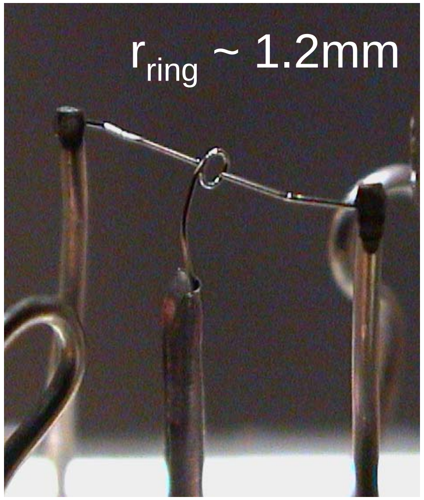

determine the quadrupole part of the potential:

$$\phi(r) = \sum a_{2l} (\tfrac{r}{\tilde{r}})^{2l}$$

ideal: $a_0 = a_2 = 0.5, a_{>2} = 0$ fully harmonic potential

real: $L = 0.5/a_2, L > 1$ Loss factor

main advantages:
good optical access
large observation angle

Paul trap 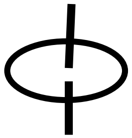

$L \geq 5$ Paul Straubel trap: ring only 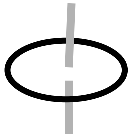

inverted Paul Straubel trap: endcaps only 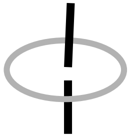

2-Dim. Paul mass filter stability diagram

time depending potential $$\Phi(x,y,t) = \Phi_0(t)\cdot(x^2 - y^2)$$

with $$\Phi_0(t) = (U + V\,cos(\Omega_{RF} t))/r_0^2$$

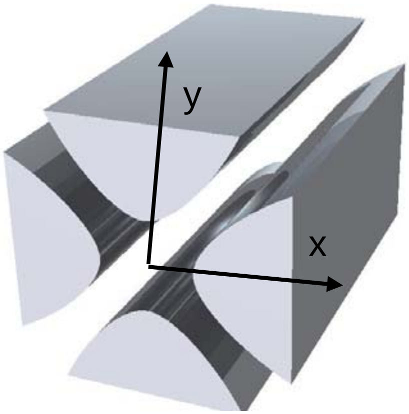

dynamical confinement in the x- y-plane

$$\boxed{\begin{aligned}\ddot{x} + (a - 2\ q\ cos(2\tau))x = 0\\ \ddot{y} - (a - 2\ q\ cos(2\tau))y = 0\end{aligned}}$$

with substitutions

$$a_i = -\frac{4QU}{mr_0^2\Omega_{RF}^2} \qquad q_i = -\frac{2QV}{mr_0^2\Omega_{RF}^2} \qquad \tau = \frac{1}{2}\Omega_{RF} t$$

radial trap radius r_0

2-Dim. Paul mass filter stability diagram

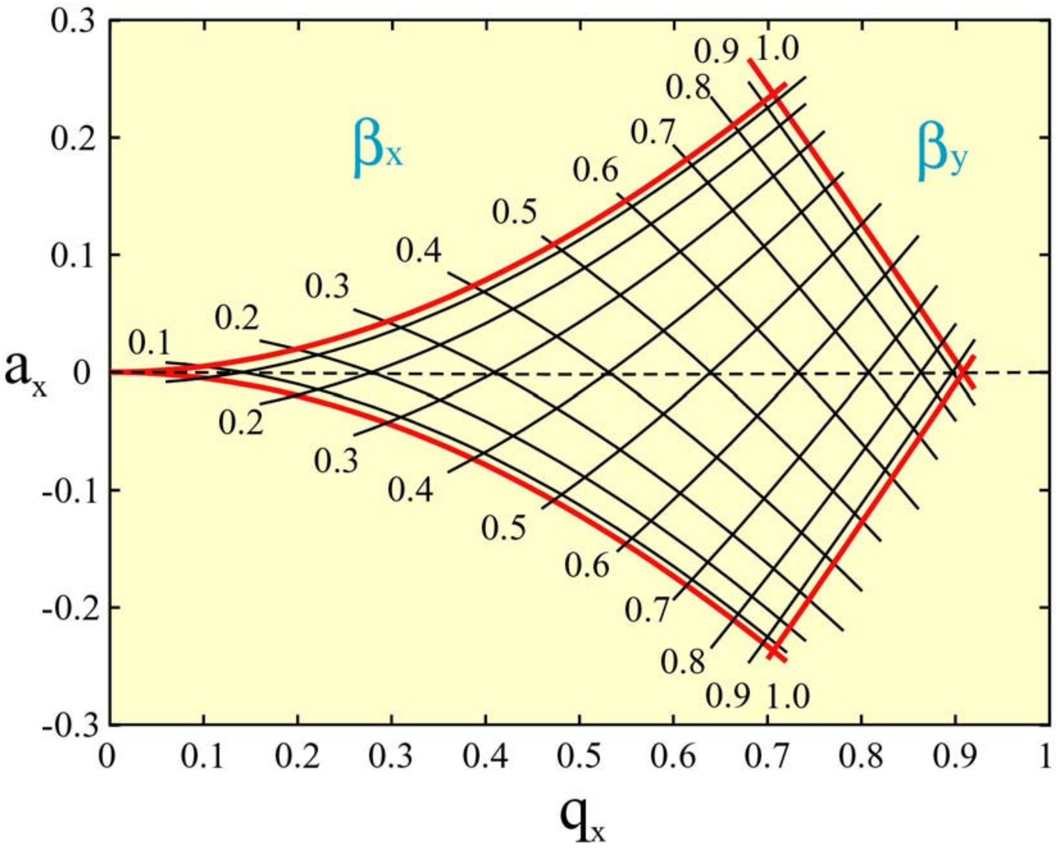

$$\omega_i = \beta_i \frac{\Omega_{RF}}{2}$$

$$\beta_i = \sqrt{a_i + \frac{q_i}{2}}$$

$$a_i = -\frac{4QU}{mr_0^2\Omega_{RF}^2} \qquad q_i = -\frac{2QV}{mr_0^2\Omega_{RF}^2} \qquad i = x, y$$

A Linear Paul trap

plug the ends of a mass filter by positive electrodes:

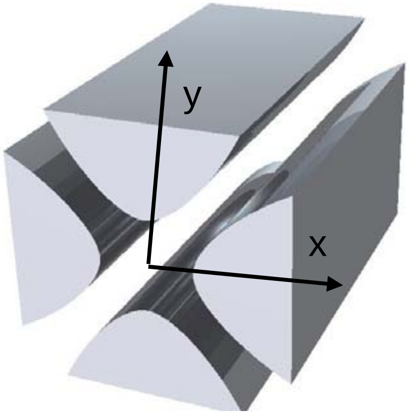

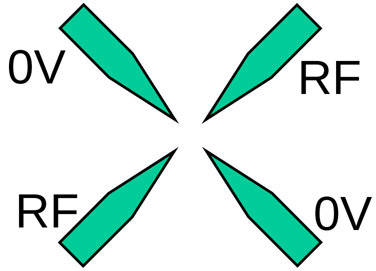

mass filter blade design

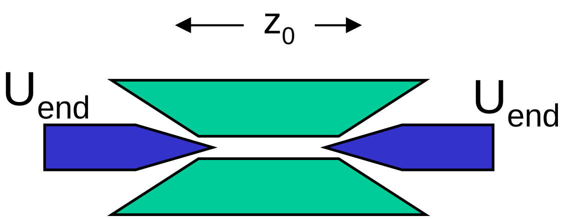

side view

numerically calculate the axial electric potential,
fit parabula into the potential
and get the axial trap frequency

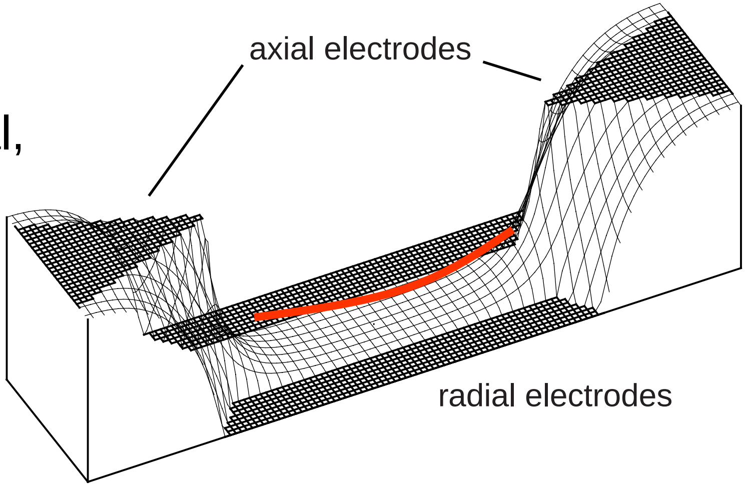

$$\boxed{\omega_z = \sqrt{\frac{2\kappa Q U_{end}}{m z_0}}}$$

with k geometry factor

Innsbruck linear ion trap

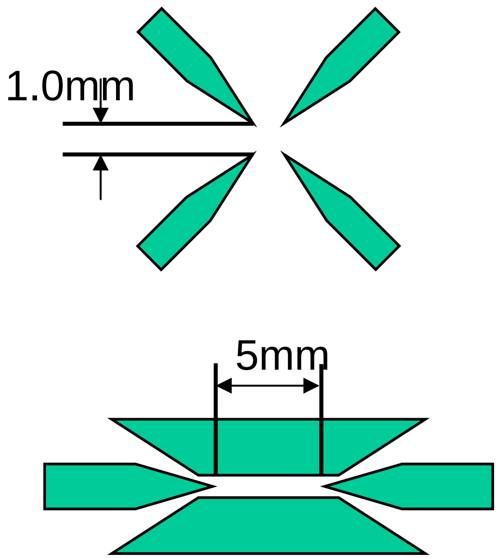

Blade design

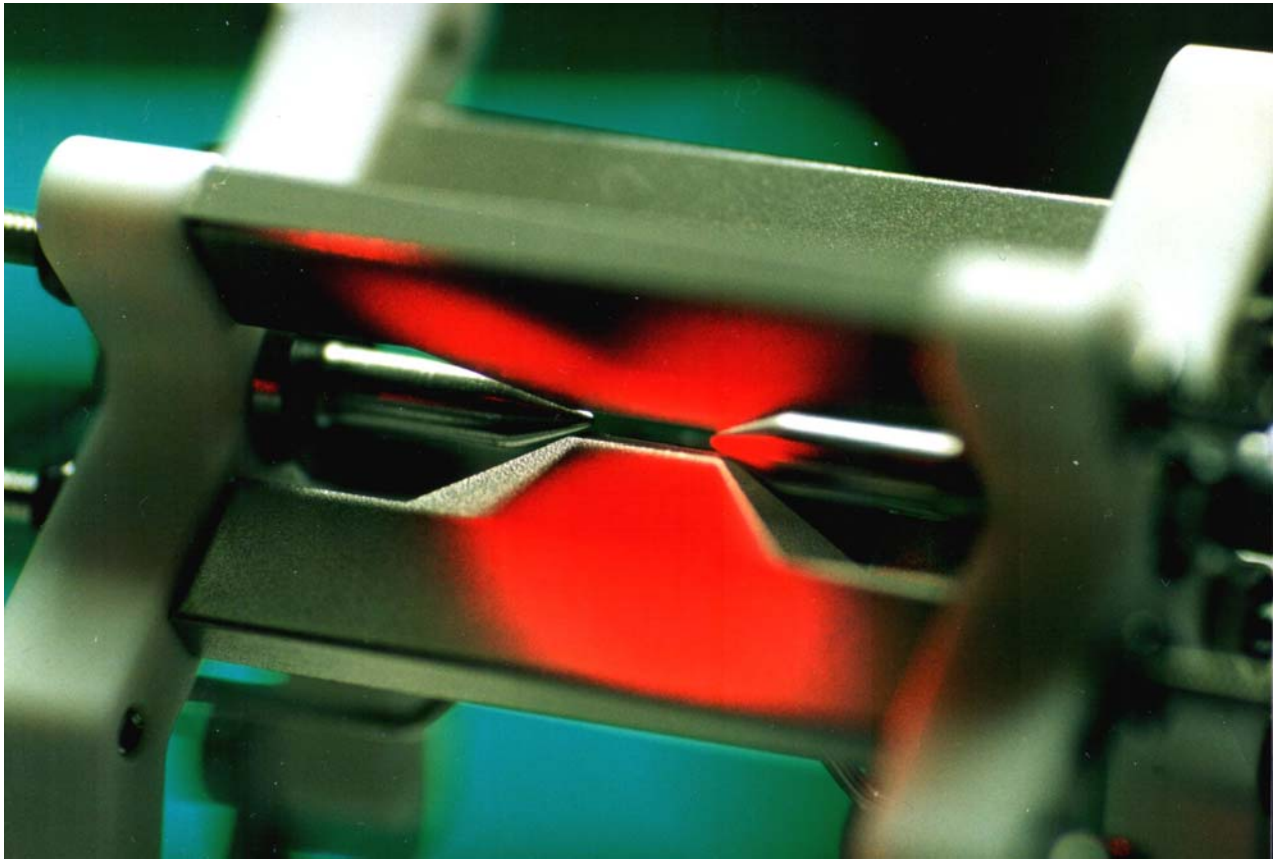

$\omega_{axial} \approx 0.7 - 2\ \mathrm{MHz}$ $\omega_{radial} \approx 5\ \mathrm{MHz}$

$$trap\ \ depth \approx eV$$

F. Schmidt-Kaler, et al.,
Appl. Phys. B 77, 789 (2003).

Innsbruck linear ion trap

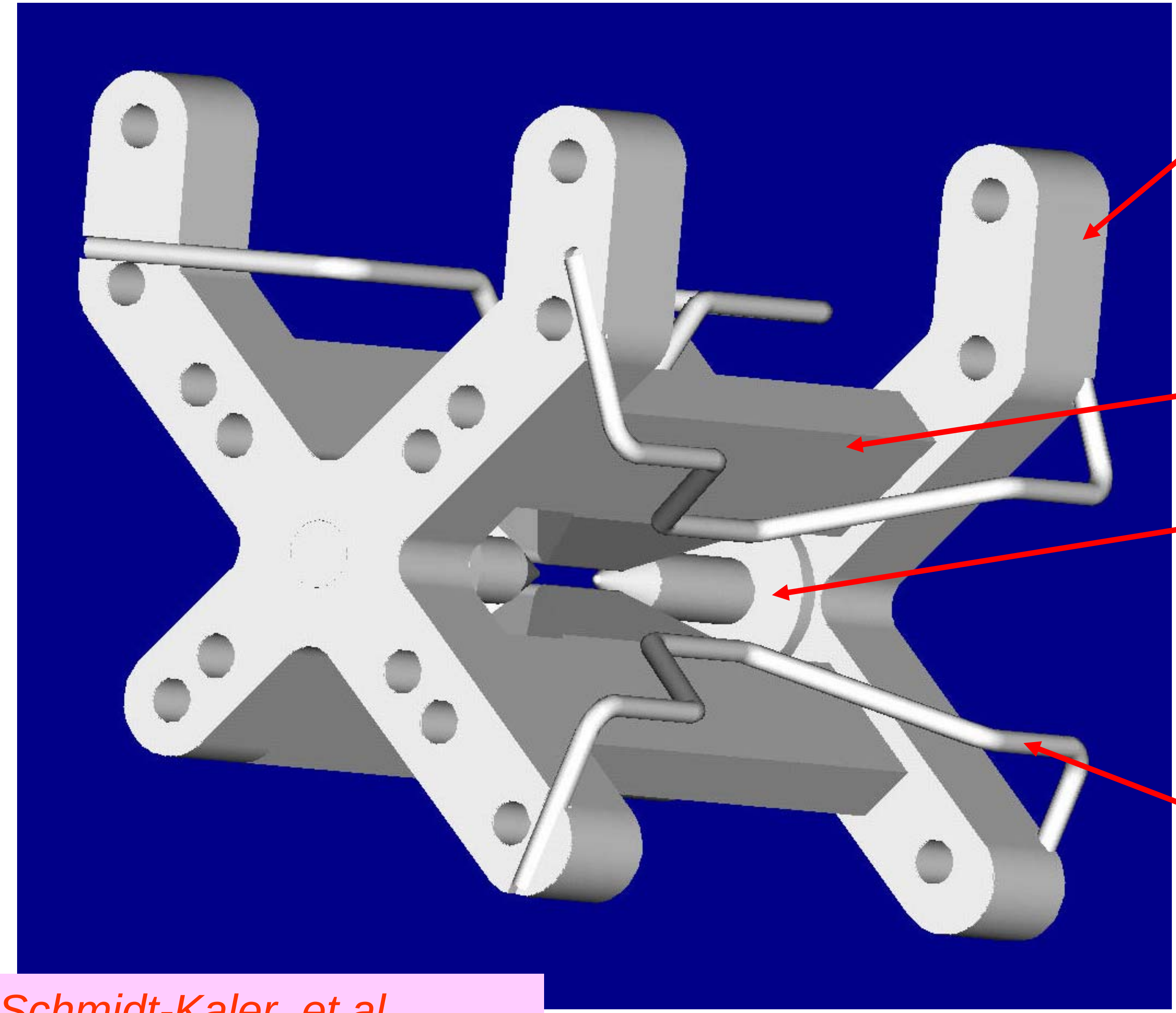

F. Schmidt-Kaler, et al.,
Appl. Phys. B 77, 789 (2003).

Linear ion traps in Rood design

trap electrodes are
nearly in ideal geometry

harmonic trapping
in a large region, and
even outside the center

Aarhus, Denmark

M. Drewsen et al. / International Journal of Mass Spectrometry 229 (2003) 83–91

(a)

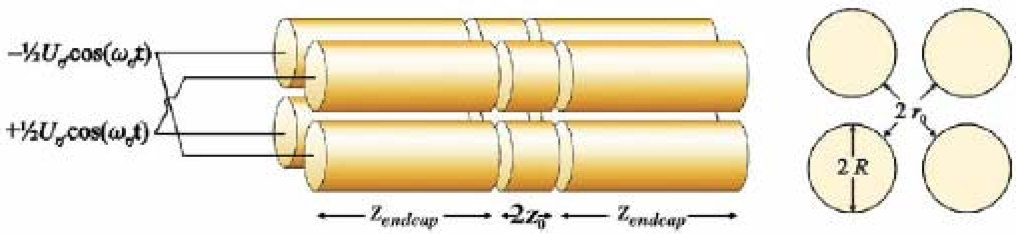

R= 4mm
r_0= 3.5mm

(b)

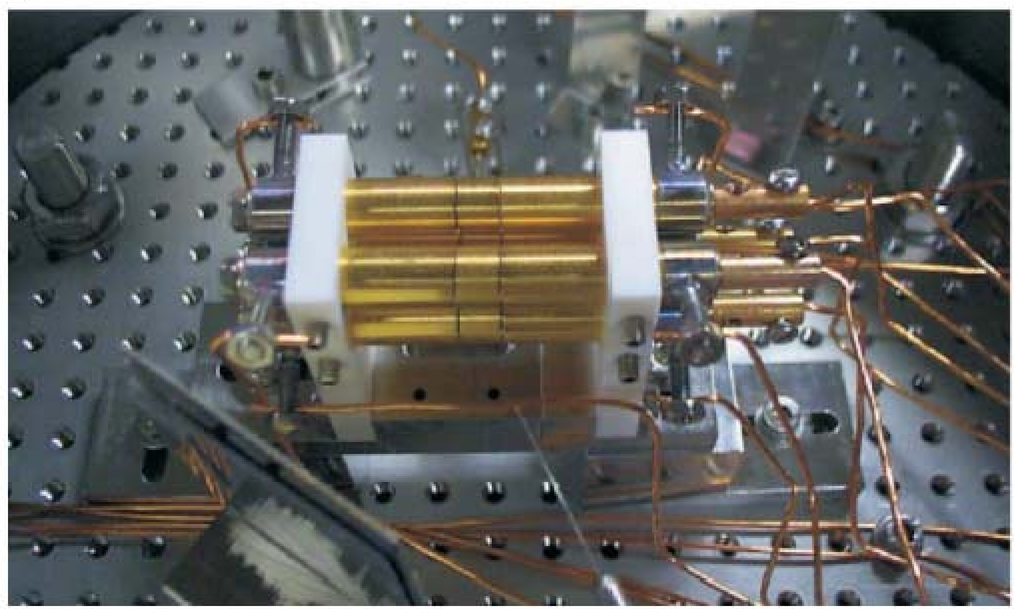

Fig. 1. (a) Sketch of the linear trap used in the experiments. The various parameters are defined in the text of Section 2. (b) Picture of the actual trap used. As a scale, the center-part of the electrode ($2z_0$) is 5.4 mm.

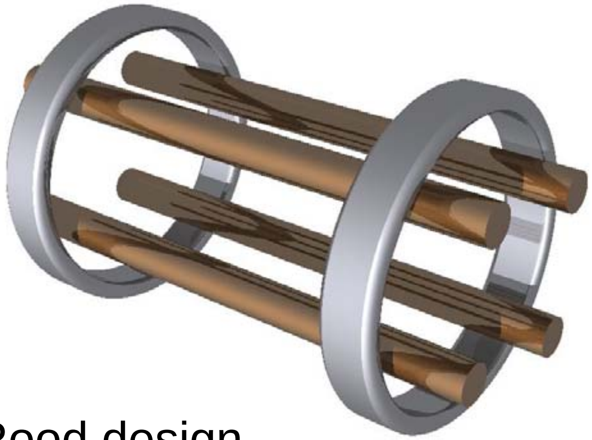

Rood design

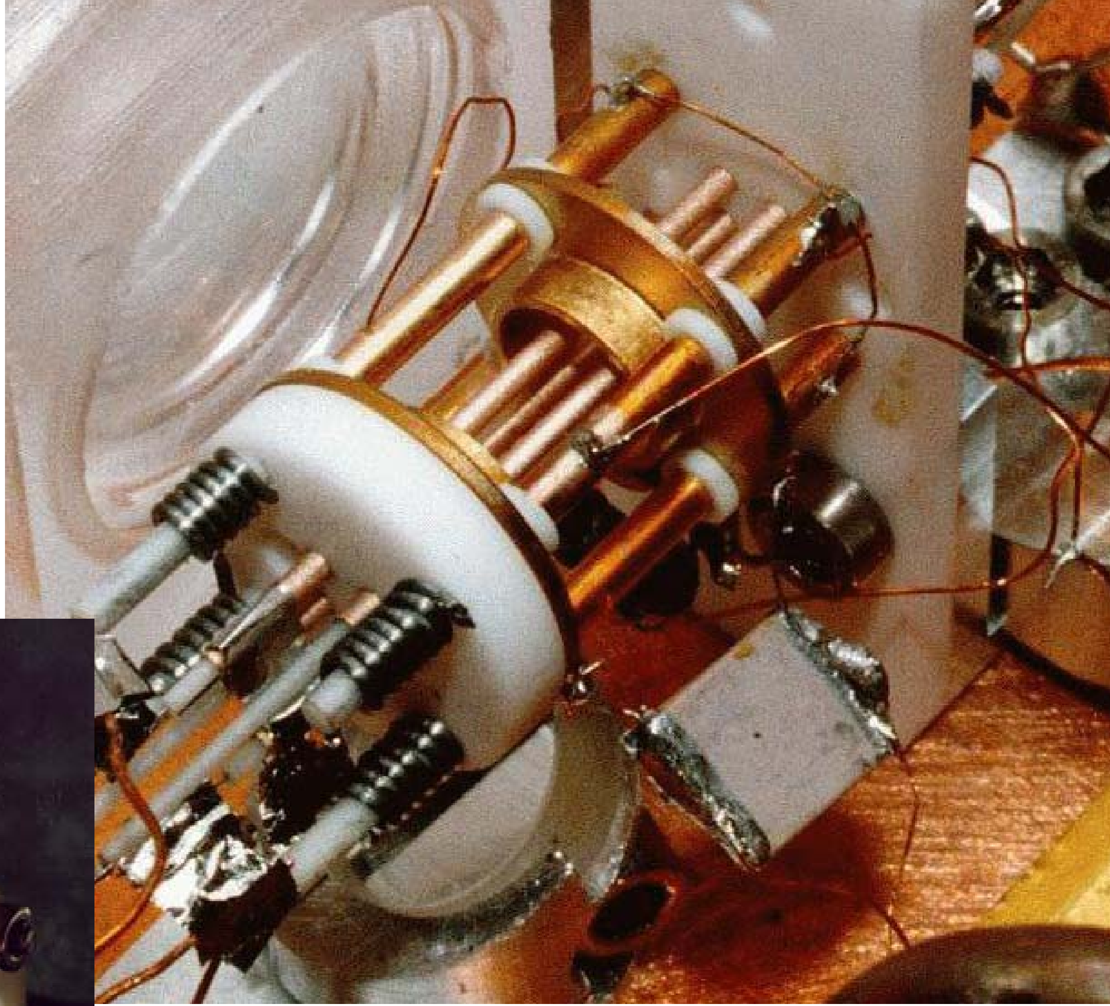

Boulder, USA

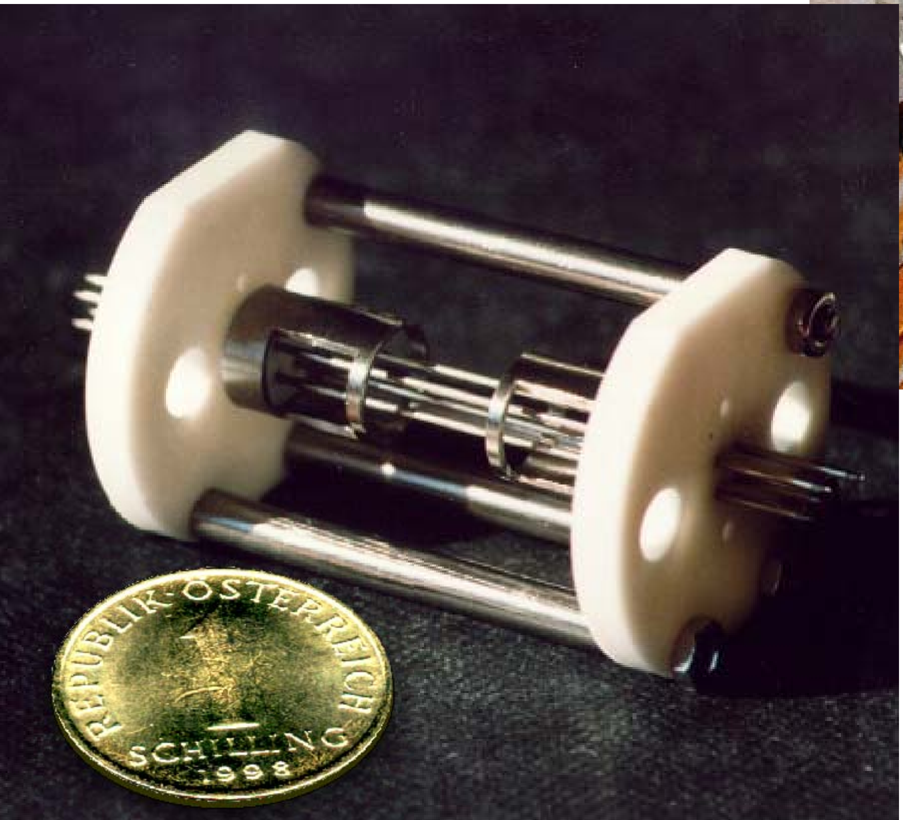

Innsbruck, Austria

Segmented micro traps overview

*Kielpinski et al,
Nature 417, 709 (2002)*

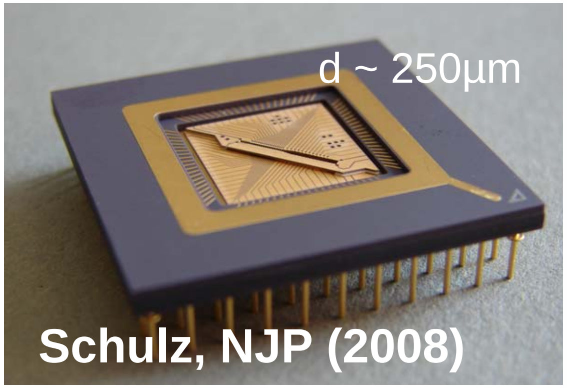

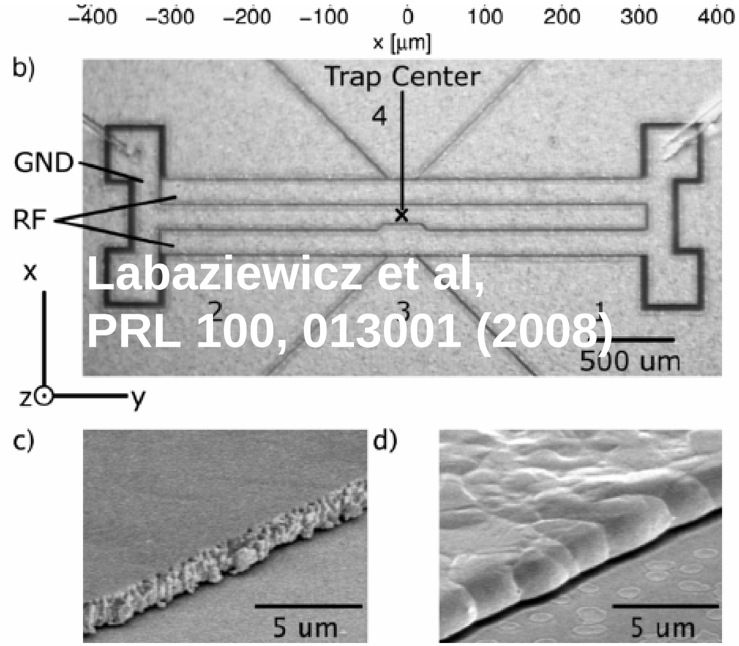

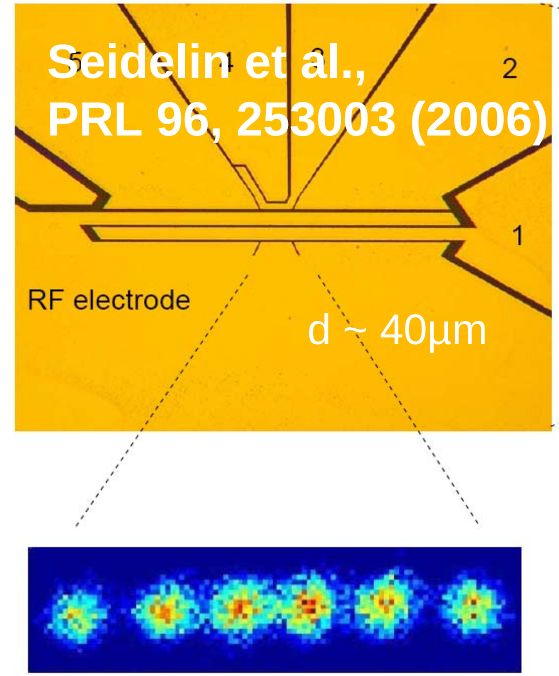

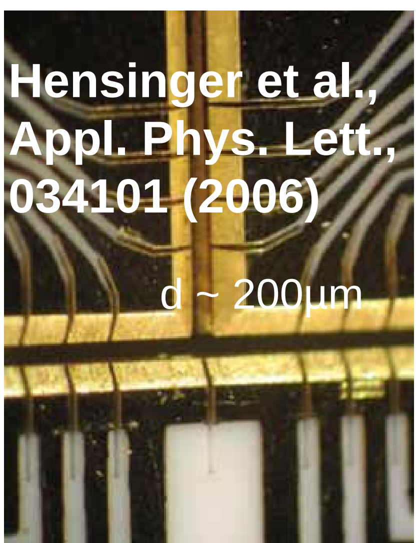

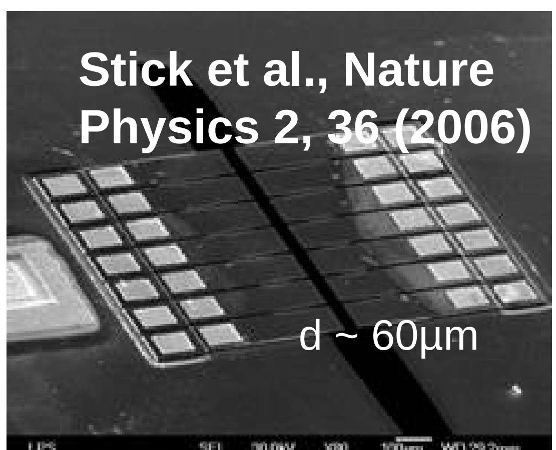

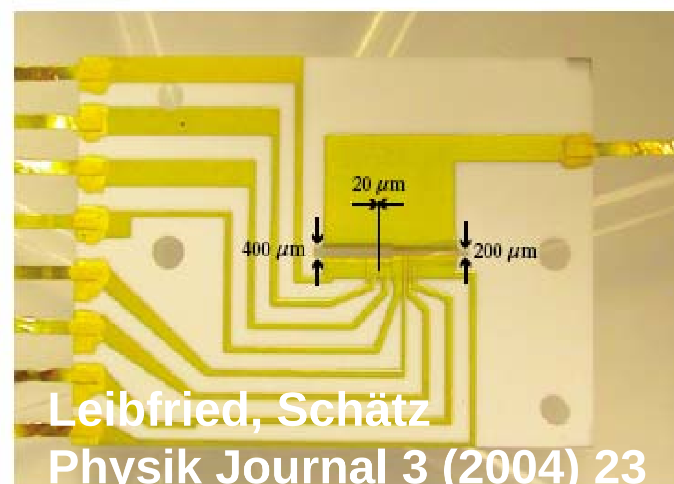

Ulm segmented micro trap

31 DC-electrode pairs
62 electrodes
individ. addressable

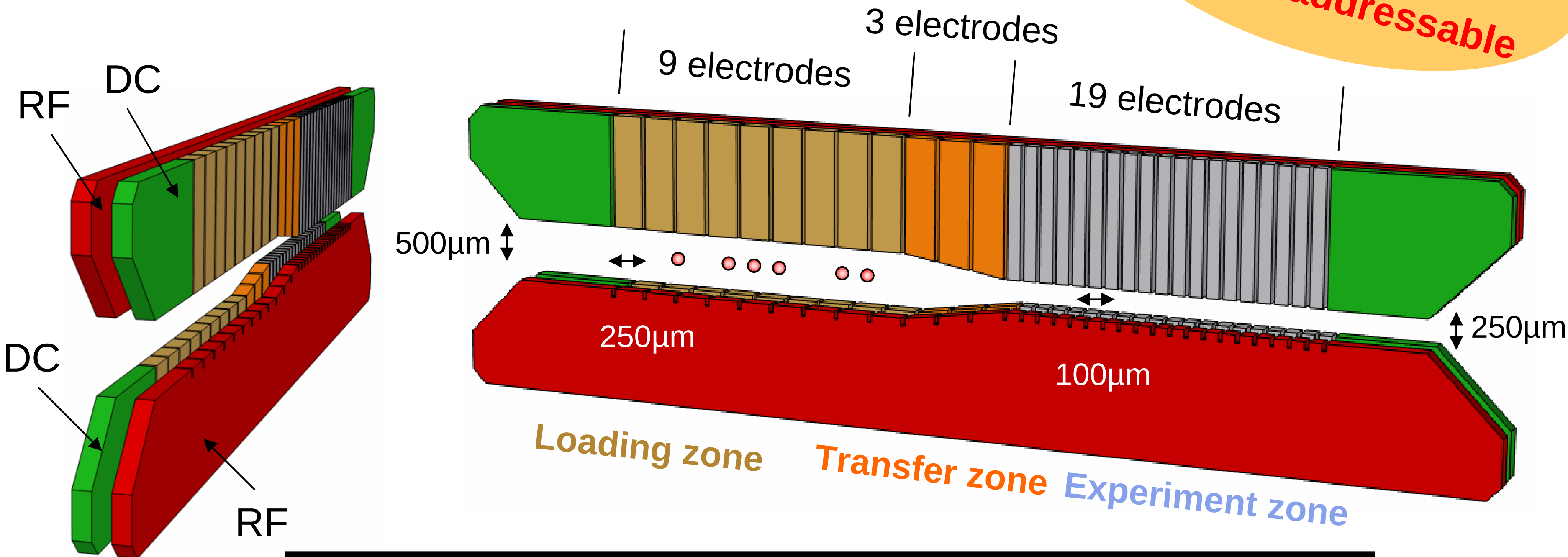

- **Micro structuring** — **- high number and density of ions**
  - high trap frequency and gate speed
- **Segmentation** — **- Processor and memory section**
  - Transport of Ion crystals
  - Separation of ions
  - Cavity QED region

Schulz et al., Fortschr. Phys. 54, 648 (2006)

Ulm segmented micro trap: Fabrication

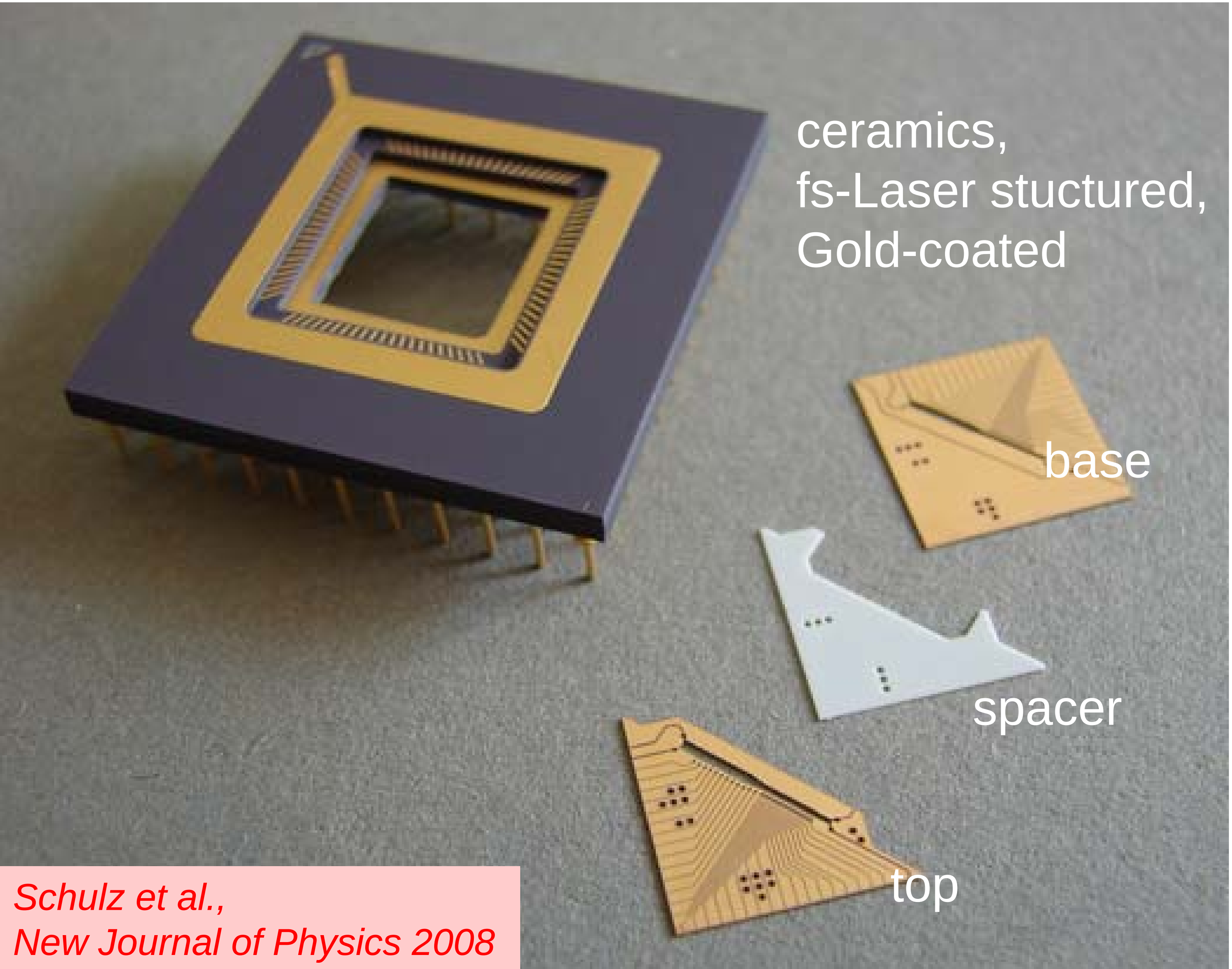

Schulz et al.,
New Journal of Physics 2008

Ulm segmented micro trap: Fabrication

- Ti/Au on Al_2O_3-Wafer (10nm/400nm)
- fs-Laser cut in Au/Ti and Al_2O_3

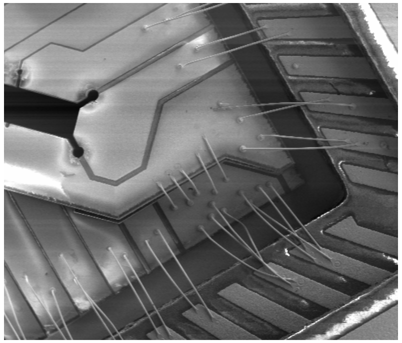

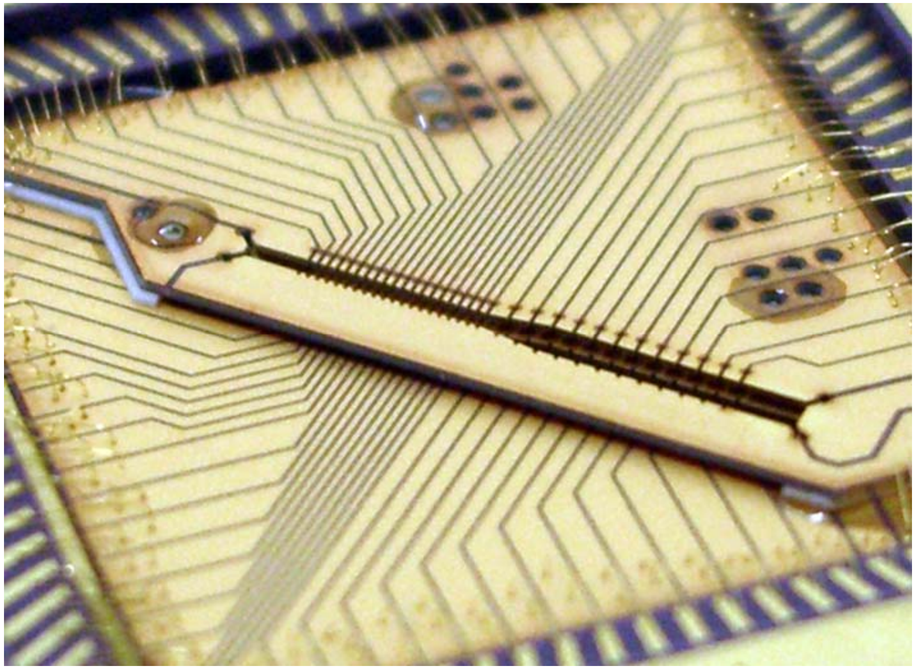

- adjusting and
- gluing into Chip Carrier
- bonding

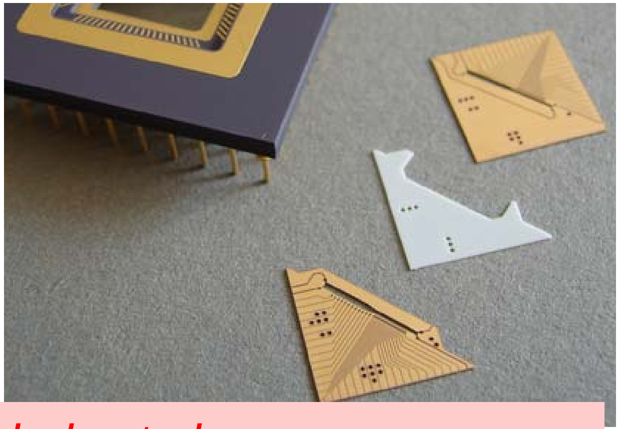

Schulz et al., New Journal of Physics 2008

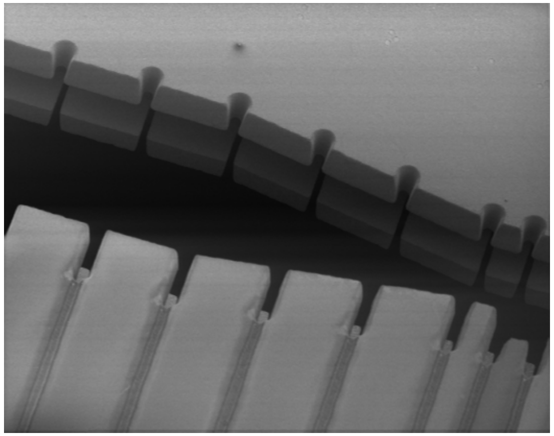

Loading zone / Transfer zone

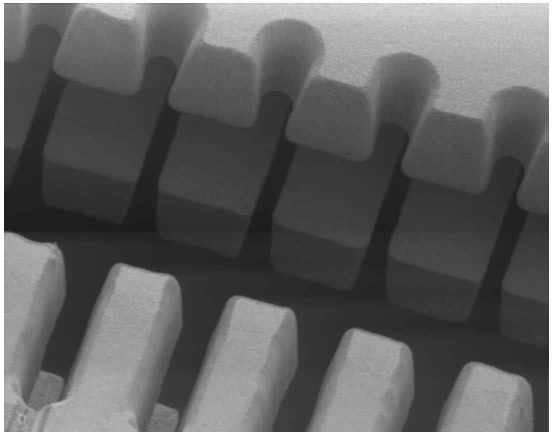

Experiment zone

… assembled and connected in the UHV recipient

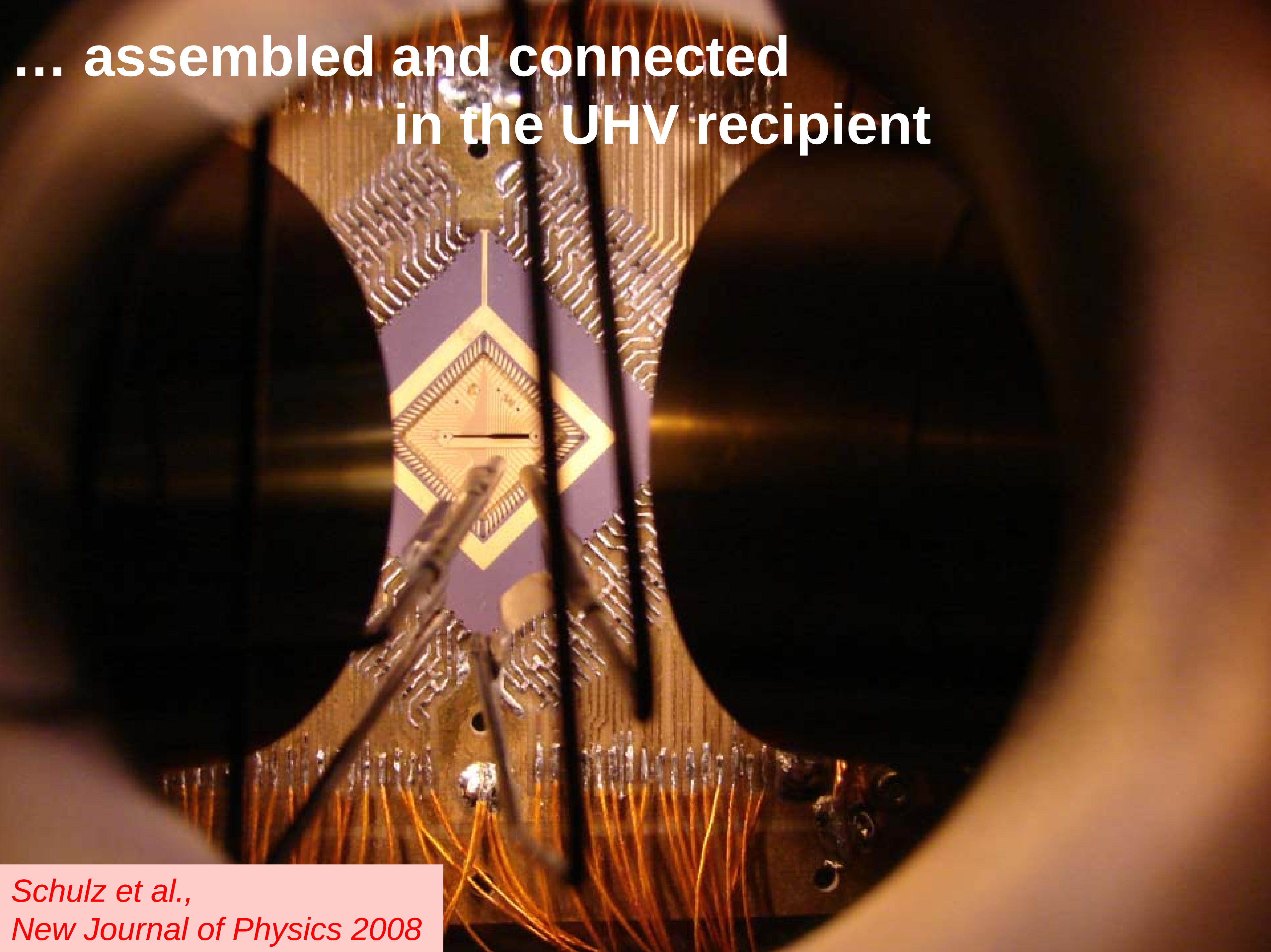

Schulz et al.,
New Journal of Physics 2008

Single Ion and cold Ion Crystal

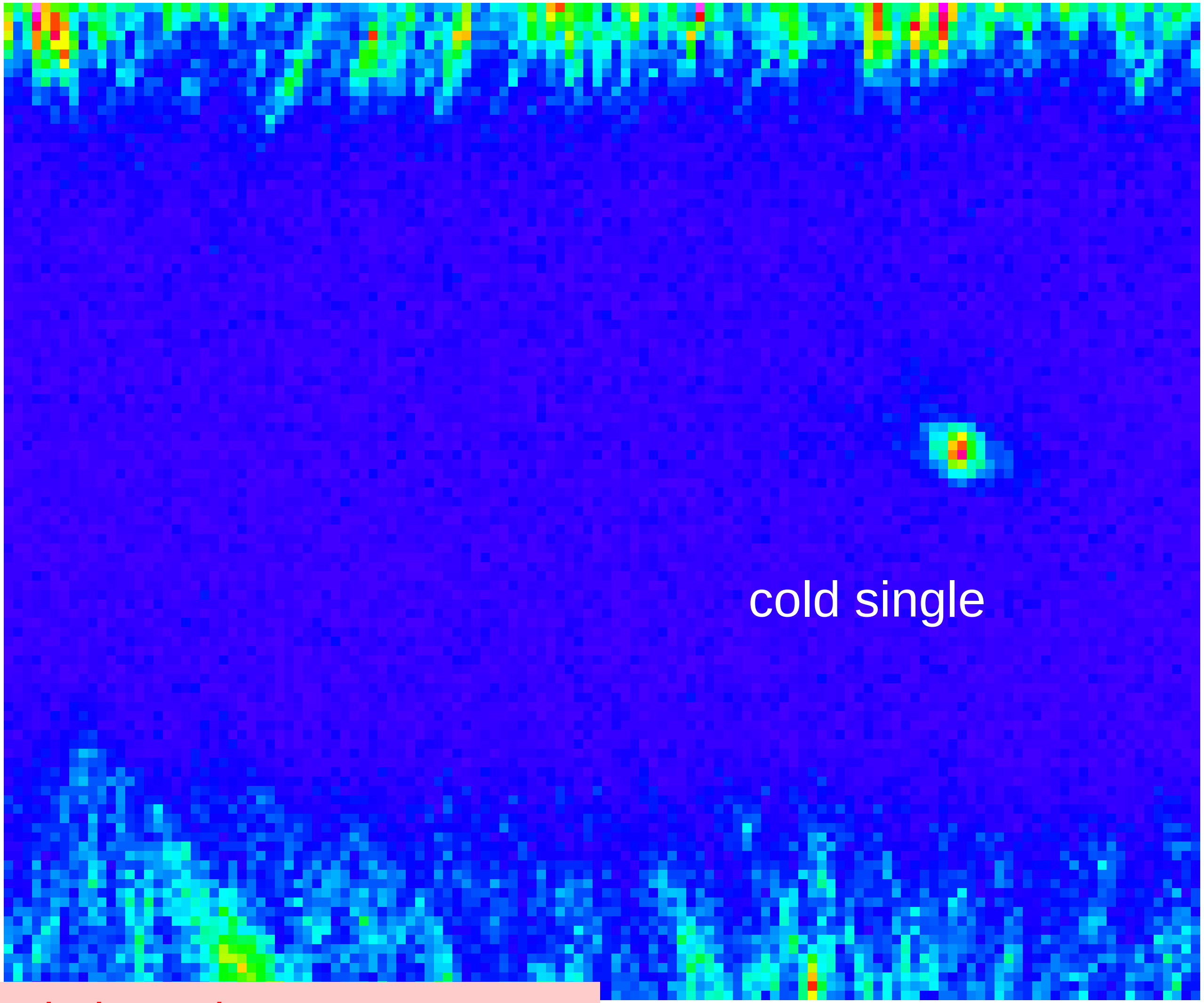

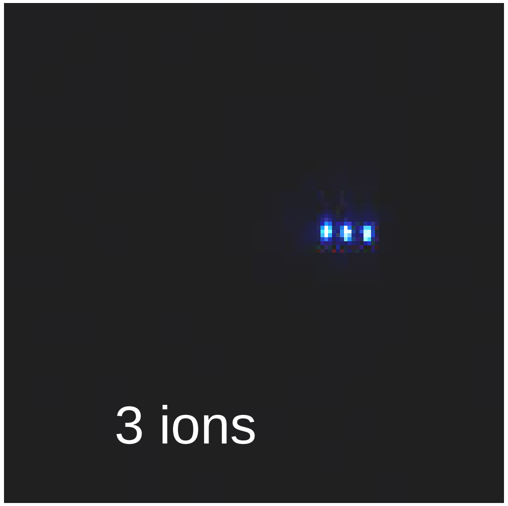

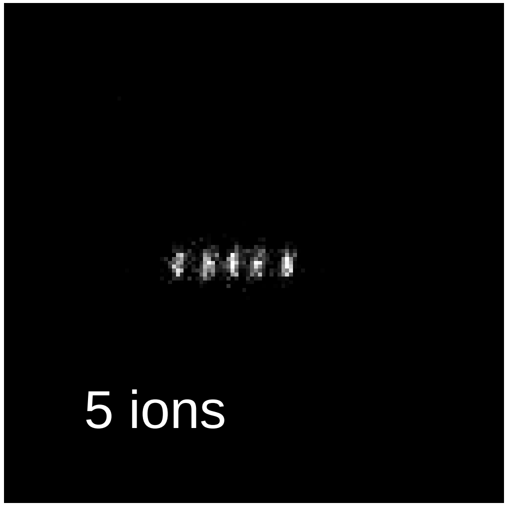

Schulz et al.,
New Journal of Physics 2008

Planar micro traps

Pros:
- Easy fabrication
- High precision
- Small sizes possible (few µm)
- high surface quality

Cons:
- shallow trap potential

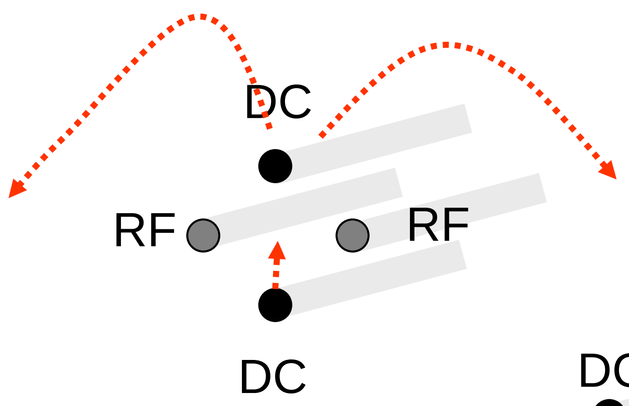

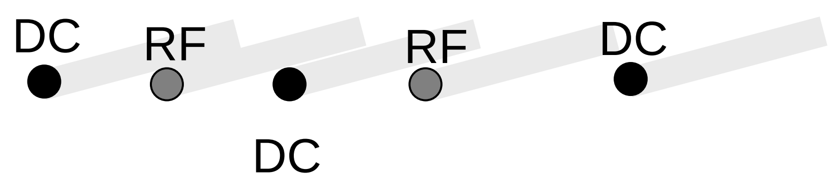

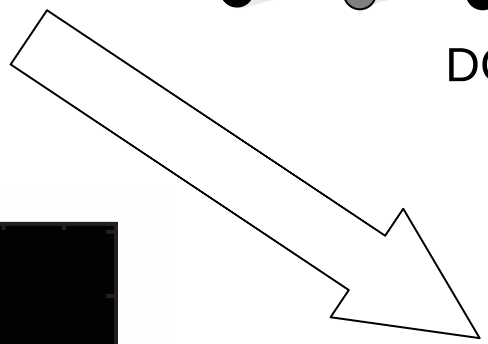

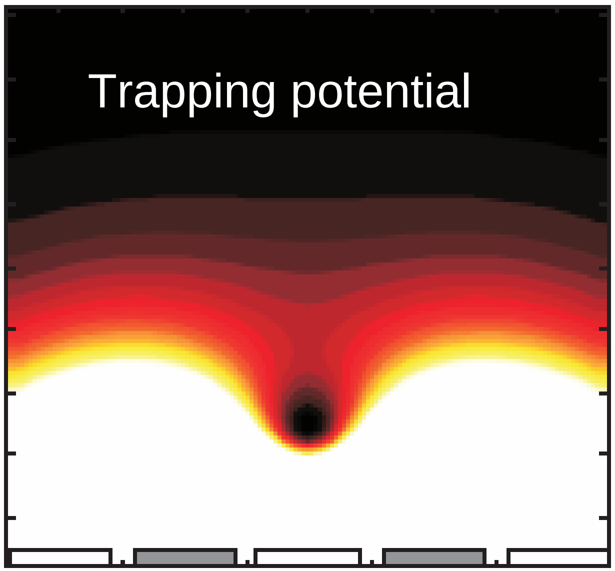

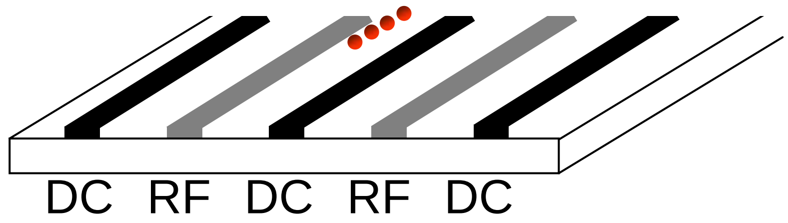

Planar micro traps

S. Seidelin, et. al.,
PRL 96 253003, (2006).

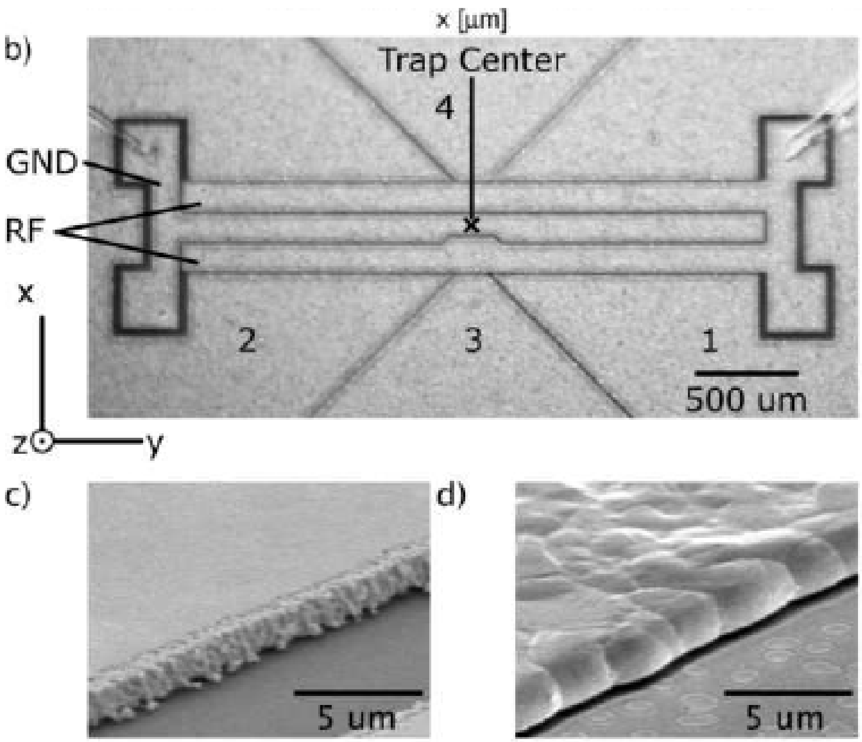

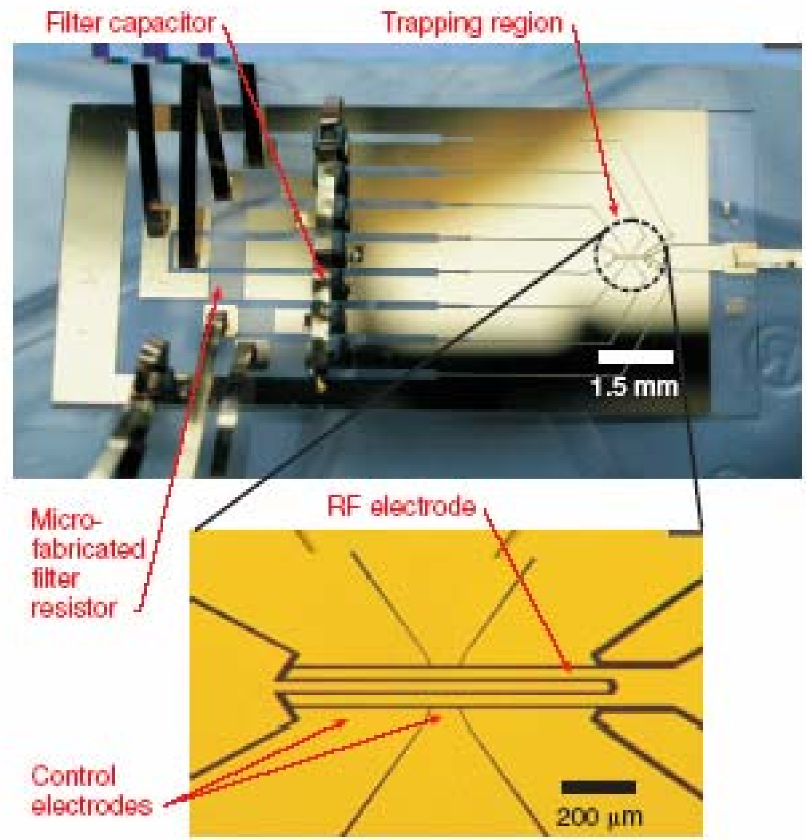

FIG. 7: Micrographs of a five-wire, one-zone linear trap fabricated of gold on fused silica. The top figure is an overview of the trap chip showing contact pads, onboard passive filter elements, leads, and trapping region. Substrate dimensions are 10 mm × 22 mm. The lower image is a detail of the trapping region indicated by the dotted ring in the top figure. The substrate material appears dark-colored in the lower image.

J. Labaziewicz, et. al.,
PRL 100, 013001 (2008).

Planar micro traps

J. Siegler, Diplom
Schulz et al., DPG 2008

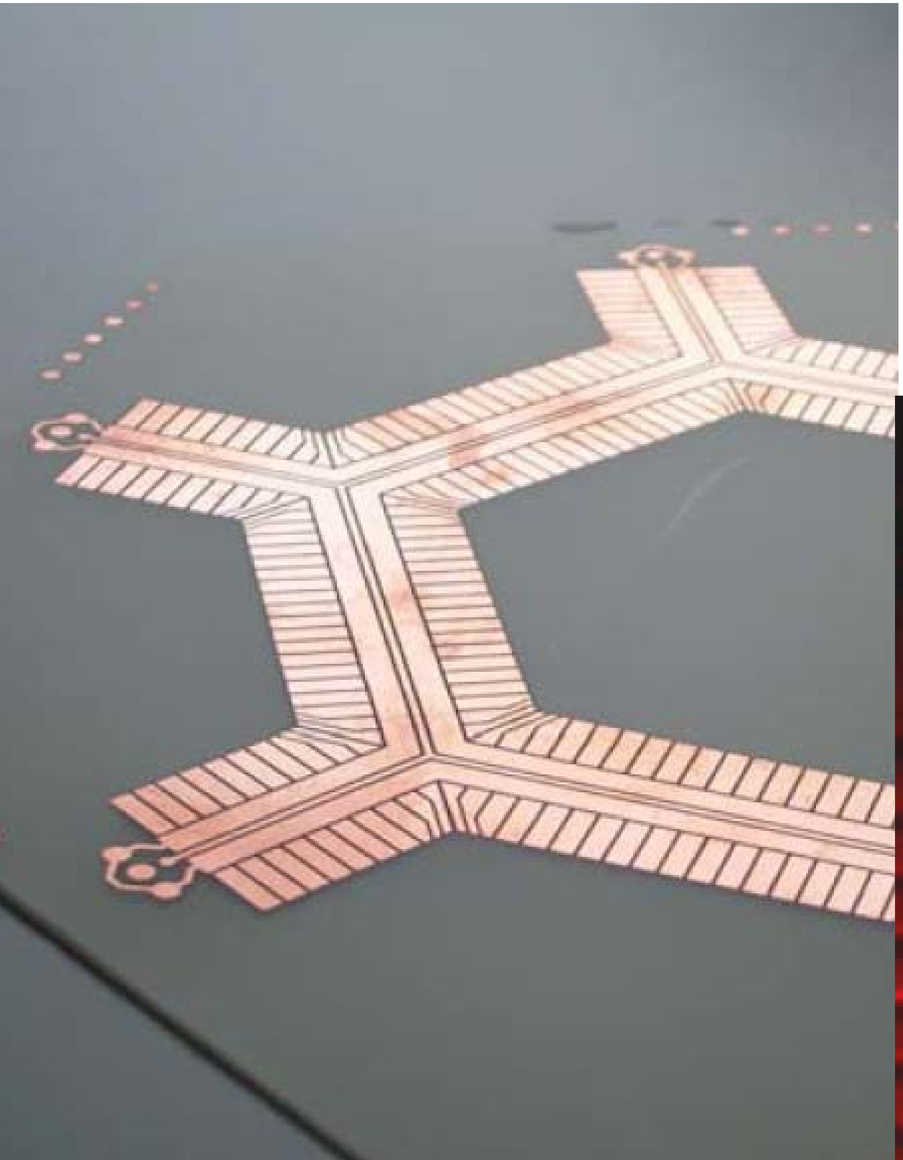

Ulm PCB planar traps:

- Transport tested
- Crossings tested

I) Trapping of single ions

Paul trap in 3D
Linear Paul trap

specialized traps:
segmented linear trap
planar segmented trap

Eigenmodes of a linear ion crystal
Stability of a linear crystal

Micromotion
Measurement and compensation

Equilibrium positions in the axial potential

$$V = \sum_{m=1}^{N} \frac{1}{2} M\nu^2 x_m(t)^2 + \sum_{\substack{n,m=1\\ m\neq n}}^{N} \frac{Z^2 e^2}{8\pi\epsilon_0} \frac{1}{|x_n(t) - x_m(t)|},$$

trap potential　　　mutual ion repulsion

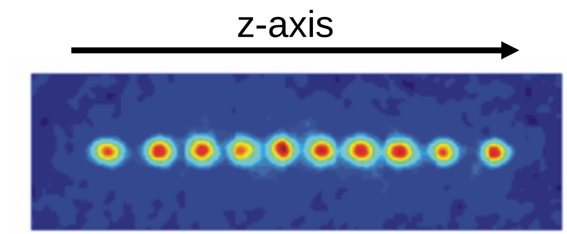

find equilibrium positions x^0: $x_m(t) \approx x_m^{(0)} + q_m(t)$ ions oscillate with *q(t)* arround

condition for equilibrium: $(\partial V/\partial x_m)_{x_m = x_m^{(0)}} = 0$

dimensionless positions $u_m = x_m^{(0)}/l$ with length scale $l^3 = \frac{Z^2 e^2}{4\pi\epsilon_0 M \omega_{ax}^2}$

$^{40}Ca^{+} at\ 1 MHz \rightarrow 4.5 \mu m$

$$\longrightarrow \quad u_m - \sum_{n=1}^{m-1} \frac{1}{(u_m - u_n)^2} + \sum_{n=m+1}^{N} \frac{1}{(u_m - u_n)^2} = 0$$

$$(m = 1, 2, \ldots N).$$

D. James, Appl. Phys. B 66, 181 (1998)

Equilibrium positions in the axial potential

$$u_m - \sum_{n=1}^{m-1} \frac{1}{(u_m - u_n)^2} + \sum_{n=m+1}^{N} \frac{1}{(u_m - u_n)^2} = 0$$

$$(m = 1, 2, \dots N) .$$

set of N equations for u_m

force of the trap potential

Coulomb force of all ions from left side

Coulomb force of all ions from left side

numerical solution (Mathematica), e.g. $N=5$ ions

```
a@Tablec;a1, a2, a3, a4, a5, a6, a7, a8, a9, a10?G;
equ5@TablecacCmGG
   0Sumc1•KacCmGG0acCnGGC^2, ;n, 1, m01?G
   .Sumc1•KacCmGG0acCnGGC^2, ;n, m.1, 5?G, ;m, 1, 5?G
aa5@TimingcFindRootcequ5, ;a1, 010?, ;a2, 01?, ;a3, 0.1?, ;a4, 1?, ;a5, 10?GG
```

```
Out[79]= =a1. 1/Ka10a2C^2 . 1/Ka10a3C^2 . 1/Ka10a4C^2 . 1/Ka10a5C^2 , a20 1/K0a1.a2C^2 . 1/Ka20a3C^2 . 1/Ka20a4C^2 . 1/Ka20a5C^2 ,
   a30 1/K0a1.a3C^2 0 1/K0a2.a3C^2 . 1/Ka30a4C^2 . 1/Ka30a5C^2 ,
   a40 1/K0a1.a4C^2 0 1/K0a2.a4C^2 0 1/K0a3.a4C^2 . 1/Ka40a5C^2 ,
   a50 1/K0a1.a5C^2 0 1/K0a2.a5C^2 0 1/K0a3.a5C^2 0 1/K0a4.a5C^2 A
```

equilibrium positions

```
Out[80]= ;0.02 Second, ;a1 Ø 01.7429, a2 Ø 00.822101, a3 Ø 2.4453 ° 10^014, a4 Ø 0.822101, a5 Ø 1.7429??
```

-1.74	-0.82	0	+0.82	+1.74

Experiment: equilibrium positions

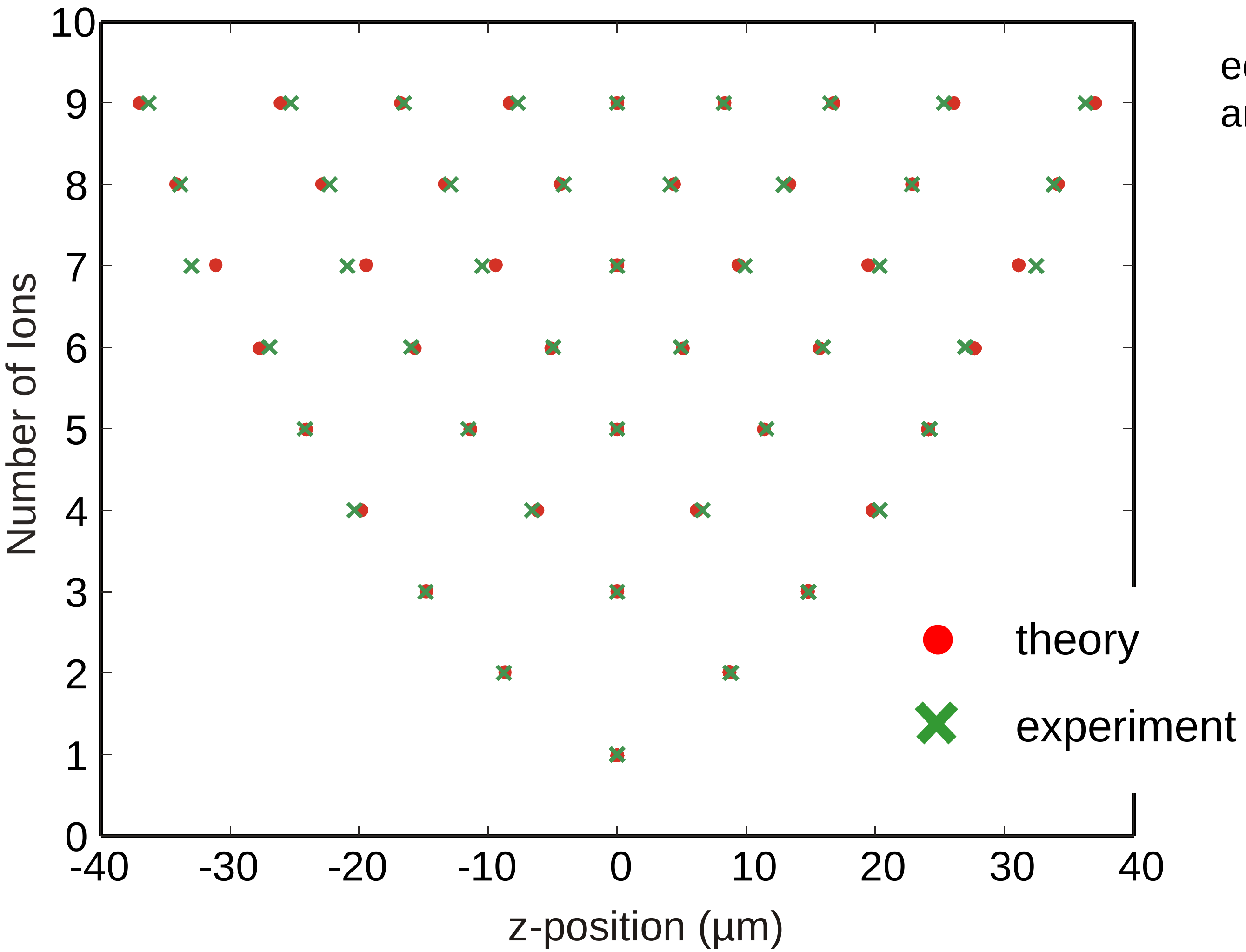

equilibrium positions
are not equally spaced

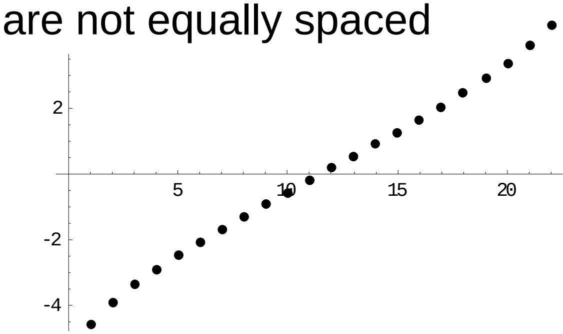

minimum inter-ion distance:

$$u_{min}(N) = \left(\frac{Z^2 e^2}{4\pi\epsilon_0 M \omega_{ax}}\right)\frac{2.018}{N^{0.559}}$$

H. C. Nägerl et al., Appl. Phys. B 66, 603 (1998)

Eigenmodes and Eigenfrequencies

Lagrangian of the axial ion motion: $L = T + V$

describes small excursions arround equilibrium positions

$$= \frac{M}{2}\sum_{m=1}^{N}(\dot{q}_m)^2 - \frac{1}{2}\sum_{m,n=1}^{N} q_n q_n \left(\frac{\partial^2 V}{\partial x_n \partial x_m}\right)_0 + \dots$$

$$= \frac{M}{2}\left(\sum_{m=1}^{N}\dot{q}_m^2 - \omega_{ax}^2 \sum_{m,n=1}^{N} A_{nm} q_n q_n\right)$$

D. James, Appl. Phys. B 66, 181 (1998)

with $$A_{mn} = 1 + 2\sum_{\substack{n \neq m \\ n = 0}}^{N} \frac{1}{|u_m - u_n|^3} \quad if \quad m = n$$

and $$A_{mn} = -\frac{2}{|u_m - u_n|^3} \quad if \quad m \neq n$$

linearized Coulomb interaction leads to Eigenmodes, but the next term in Tailor expansion leads to mode coupling, which is however very small.

C. Marquet, et al., Appl. Phys. B 76, 199 (2003)

Eigenmodes and Eigenfrequencies

numerical solution (Mathematica), e.g. *N=4* ions

```
A4 @ TableC
    IfCm $@ n,
     02 • AbsCu4CCmGG 0 u4CCnGGG^3,
     1. . 2 SumC IfC i û m, 1. • AbsCKu4CCmGG 0 u4CCiGGO^3G , 0G, ;i, 1, 4?G  G,
                                                      ;m, 1, 4?, ;n, 1, 4?G;
TableFormCA4G
TableFormCEigenvectorsCA4GG
freq4 @ SqrtCEigenvaluesCA4GG   K- Modenfrequenzen -O
```

Matrix, to diagonize

Out[36]//TableForm=

3.48927	-2.1093	-0.295686	-0.0842851
-2.1093	6.0699	-2.66491	-0.295686
-0.295686	-2.66491	6.0699	-2.1093
-0.0842851	-0.295686	-2.1093	3.48927

Eigenvectors

Out[37]//TableForm=

-0.213213	0.674196	-0.674196	0.213213
0.5	-0.5	-0.5	0.5
-0.674196	-0.213213	0.213213	0.674196
0.5	0.5	0.5	0.5

pictorial

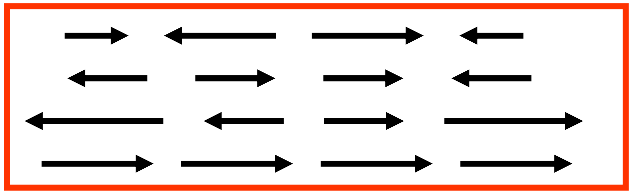

Out[38]= {3.05096, 2.41039, 1.73205, 1.} Eigenvalues

$$(3.059 \pm 0.008)\omega_{ax} \quad \sqrt{29/5}\,\omega_{ax} \quad \sqrt{3}\,\omega_{ax} \quad 1\omega_{ax}$$

depends on *N* does not

for the radial modes:
Market et al., Appl. Phys. B76, (2003) 199

Common mode excitation: Experiment

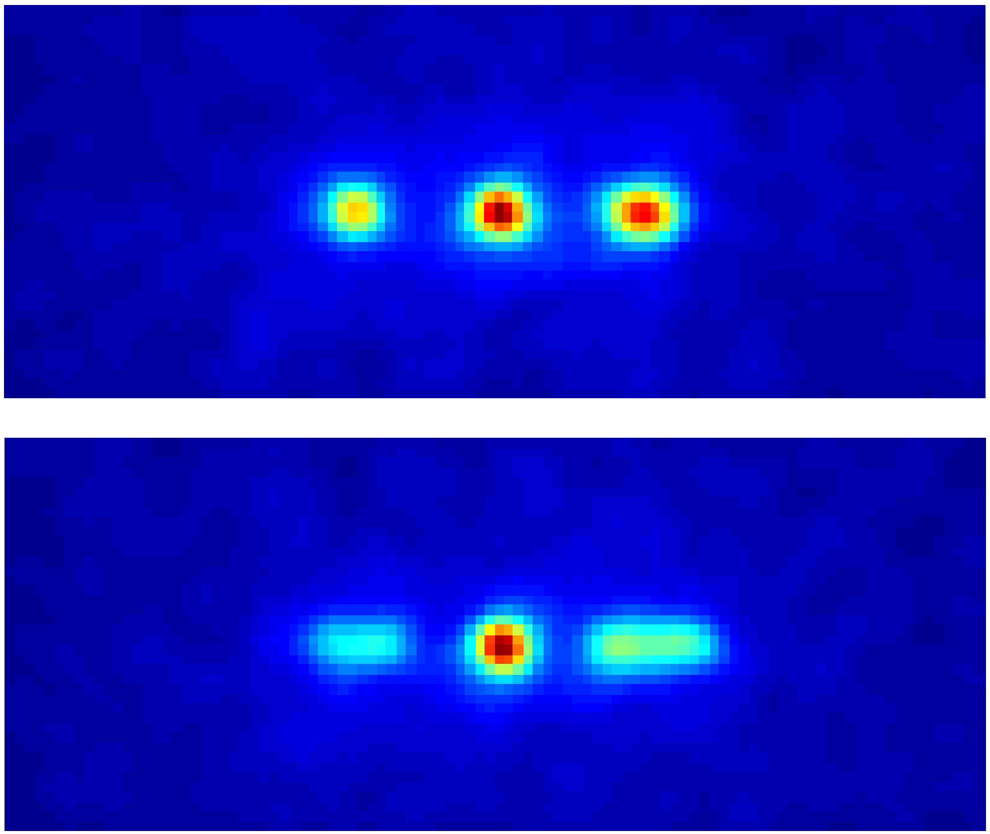

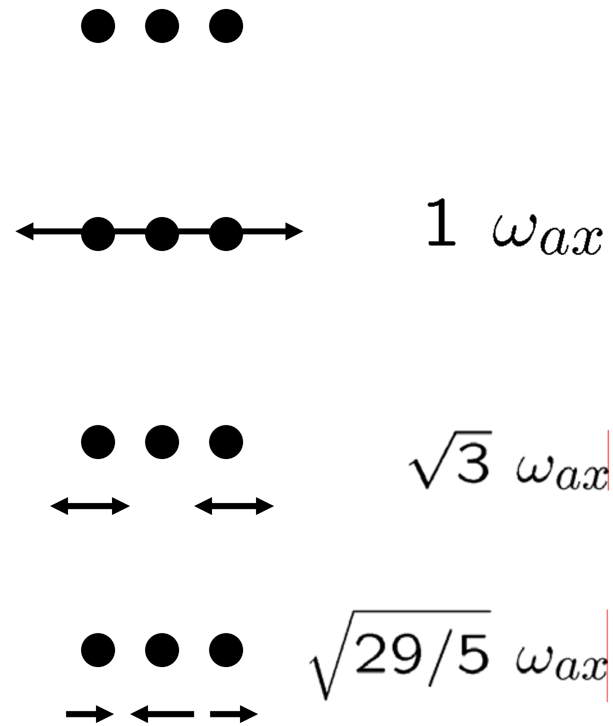

H. C. Nägerl, Optics Express / Vol. 3, No. 2 / 89 (1998).

Common mode excitations

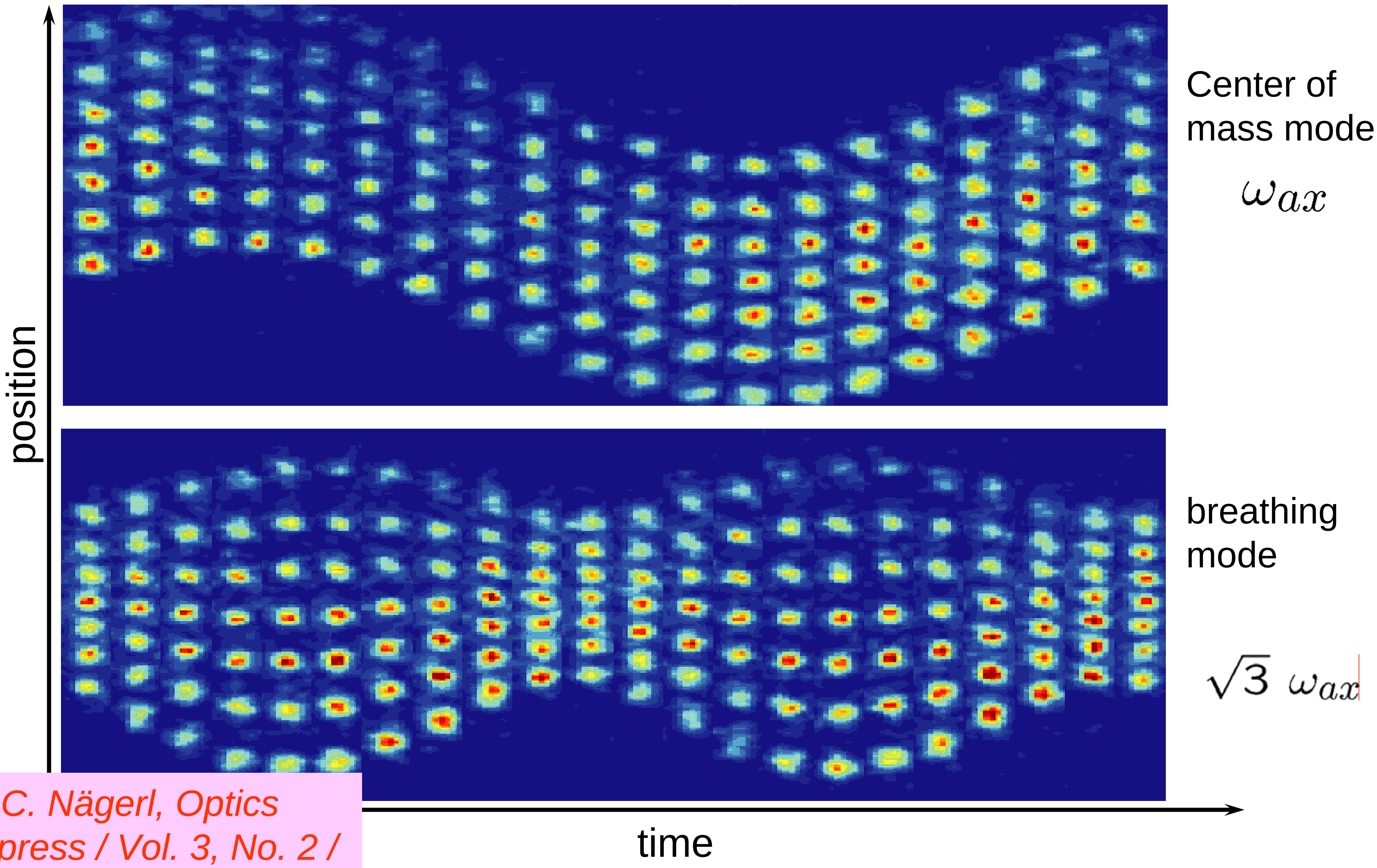

H. C. Nägerl, Optics Express / Vol. 3, No. 2 / 89 (1998).

Breathing mode excitation

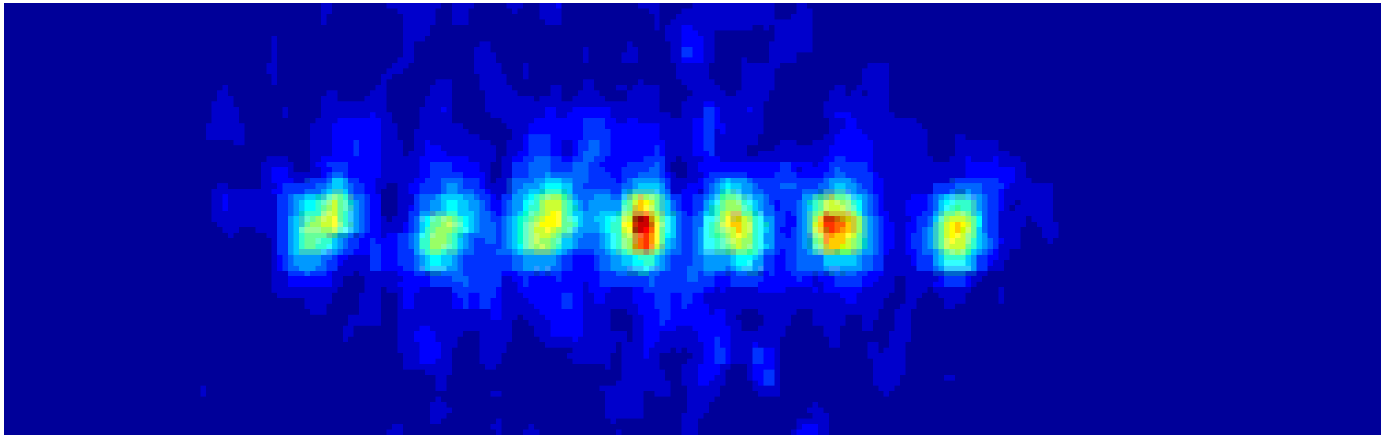

H. C. Nägerl, Optics Express / Vol. 3, No. 2 / 89 (1998).

linear crystal ⟺ zig zag crystal

with higher *N* of ions the linear configuration becomes unstable and ions arrange in 3d

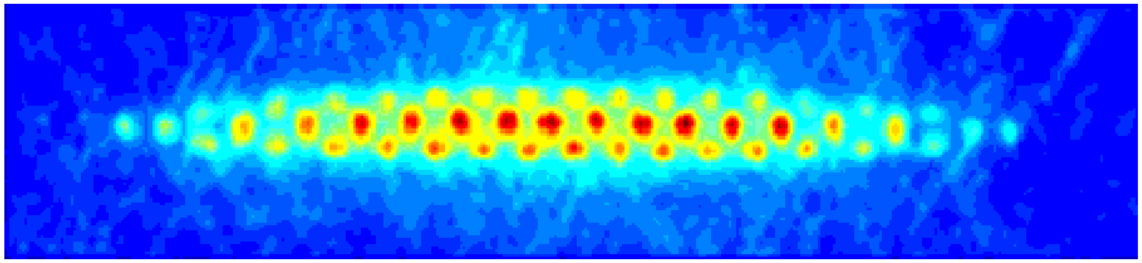

Ca^+ crystal with about 70 ions

$$\alpha = (\omega_{ax}/\omega_{rad})^2$$

$$\alpha_{crit} = 2.94 N e^{-1.8}$$

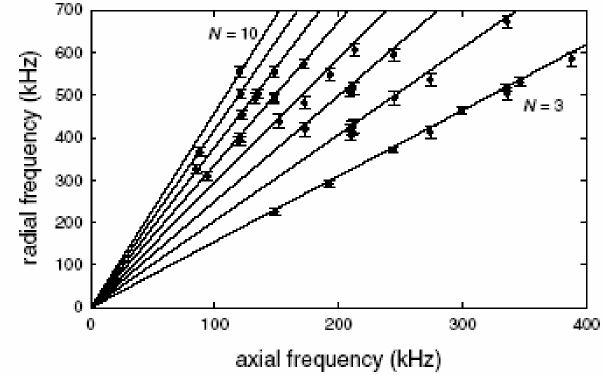

FIG. 2. Measured radial versus axial frequencies (points), at the onset of the zigzag instability, agree well with the prediction of our theoretical analysis (lines). Measurements were taken on seven different days, with some days dedicated to a particular length ion string and other days spent studying up to six different length strings. Theory lines pass through the origin and have slopes $\nu_r/\nu_z = (\alpha_{\rm crit})^{-1/2}$, increasing with ion number for $N = 3$ (minimum slope shown) through $N = 10$ (maximum slope shown). Error bars (see text) are dominated by the uncertainty in determining the critical rf voltage for zigzag onset while the axial frequency is held fixed.

VOLUME 85, NUMBER 12 PHYSICAL REVIEW LETTERS 18 SEPTEMBER 2000

Observation of Power-Law Scaling for Phase Transitions in Linear Trapped Ion Crystals

D. G. Enzer, M. M. Schauer, J. J. Gomez, M. S. Gulley, M. H. Holzscheiter, P. G. Kwiat, S. K. Lamoreaux, C. G. Peterson, V. D. Sandberg, D. Tupa, A. G. White, and R. J. Hughes

Physics Division, Los Alamos National Laboratory, Los Alamos, New Mexico 87545

D. F. V. James

Theoretical Division, Los Alamos National Laboratory, Los Alamos, New Mexico 87545

(Received 14 January 2000)

We report an experimental confirmation of the power-law relationship between the critical anisotropy parameter and ion number for the linear-to-zigzag phase transition in an ionic crystal. Our experiment uses laser cooled calcium ions confined in a linear radio-frequency trap. Measurements for up to ten ions are in good agreement with theoretical and numeric predictions. Implications on an upper limit to the size of data registers in ion trap quantum computers are discussed.

Micro-motion

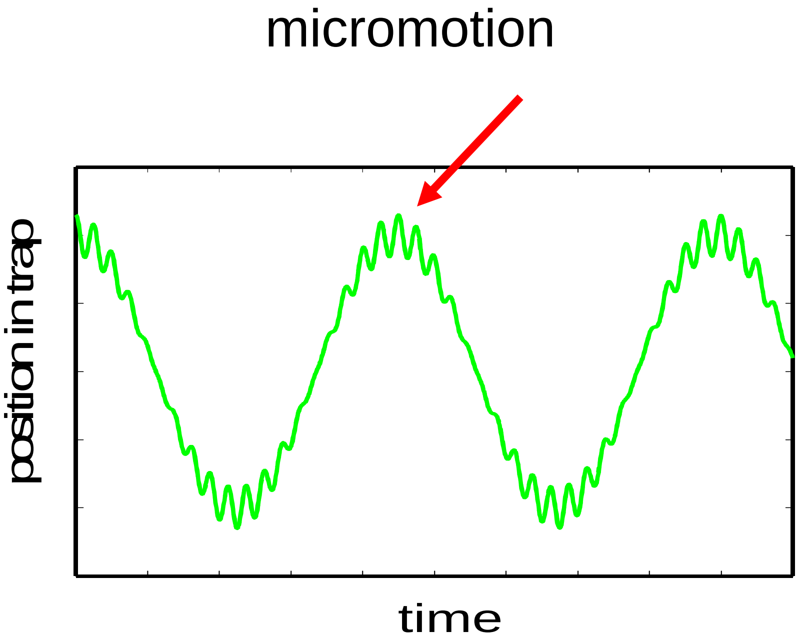

Problems due to micro-motion:

a) relativistic Doppler shift in
frequency measurements

b) less scattered photons
due to broader resonance line

c) imperfect Doppler cooling
due to line broadening

d) AC Stark shift of the clock transition
due to trap drive field Ω

f) for larger # of ions: mutual coupling
of ions can lead to coupling of secular
frequency ω and drive frequency Ω.
Heating of the ion motion

Micro-motion

frequency Ω : Micro-motion
Ion is shaken with the RF drive frequency

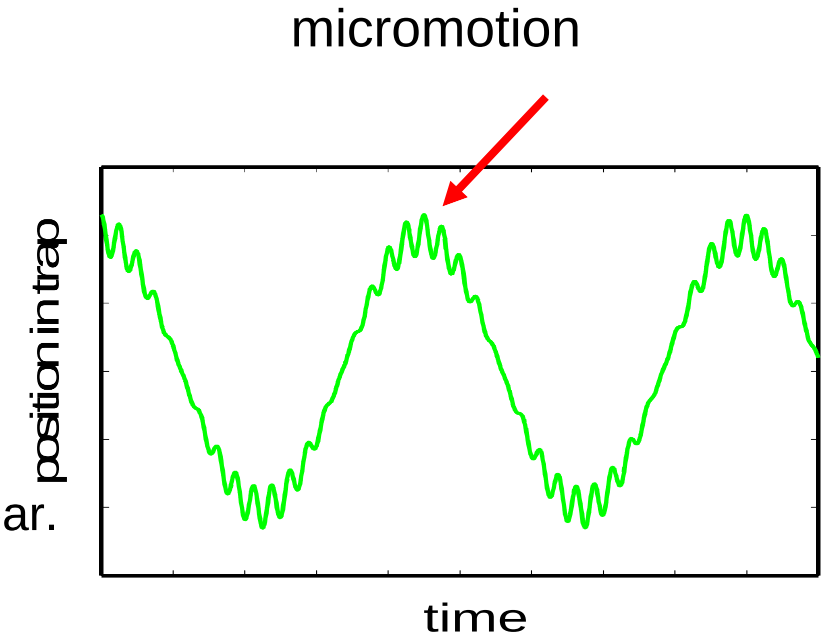

alters the optical spectrum of the trapped ion due to Doppler shift, Bessel functions $J_n(b)$ appear.
Electric field seen by the ion:

$$E = \sum J_n(\beta) e^{-in\Omega t}$$

a) broadening of the ion's resonance

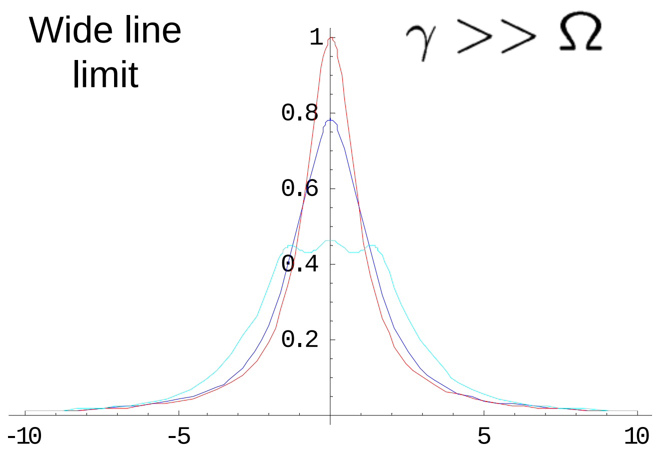

b) appearing of micro-motion sidebands

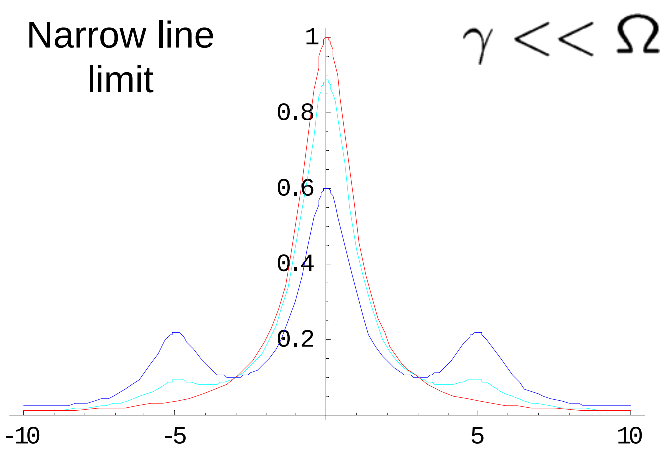

Compensate micro-motion

how to detect micro-motion:

a) detect the Doppler shift
and Doppler broadening

→ Fluorescence modulation technique:

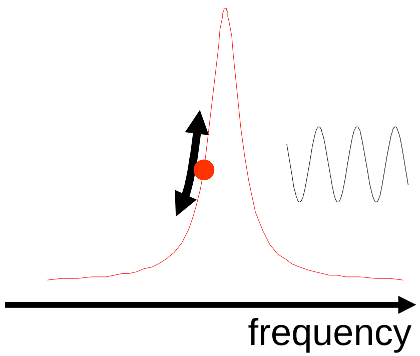

ion oscillation leads a modulation in # of scattered photons. Synchron detection via a START (photon) STOP (W_{RF} trigger) measurement

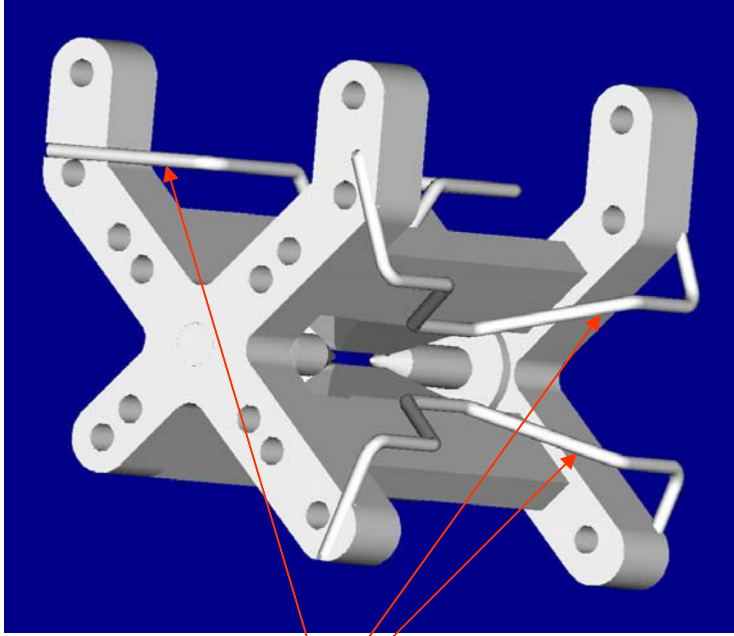

apply voltages here
and shift the ion into the symetry center
of the linear quadrupole

J. Appl. Phys. 83, 5025

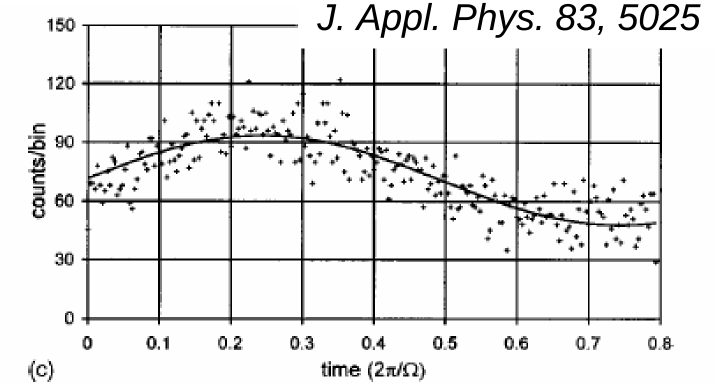

FIG. 4. Experimental fluorescence modulation signals for beam 1 of Fig. 3, using eight ions in the linear trap (points) and fit (solid line). Displacement of the ions from the trap axis along $(\hat{x}+\hat{y})/\sqrt{2}$ is (a) 0.9±0.3 μm, (b) 6.7 ±0.4 μm, and (c) −6.7±0.4 μm.

b) detect micro-motional sidebands

→ Sideband spectroscopy

Cold Ions and their Applications for Quantum Computing and Frequency Standards

- Trapping Ions
- **Cooling Ions**
- Superposition and Entanglement
- Quantum computer: basics, gates, algorithms, future challenges
- Ion clocks: from Ramsey spectroscopy to quantum techniques

Ferdinand Schmidt-Kaler
Institute for Quantum Information Processing
www.quantenbit.de

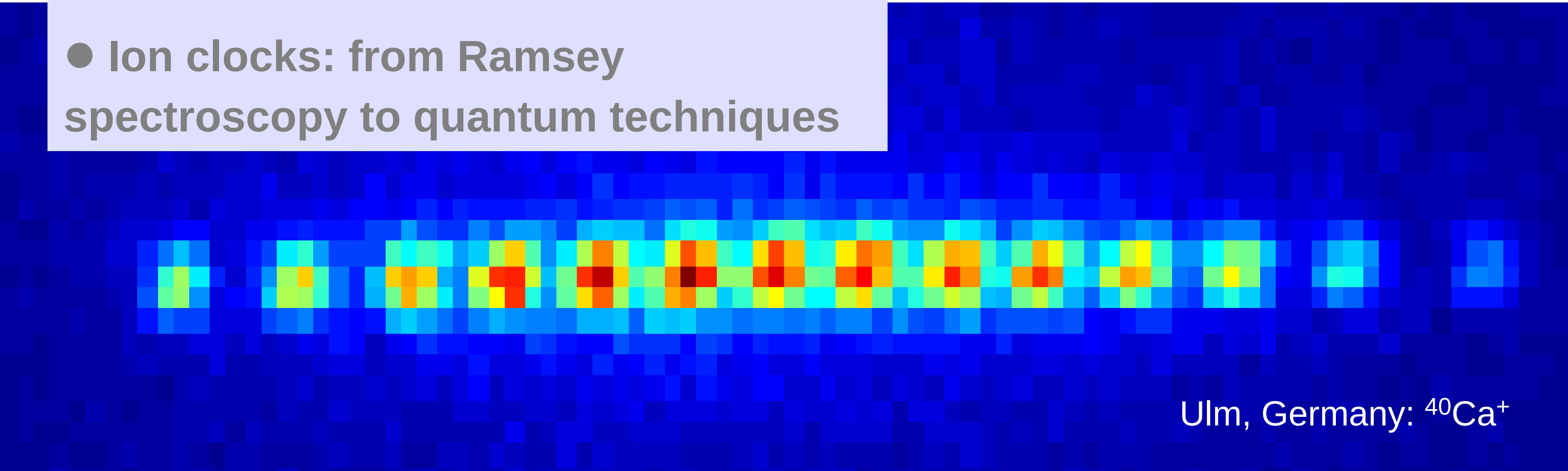

Ulm, Germany: $^{40}Ca^{+}$

II) Laser cooling

Laser-ion interaction

- Lamb Dicke parameter
- Strong and weak confinement regime

Rate equation model
Cooling rate and cooling limit
Doppler cooling of ions

Dopper recooling measurements
to determine heating rates and
to optimize the transport of ions

Resolved sideband spectroscopy

Temperature measurement techniques

- Sideband Rabi oscillations
- Red / blue sideband ratio
- Carrier Rabi oscillations

Resolved sideband cooling

- Quadrupole transition
- Optimizing the cooling rate
- Raman transition

Heating rate
Coherence of vibrational superposition states

Cooling in multi-level systems

- Dark resonances
- EIT cooling

Basics: Harmonic oscillator

Why? The trap confinement is leads to three independend harmonic oscillators !

$$E = E_{kin} + E_{pot} = \frac{\vec{p}^2}{2m} + \frac{m}{2}\omega_{ax}^2 x^2$$

here only for the linear direction of the linear trap $\longrightarrow$ no micro-motion

treat the oscillator quantum mechanically and introduce *a*+ and *a*

$$x = \sqrt{\frac{\hbar}{2m\omega_{ax}}}(a + a^\dagger) \qquad p_x = i\sqrt{\frac{\hbar m\omega_{ax}}{2}}(a^\dagger - a)$$

and get Hamiltonian

$$\boxed{H_{oscillator} = \hbar\omega_{ax}(a^\dagger a + \frac{1}{2})}$$

Eigenstates |*n*> with:

$$H|n\rangle = \hbar\omega_{ax}(n + \frac{1}{2})|n\rangle$$

$$a^\dagger|n\rangle = \sqrt{n}|n-1\rangle$$

$$a|n\rangle = \sqrt{n+1}|n+1\rangle$$

Harmonic oscillator wavefunctions

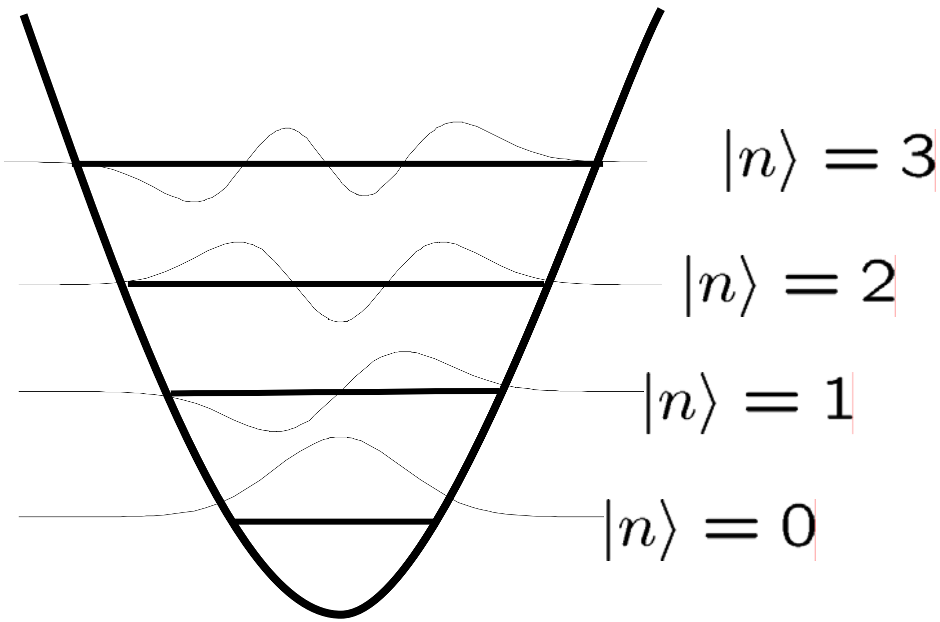

Eigen functions

$$u(x) \sim H(n,x)\, e^{-x^2}$$

with orthonormal Hermite polynoms
and energies:

$$E(n) = \hbar\omega_{ax}(n + \tfrac{1}{2})$$

Two – level atom

Why? Is an idealization which is a good approximation to real physical system in many cases

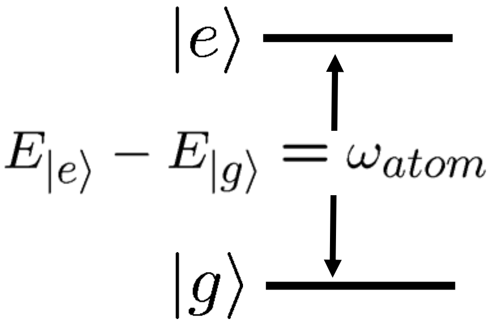

$$
\begin{aligned}
H_{atom} &= \hbar\omega_{atom}(|e\rangle\langle e| - |g\rangle\langle g|) \\
&= \hbar\omega_{atom}\sigma_z
\end{aligned}
$$

two level system is connected with spin ½ algebra using the Pauli matrices

$$
\begin{aligned}
|g\rangle\langle g| + |e\rangle\langle e| &\rightarrow \hat{I} \\
|g\rangle\langle e| + |e\rangle\langle g| &\rightarrow \widehat{\sigma_x} \\
i(|g\rangle\langle e| - |e\rangle\langle g|) &\rightarrow \widehat{\sigma_y} \\
|e\rangle\langle e| - |g\rangle\langle g| &\rightarrow \widehat{\sigma_z}
\end{aligned}
$$

D. Leibfried, C. Monroe,
R. Blatt, D. Wineland,
Rev. Mod. Phys. 75, 281 (2003)

Two – level atom

Why? Is an idealization which is a good approximation to real pyhsical system in many cases

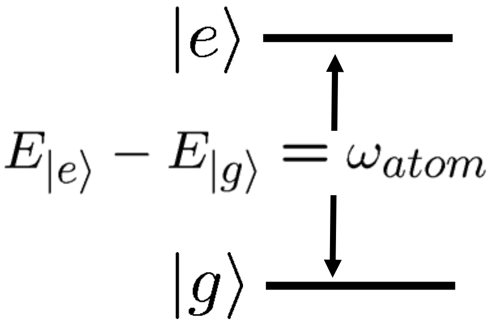

$$\boxed{\begin{aligned} H_{atom} &= \hbar\omega_{atom}(|e\rangle\langle e| - |g\rangle\langle g|) \\ &= \hbar\omega_{atom}\sigma_z \end{aligned}}$$

together with the harmonic oscillator leading to the ladder of eigenstates |g,n>, |e,n>:

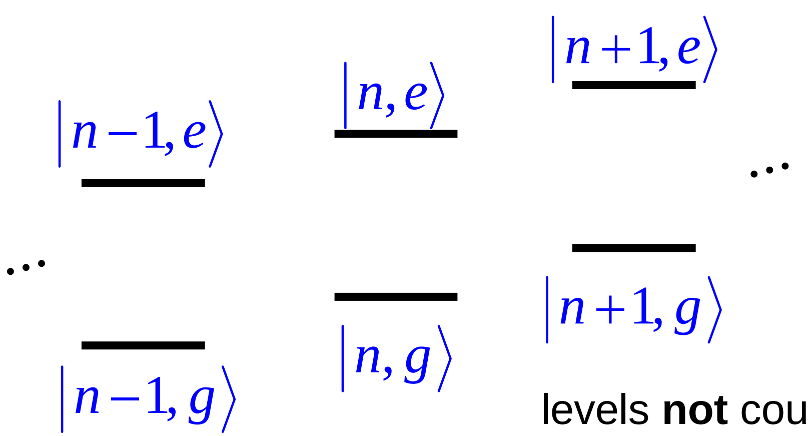

$$\boxed{H_0 = \frac{p^2}{2m_0} + \frac{1}{2}m_0\omega^2 x^2 + \frac{1}{2}\hbar\omega_a\sigma_z}$$

levels **not** coupled

Laser coupling

dipole interaction, Laser radiation with frequency ω_l, and intensity $|E|^2$

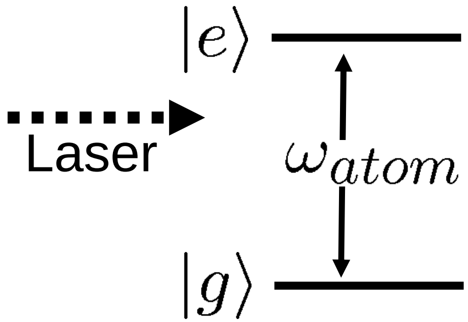

Rabi frequency: $\Omega_R = \langle g|\vec{d}\cdot\vec{E}|e\rangle$

$$\boxed{\begin{aligned} H_{ge} &= \hbar\frac{\Omega_R}{2}(|g\rangle\langle e| + |e\rangle\langle g|) \\ &= \hbar\frac{\Omega_R}{2}(\sigma^+ + \sigma^-) \end{aligned}}$$

with
$$|e\rangle\langle g| \rightarrow \sigma^+ = (\sigma_x + i\sigma_y)/2$$
$$|g\rangle\langle e| \rightarrow \sigma^- = (\sigma_x - i\sigma_y)/2$$

the laser interaction (running laser wave) has a spatial dependence:

$$\vec{d}\cdot\vec{E} \rightarrow \vec{d}\cdot\vec{E}e^{ikx}$$

momentum kick, recoil: e^{ikx}

$$\boxed{\begin{aligned} H_{ge} &= \hbar\frac{\Omega_R}{2}(|g\rangle\langle e|e^{ikx} + |e\rangle\langle g|e^{-ikx}) \\ &= \frac{1}{2}\hbar\Omega(\sigma^+ + \sigma^-)(e^{i(kx-\omega_l t+\phi)} + e^{-i(kx-\omega_l t+\phi)}) \end{aligned}}$$

Laser coupling

in the rotating wave approximation

$$\boxed{H_{ge} = \frac{1}{2}\hbar\Omega(\sigma^+ e^{i(\eta(a+a^\dagger)} e^{-i\omega_l t} + \sigma^- e^{-i\eta(a+a^\dagger)} e^{\omega_l t})}$$

using $x = \sqrt{\frac{\hbar}{2m\omega_{ax}}}(a + a^\dagger)$

and defining the Lamb Dicke parameter η:

$$\boxed{\eta = k\sqrt{\frac{\hbar}{2m\omega_{ax}}}}$$

if the laser direction is at an angle ϕ to the vibration mode direction:

single photon transition

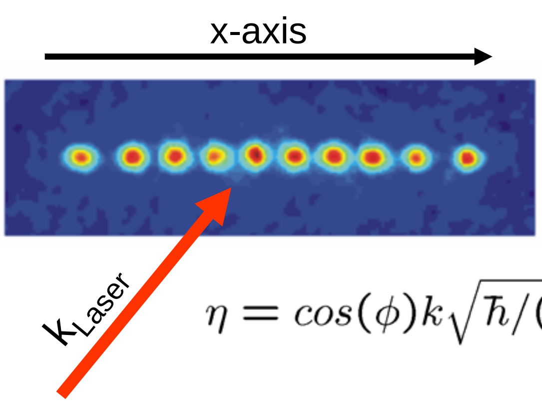

$\eta = cos(\phi)k\sqrt{\hbar/(2m\omega_{ax}}$

Raman transition: projection of $\Delta k = k_1 - k_2$

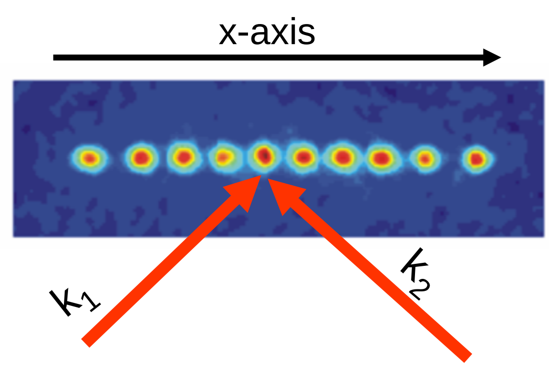

Interaction picture

$$H_{ge} = \frac{1}{2}\hbar\Omega(\sigma^{+}e^{i(\eta(a+a^{\dagger})}e^{-i\omega_l t} + \sigma^{-}e^{-i\eta(a+a^{\dagger})}e^{\omega_l t})$$

In the interaction picture defined by $U = e^{iHt/\hbar}$

we obtain for the Hamiltonian $H_I = U^{\dagger}HU$

$$\boxed{H_I = \frac{1}{2}\hbar\Omega\left(e^{i\eta(\hat{a}+\hat{a}^{\dagger})}\sigma^{+}e^{-i\Delta t} + e^{-i\eta(\hat{a}+\hat{a}^{\dagger})}\sigma^{-}e^{i\Delta t}\right)}$$

with $\hat{a} = ae^{i\omega t}, \Delta = \omega_{laser} - \omega_{atom}$ laser detuning Δ

coupling states $|g, n\rangle \leftrightarrow |e, n'\rangle$ with vibration quantum numbers n, n'

Laser coupling

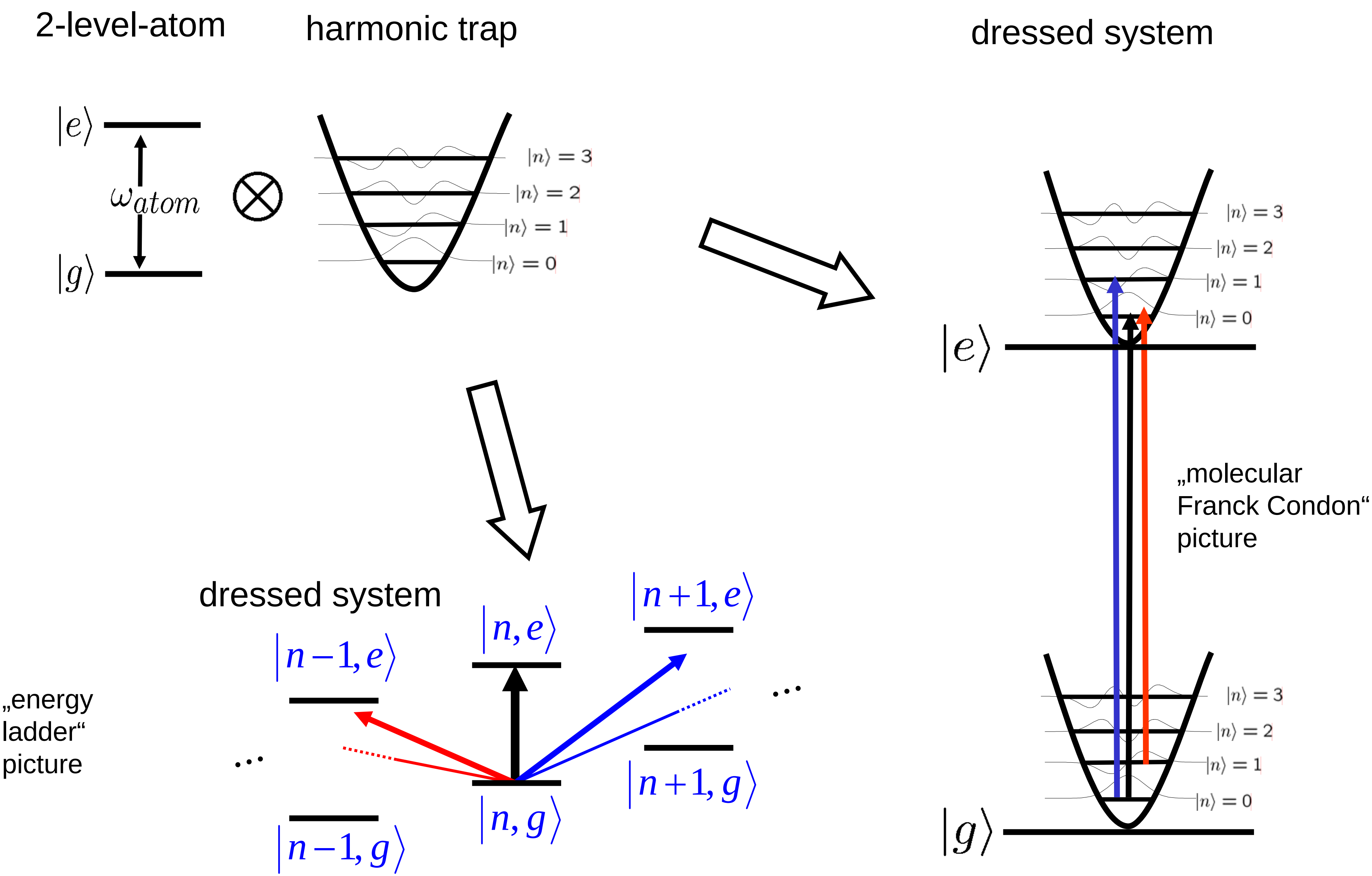

Lamb Dicke Regime

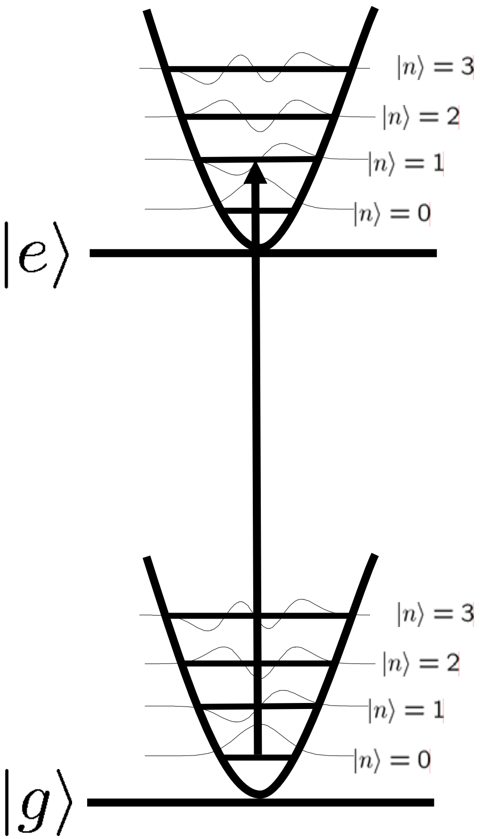

$$\langle g,n|\vec{d}\cdot\vec{E}e^{ikx}|e,m\rangle =$$

$$\langle g|\vec{d}\cdot\vec{E}|e\rangle\langle n|e^{ikx}|m\rangle =$$

$$\hbar\frac{\Omega_{Rabi}}{2}\langle n|e^{i\eta(a+a^\dagger)}|m\rangle \approx$$

$$\boxed{\eta^2(a+a^\dagger)^2 << 1 \rightarrow \eta^2(2n+1) << 1}$$

$$\hbar\frac{\Omega_{Rabi}}{2}\langle n|1+(i\eta(a+a^\dagger)|m\rangle =$$

$$\boxed{\hbar\frac{\Omega_{Rabi}}{2}\ (\delta_{n,m}+i\eta\sqrt{n}\delta_{m=n-1}+i\eta\sqrt{n+1}\delta_{m=n+1})}$$

laser is tuned to the resonances:

carrier: $\Omega_{Rabi}\ (1-\eta^2(2n+1))$

blue sideband: $\Omega_{Rabi}\ \eta\sqrt{n+1}$

red sideband: $\Omega_{Rabi}\ \eta\sqrt{n}$

Wavefunctions in momentum space

$$\eta = \sqrt{\frac{\hbar k}{2m\omega_{trap}}} = \sqrt{\frac{\omega_{recoil}}{\omega_{trap}}}$$

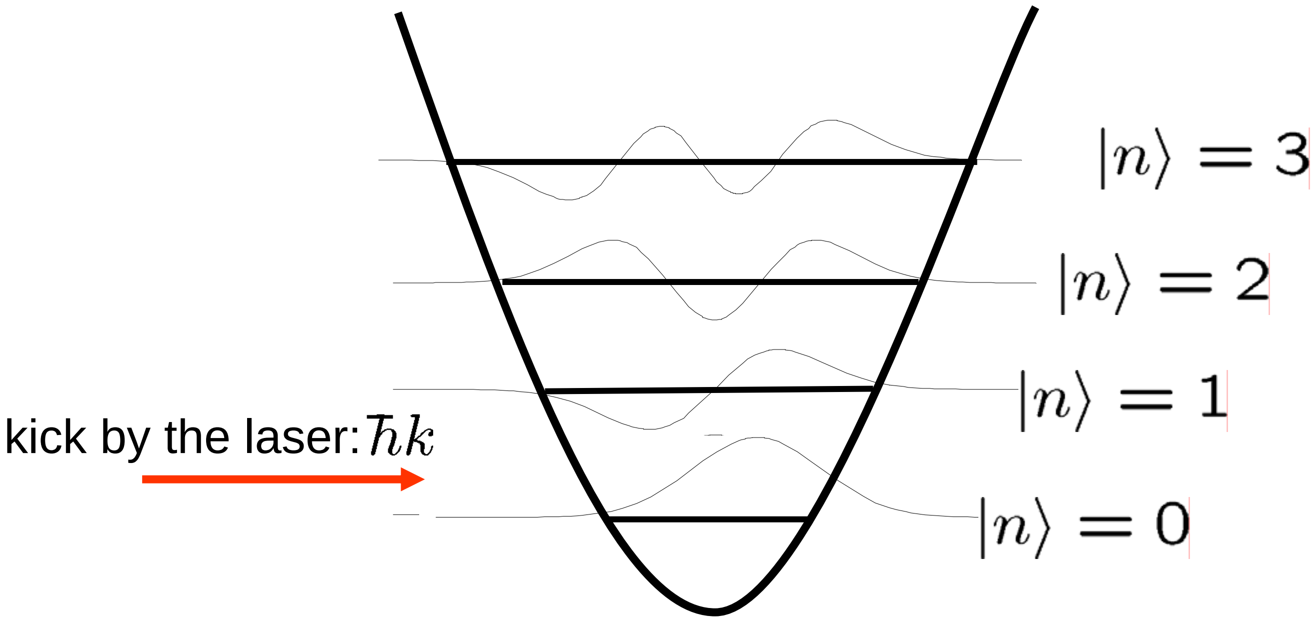

kicked wave function is **non-**orthogonal to the other wave functions

Experimental example

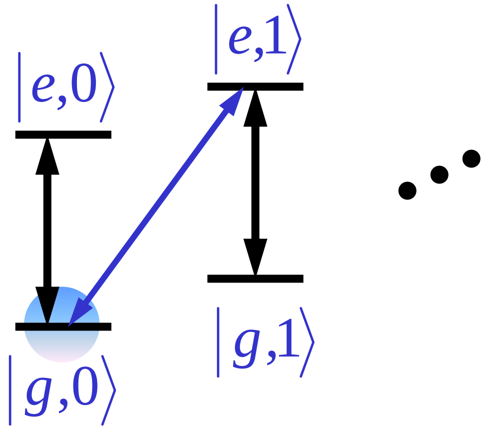

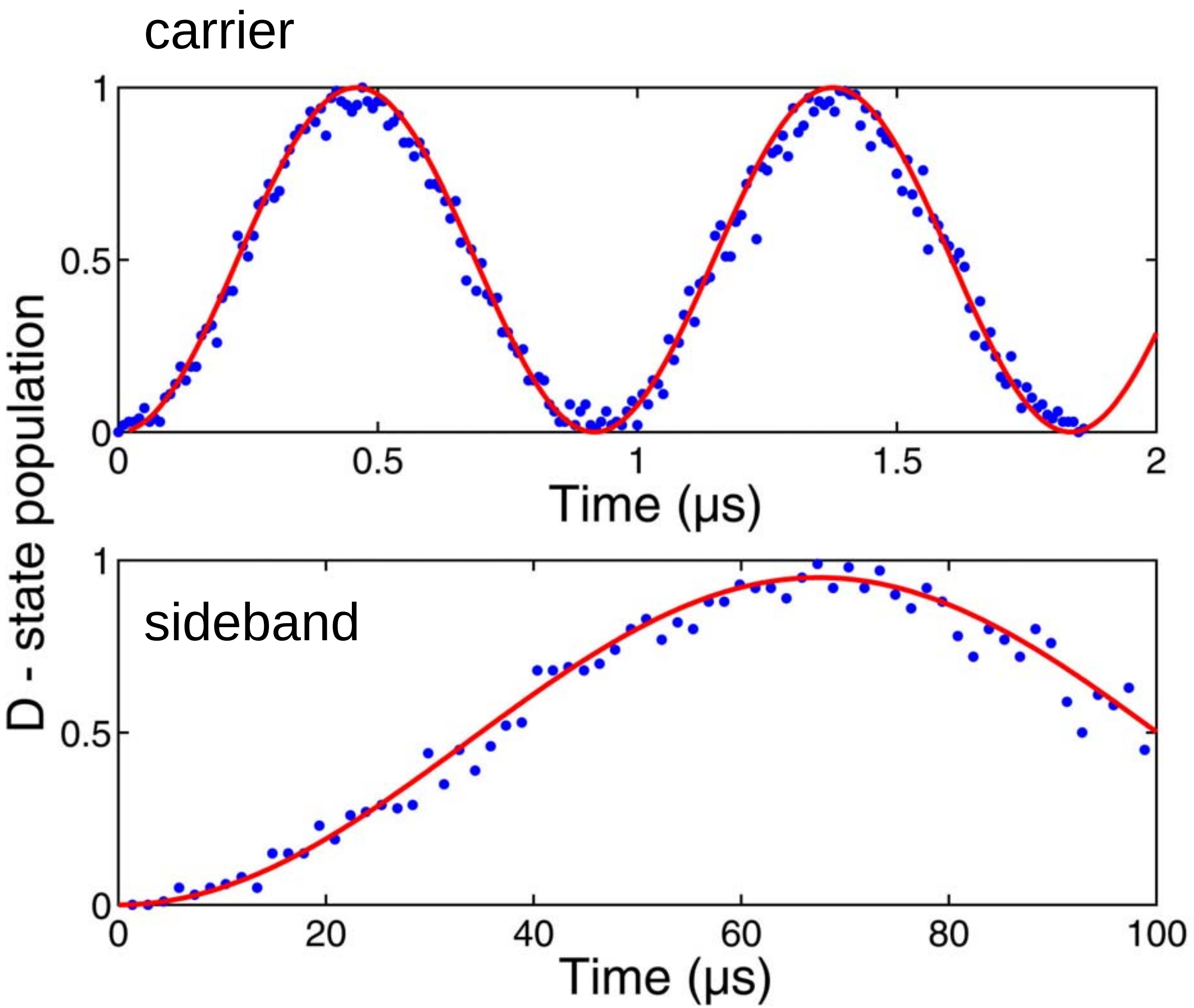

carrier and sideband
Rabi oscillations
with Rabi frequencies

Ω_{Rabi} and $\Omega_{Rabi}\ \eta$

Outside Lamb Dicke Regime

$$\hbar \frac{\Omega_{Rabi}}{2} \langle n | e^{i\eta(a+a^\dagger)} | m \rangle =$$

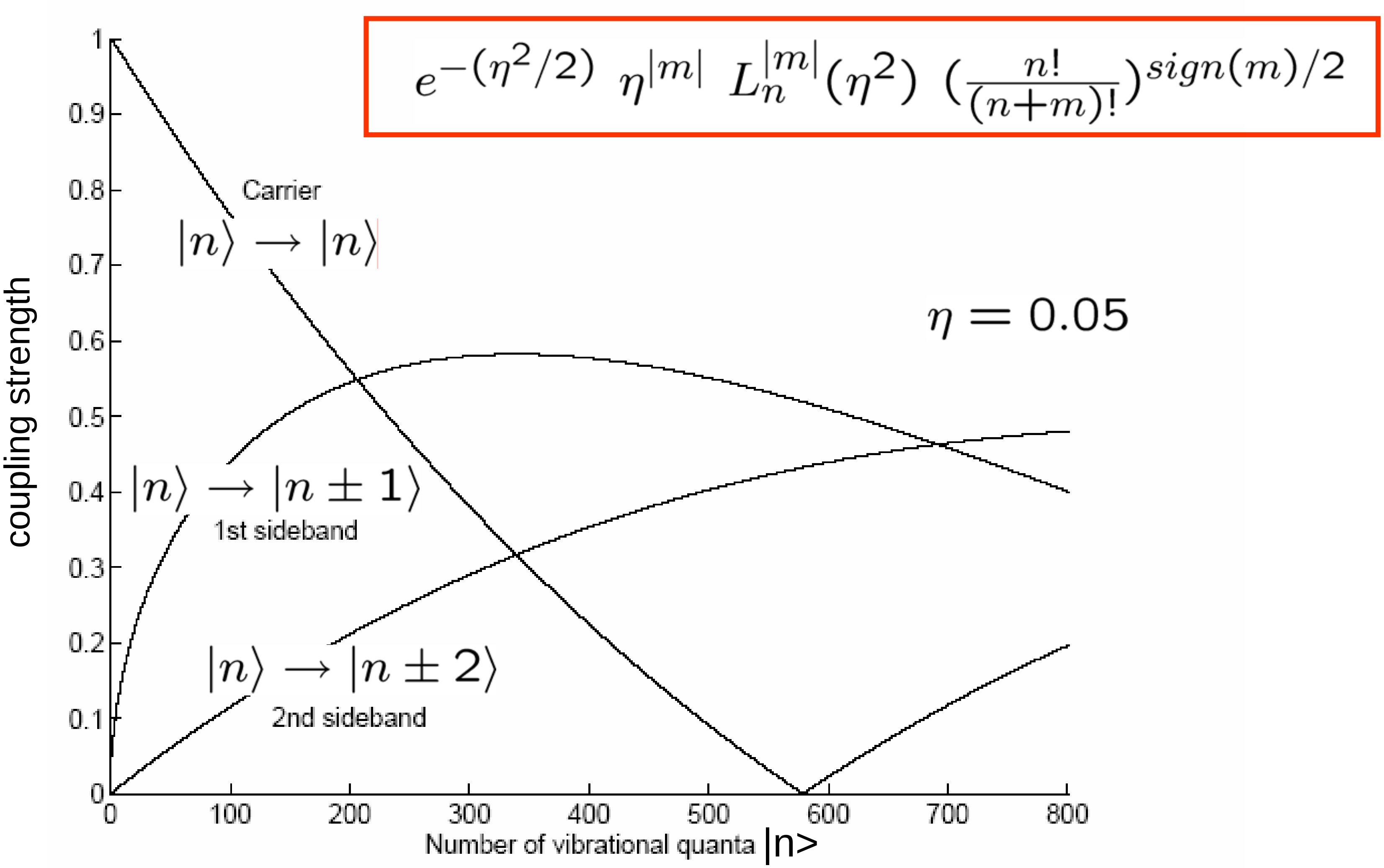

„Strong confinement“

$$\boxed{\omega_{trap} >> \gamma}$$

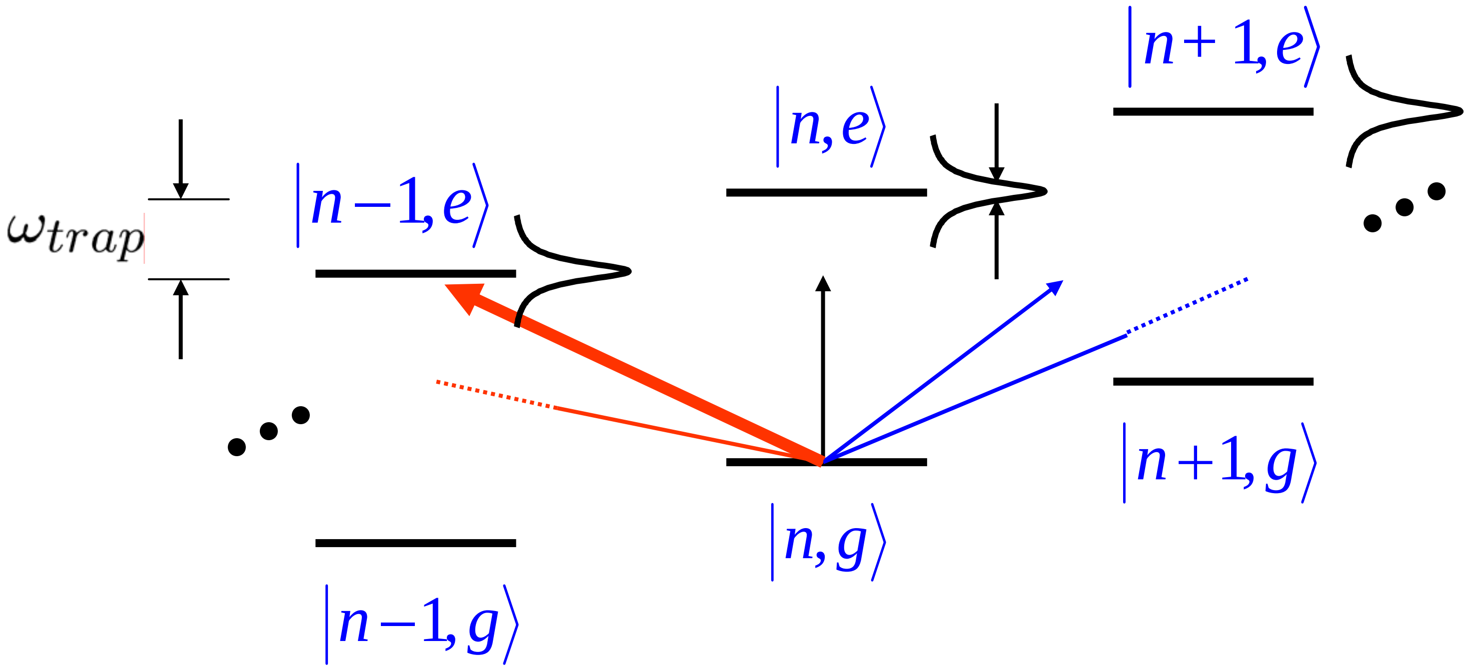

strong confinement – well resolved sidebands:
Selective excitation of a single sideband only,
e.g. here the red SB

„Weak confinement“

$$\boxed{\omega_{trap} << \gamma}$$

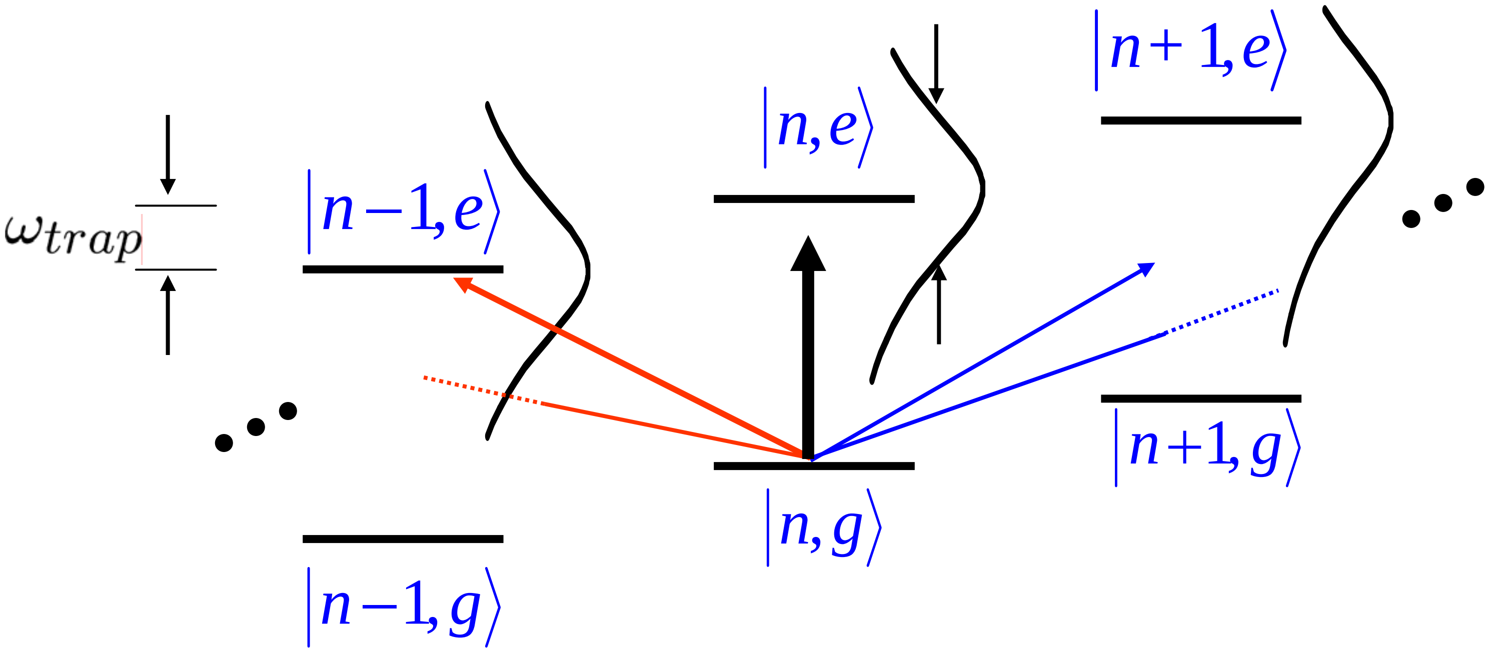

weak confinement:
Sidebands are not resolved on that transition.
Simultaneous excitation of several vibrational states

Two-level system dynamics

spont. decay rate γ

Rabi frequency Ω

incoherent: $\Omega < \gamma$

coherent: $\Omega > \gamma$

Solution of
optical Bloch equations

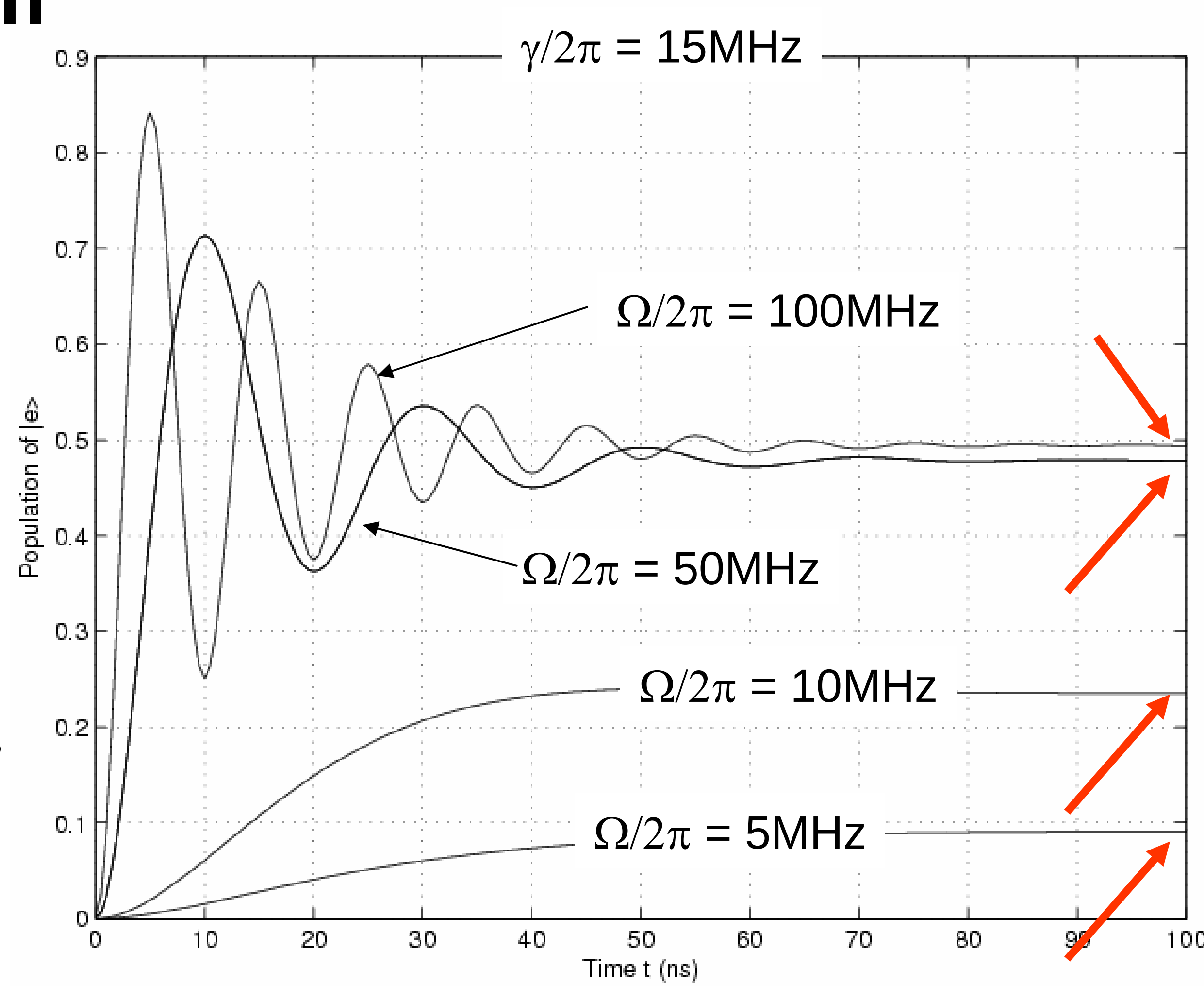

Steady state population of |e>:

$$\rho_{ee}(t \rightarrow \infty) = \frac{(\Omega/2)^2}{\Delta^2 + (\gamma/2)^2 + 2(\Omega/2)^2} \simeq \left(\frac{\Omega}{\gamma}\right)^2 \frac{1}{1 + (2\Delta/\gamma)^2} = \left(\frac{\Omega}{\gamma}\right)^2 W(\Delta)$$

Rate equations of absorption

excitation probabilities in pertubative regime:

incoherent excitation if $\Omega_{Rabi} << \gamma$

$$\rho_{ee}(t \rightarrow \infty) = \frac{(\Omega/2)^2}{\Delta^2 + (\gamma/2)^2 + 2(\Omega/2)^2}$$

$$\simeq (\frac{\Omega}{\gamma})^2 \frac{1}{1+(2\Delta/\gamma)^2} = (\frac{\Omega}{\gamma})^2 \; W(\Delta)$$

photon scatter rate: $S = \gamma \rho_{ee}$

spont. decay rate: γ

absorption

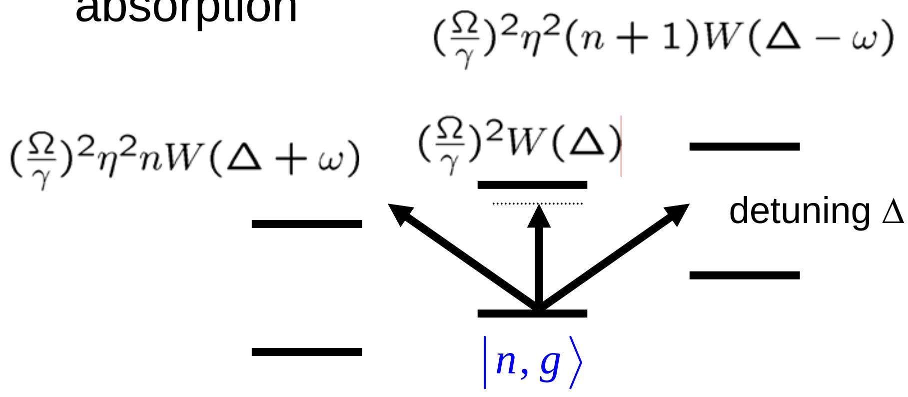

Rate equations of absorption and emission

excitation probabilities in pertubative regime:
incoherent excitation if $\Omega_{Rabi} << \gamma$

$$\rho_{ee}(t \rightarrow \infty) = \frac{(\Omega/2)^2}{\Delta^2+(\gamma/2)^2+2(\Omega/2)^2}$$

$$\simeq (\frac{\Omega}{\gamma})^2 \frac{1}{1+(2\Delta/\gamma)^2} = (\frac{\Omega}{\gamma})^2 \; W(\Delta)$$

photon scatter rate: $S = \gamma \rho_{ee}$

spont. decay rate: γ

emission

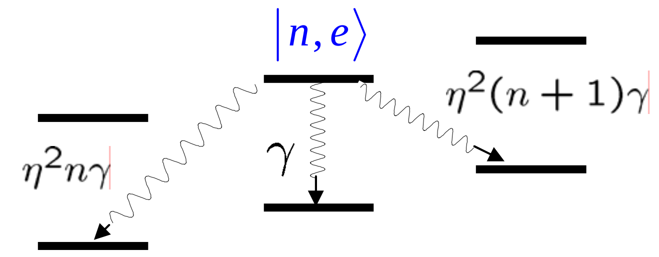

take all physical processes that change *n*, in lowest order of η

cooling:

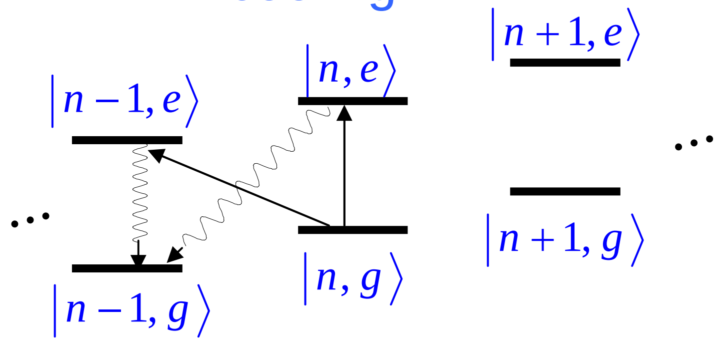

heating:

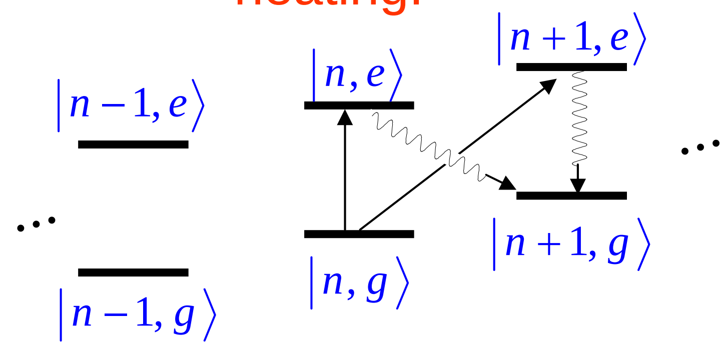

S. Stenholm, Rev. Mod. Phys. ***58****, 699 (1986)*

Rate equations for cooling and heating

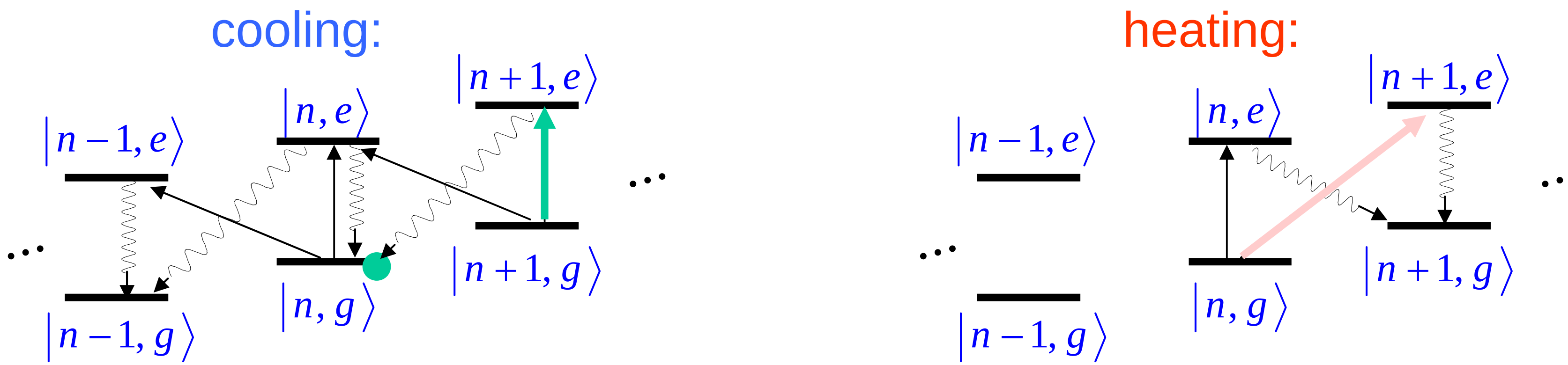

probability for population in |g,n>: loss and gain from states with |±n>

$$\dot{P}_{g,n} = \eta^2\gamma\left(\frac{\Omega}{\gamma}\right)^2 \cdot \left[\begin{array}{l|l} -nW(\Delta)P_n & -(n+1)W(\Delta)P_n \\ -nW(\Delta+\omega)P_n & \boxed{-(n+1)W(\Delta-\omega)P_n} \\ \hline \boxed{+(n+1)W(\Delta)P_{n+1}} & +nW(\Delta)P_{n-1} \\ +(n+1)W(\Delta+\omega)P_{n+1} & +nW(\Delta-\omega)P_{n-1} \end{array}\right] \begin{array}{l} \text{loss} \\ \\ \text{gain} \end{array}$$

cooling | heating

S. Stenholm, Rev. Mod. Phys. ***58****, 699 (1986)*

Rate equation

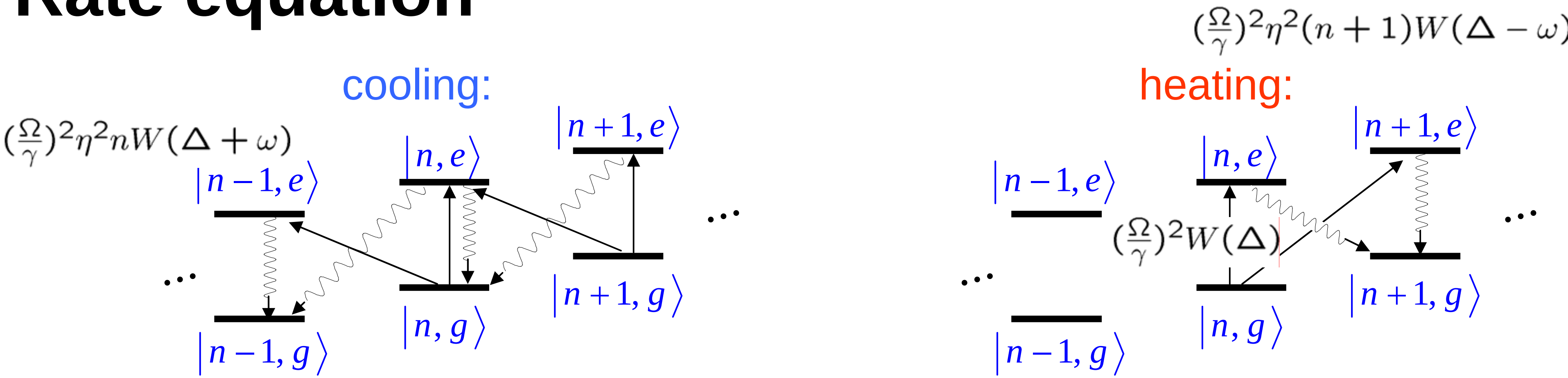

$$A_- = W(\Delta) + W(\Delta+\omega) \quad \text{cooling}$$

$$A_+ = W(\Delta) + W(\Delta-\omega) \quad \text{heating}$$

$$A_- - A_+ = W(\Delta+\omega) - W(\Delta-\omega)$$

different illustration:

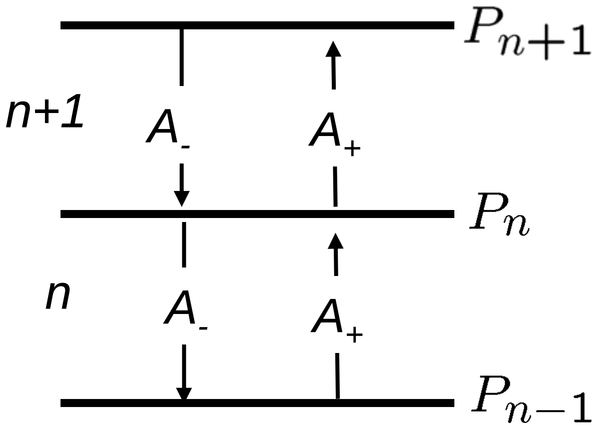

$$\langle \dot{n} \rangle = \frac{(\eta\Omega)^2}{\gamma} \sum n \frac{dP_n}{dt}$$

$$\Longrightarrow \quad \langle \dot{n} \rangle \sim -(A_- - A_+)\langle n \rangle + A_+$$

$$\langle n \rangle_{ss} = \frac{A_+}{A_- - A_+} \qquad 1/\tau_{cool} = \frac{(\eta\Omega)^2}{\gamma}(A_- - A_+)$$

steady state phonon number — cooling rate

How to reach $A_- > A_+ \Rightarrow W(\Delta+\omega) > W(\Delta-\omega) \Rightarrow$ red detuning $\Delta < 0$

****

$$\dot{m} = \langle \dot{n} \rangle = \sum n \, \frac{dP_n}{dt} =$$

$$\sum_{n=1} A_- P_{n+1}(n+1)(n) - A_- P_n(n)(n) + A_+ P_{n-1}(n)(n) - A_+ P_n(n+1)(n)$$

$$= A_-(P_2 \cdot 2 \cdot 1 + P_3 \cdot 3 \cdot 2 + \ldots - P_1 \cdot 1 \cdot 1 - P_2 \cdot 2 \cdot 2 - \ldots)$$
$$+ A_+(P_0 \cdot 1 \cdot 1 + P_1 \cdot 2 \cdot 2 + \ldots - P_1 \cdot 2 \cdot 1 - P_2 \cdot 3 \cdot 2 - \ldots)$$

$$= A_-(P_1 - P_2 \cdot 2 - P_3 \cdot 3 \ldots)$$
$$+ A_+(P_0 + P_1 \cdot 2 - P_2 \cdot 3 - P_3 \cdot 4 \ldots)$$

$$= -A_- \sum n \cdot P_n \; + A_+ \sum (n+1) \cdot P_n$$

$$= -A_- \langle n \rangle + A_+ \langle n \rangle + A_+ \cdot \sum P_n$$

$$= -A_- \langle n \rangle + A_+ \langle n \rangle + A_+$$

$$\langle \dot{n} \rangle = 0 \quad \Longrightarrow \quad \langle n \rangle = \frac{A_+}{A_- - A_+}$$

hurra !

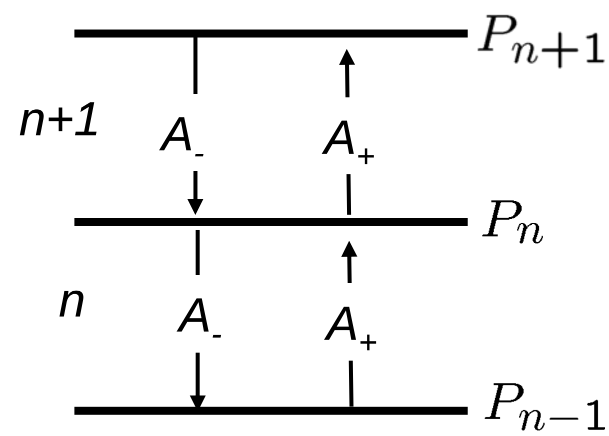

„Weak confinement“

$$\boxed{\omega_{trap} << \gamma}$$

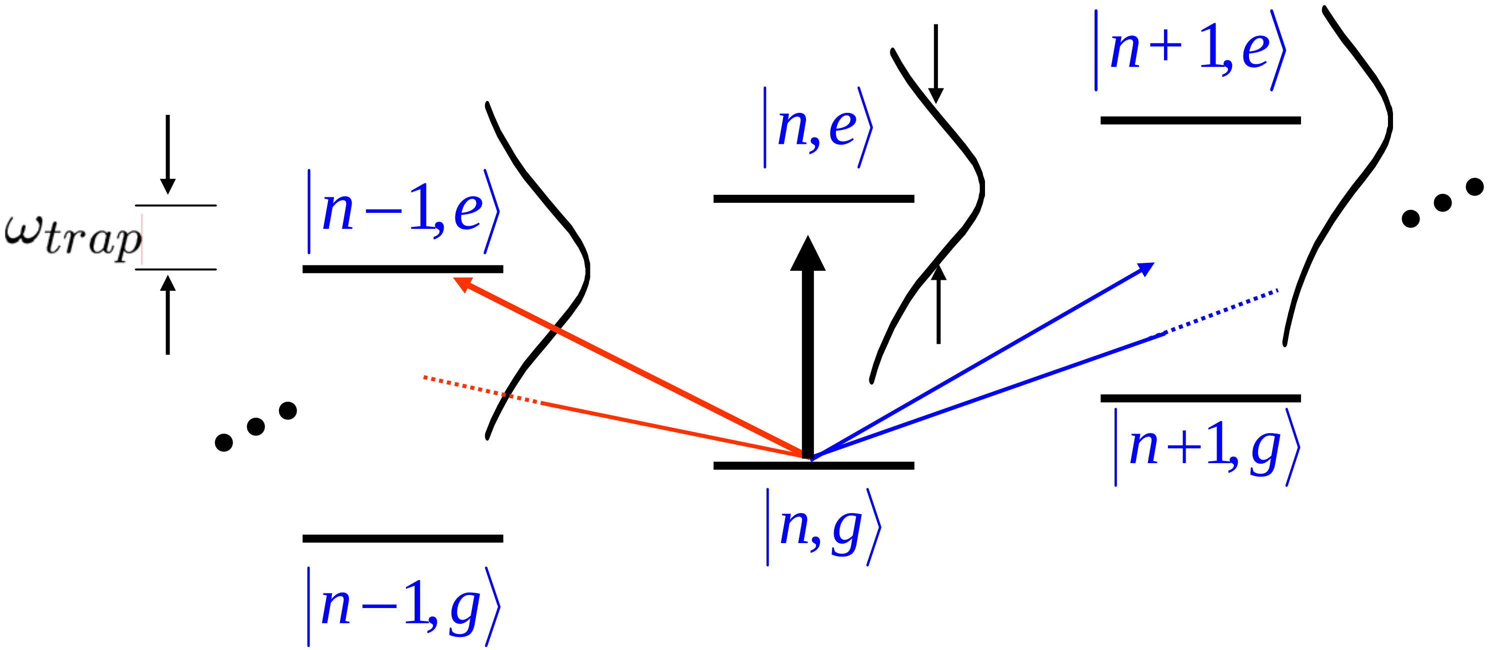

weak confinement:
Sidebands are not resolved on that transition.
Small differences in $W(\Delta \pm \omega), W(\Delta - \omega)$

detuning for optimum cooling $\Delta = -\gamma/2$ $\Rightarrow$ $\langle n \rangle_{ss} = \frac{\gamma/2}{\omega_{trap}}$

„Weak confinement“

$$\boxed{\omega_{trap} << \gamma}$$

Lorentzian has the steepest slope at $-\gamma/2$

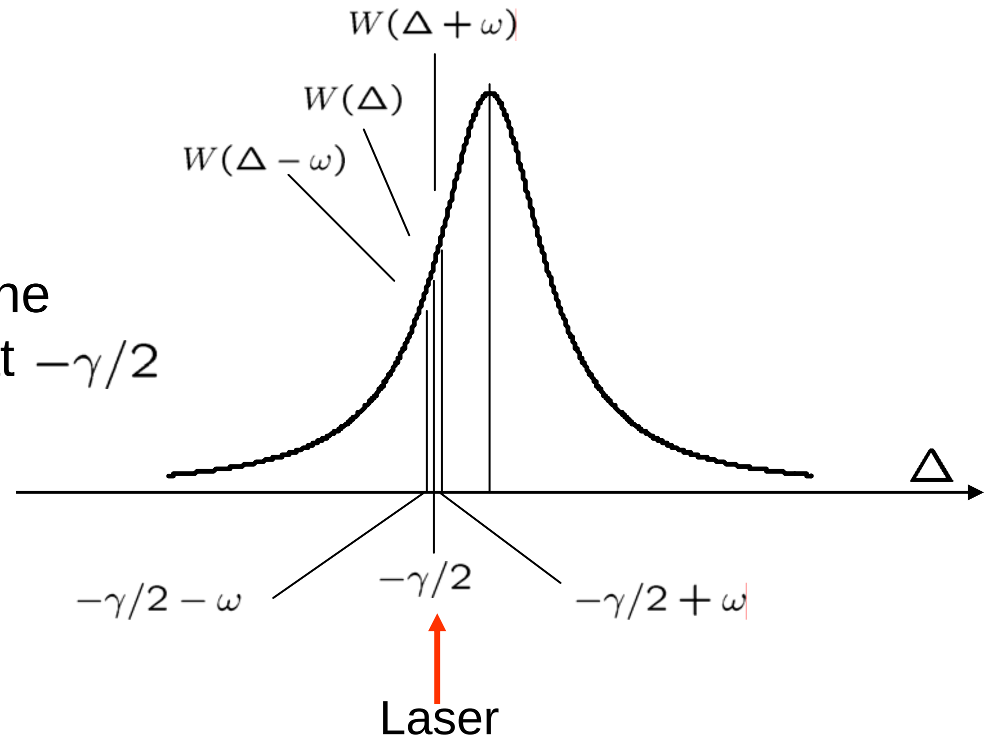

complications:

- $\eta_{laser} < \eta_{spontaneous}$
- saturation effects
- optical pumping

weak confinement:
Sidebands are not resolved on that transition.
Small differences in $W(\Delta \pm \omega), W(\Delta - \omega)$

$$\boxed{\text{detuning for optimum cooling } \Delta = -\gamma/2 \quad \Rightarrow \quad \langle n \rangle_{ss} = \frac{\gamma/2}{\omega_{trap}}}$$

Transport of Ions and Doppler recooling

Fast shuttle of ions is important

-to bring the ions in an optical cavity zone

-to allow scalable quantum computing

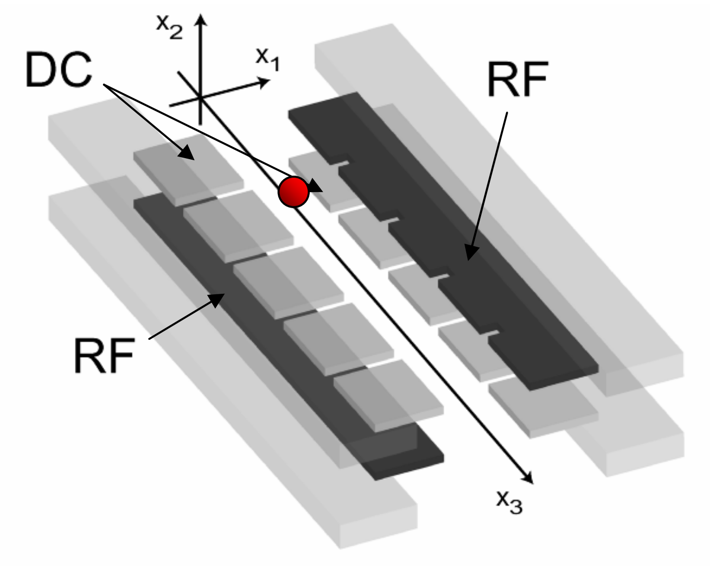

Control voltages: $U_1, U_2, U_3, \ldots, U_n$

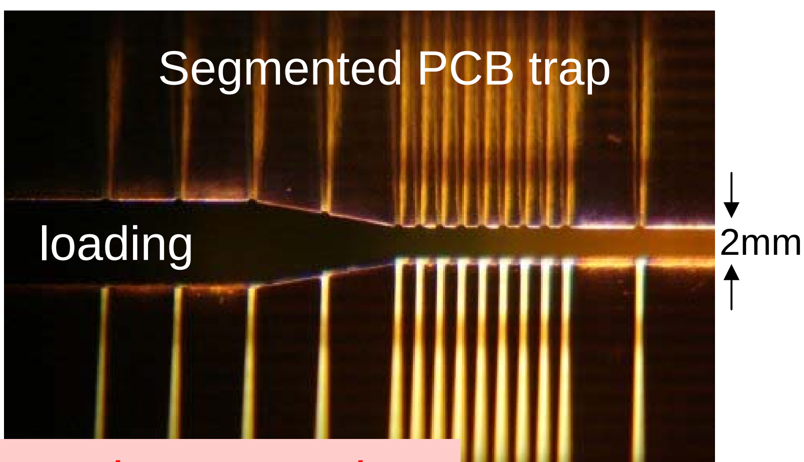

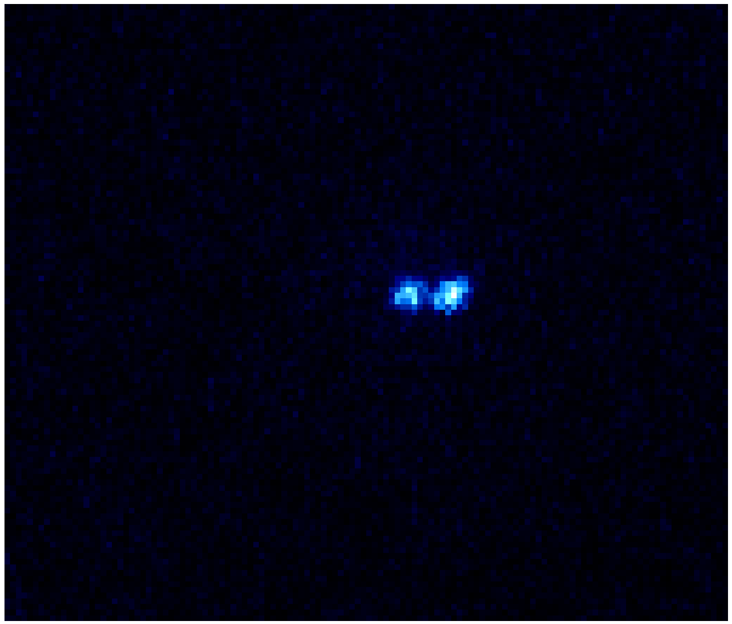

Huber et al., New J. Phys. 10 013004 (2008)

Non-adiabatic, fast transport

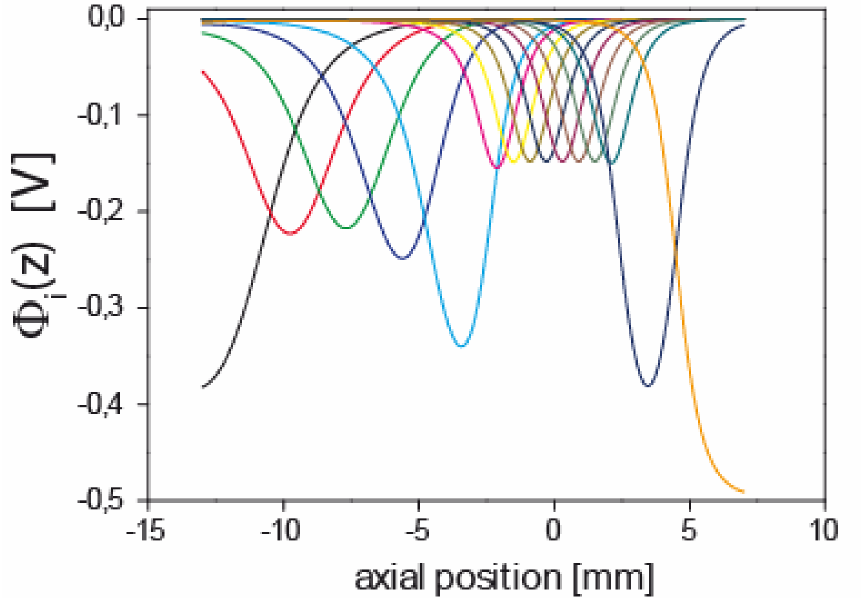

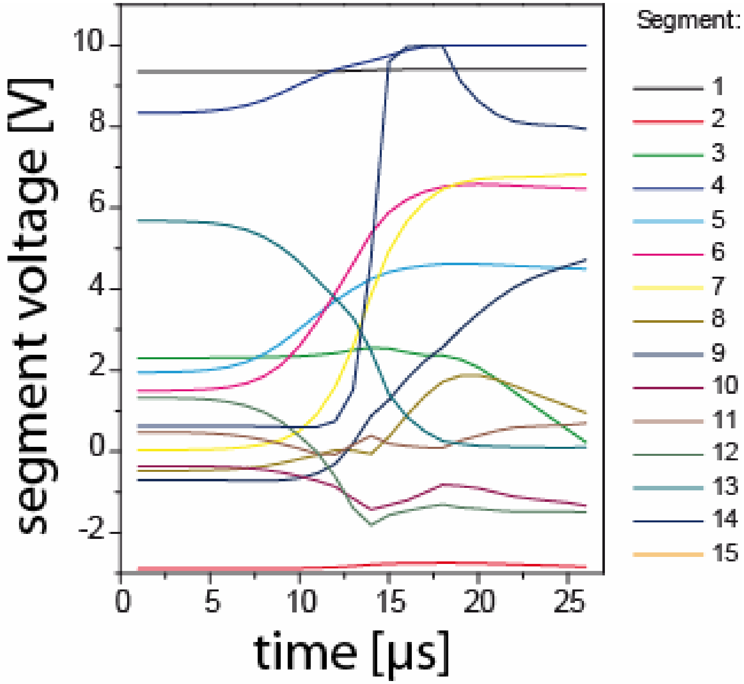

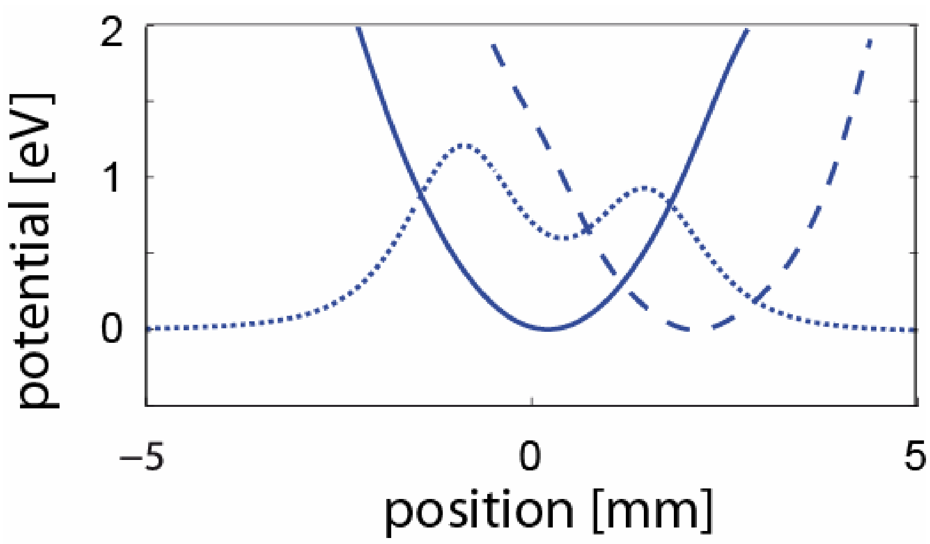

Doppler recooling after fast transport

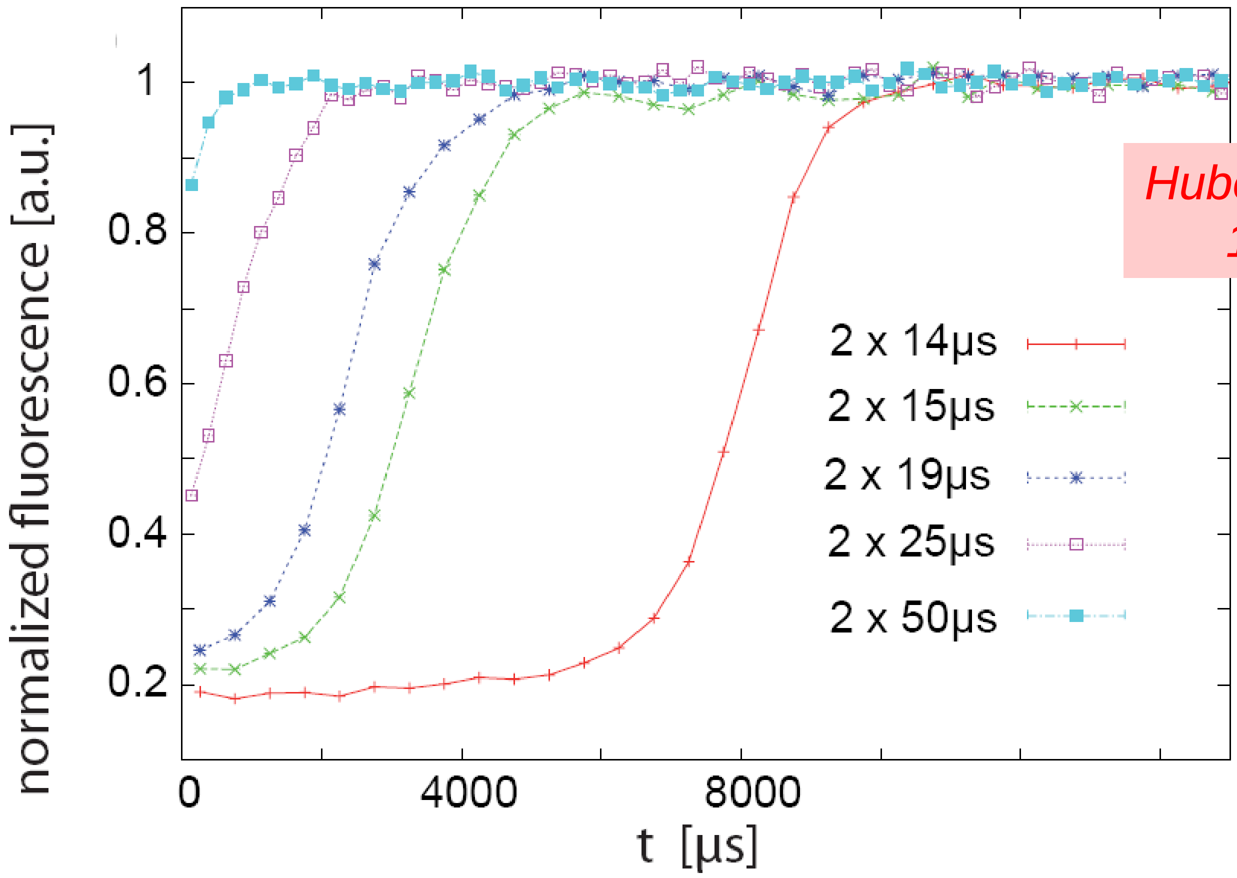

Huber et al., New J. Phys. 10, 013004 (2008)

See also: *J.H. Wesenberg, et. al., arXiv:quant-ph/0707.1314, (2007).*

„Strong confinement“

$$\boxed{\omega_{trap} >> \gamma}$$

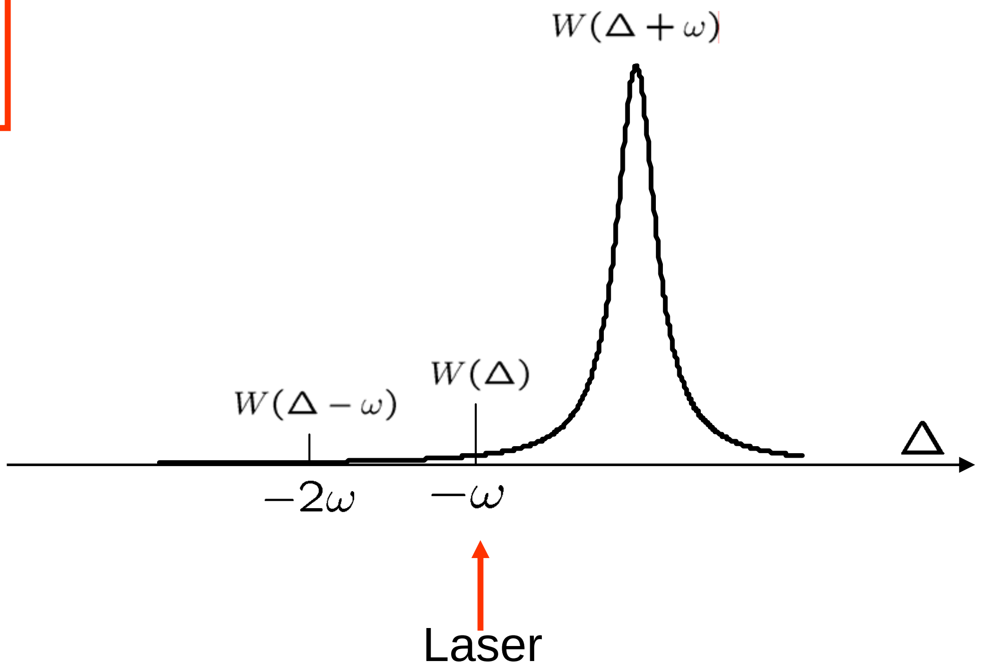

ground state cooling

strong confinement – well resolved sidebands:
detuning for optimum cooling

$$\boxed{\Delta = -\omega_{trap} \;\Rightarrow\; \langle n \rangle_{ss} \approx \left(\frac{\gamma/2}{\omega_{trap}}\right)^2 << 1}$$

„Strong confinement“

$$\boxed{\omega_{trap} >> \gamma}$$

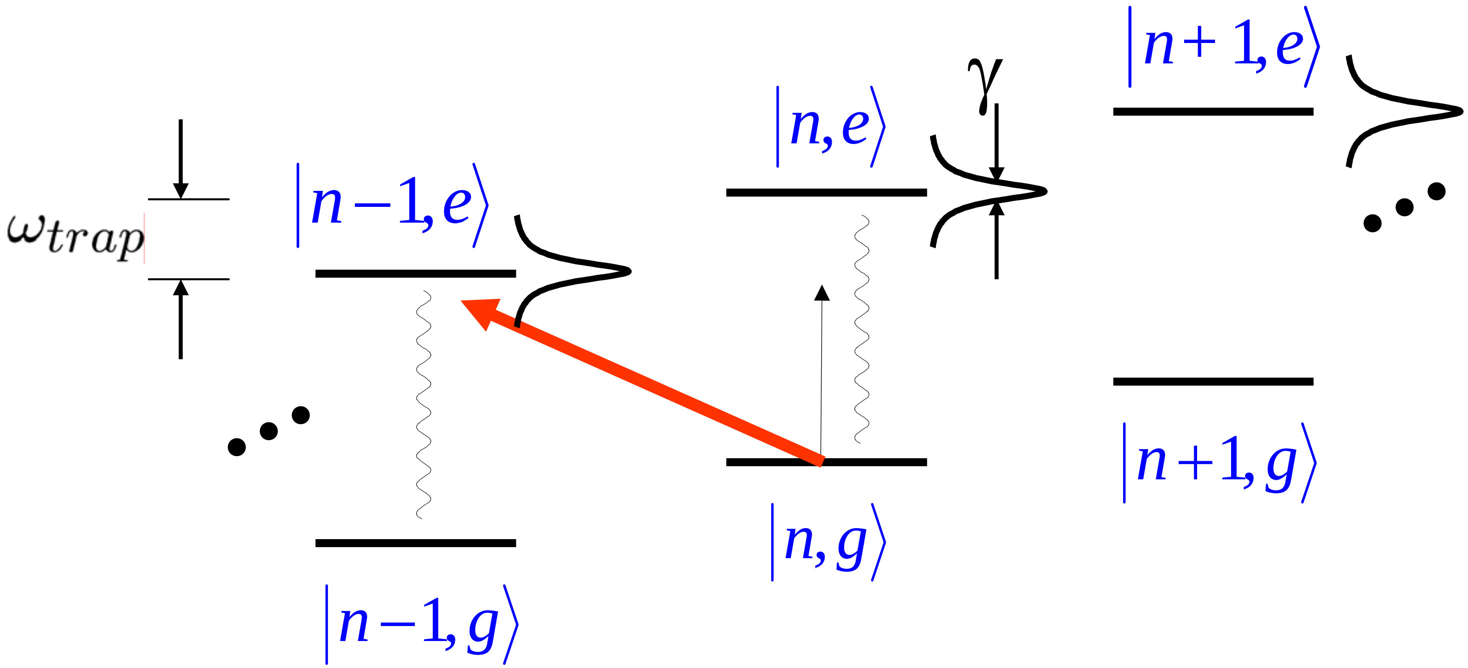

strong confinement – well resolved sidebands:
detuning for optimum cooling

$$\boxed{\Delta = -\omega_{trap} \;\Rightarrow\; \langle n\rangle_{ss} \approx \left(\frac{\gamma/2}{\omega_{trap}}\right)^2 << 1}$$

Cooling limit

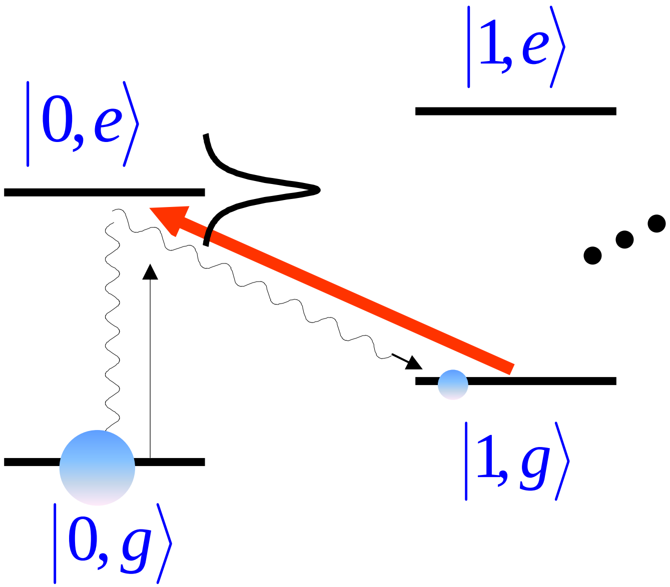

$$\Delta = -\omega_{trap}$$

Limit of SB cooling

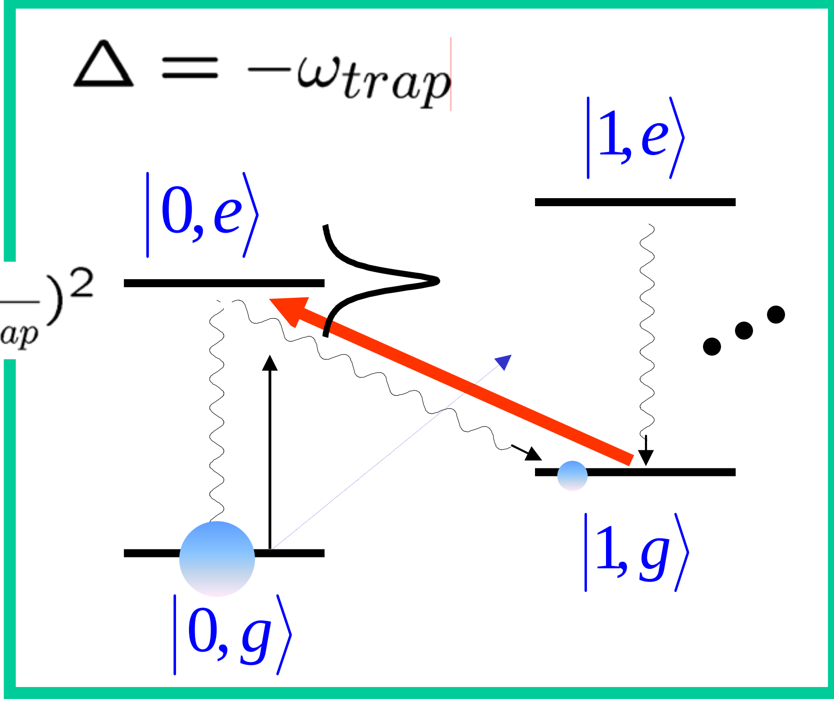

off resonant
carrier excitation: $(\frac{\Omega}{\gamma_{eff}})^2 \frac{1}{1+(2\Delta/\gamma_{eff})^2} \overset{\Delta=-\omega_{trap}}{=} (\frac{\Omega}{2\omega_{trap}})^2$

subsequent blue SB decay: $\eta_{spont}^2 \gamma_{eff}$
with an „effective" γ
and the η of spont. emission

leads to heating: $\eta_{spont}^2 \gamma_{eff} \Omega^2/(2\omega_{trap})^2$

off resonant blue SB excitation $\Delta = -2\omega_{trap}$
leads to heating: $\gamma_{eff}\ (\eta_{laser}\Omega)^2/(4\omega_{trap})^2$

$$\boxed{\dot{p_0} = p_1 \frac{(\eta_{laser}\Omega)^2}{\gamma_{eff}} - p_0\ (\frac{\Omega}{2\omega_{trap}})^2 \eta_{spont}^2 \gamma_{eff} - p_0\ (\frac{\eta_{laser}\Omega}{4\omega_{trap}})^2 \gamma_{eff}, \quad \dot{p_0} = -\dot{p_1}}$$

with: $\dot{p_0} = 0, p_1 = 1 - p_0$

$$\boxed{n \approx p_1 \approx (\frac{\gamma_{eff}}{2\omega_{trap}})^2((\frac{\eta_{spont}}{\eta_{laser}})^2 + \frac{1}{4})}$$

typical experimental
parameters: $n \approx (\frac{5kHz}{5MHz})^2((\frac{0.05}{0.02})^2 + \frac{1}{4}) \approx 5\text{x}10^{-6}$

II) Laser cooling

Laser-ion interaction
- Lamb Dicke parameter
- Strong and weak confinement regime

Rate equation model
Cooling rate and cooling limit
Doppler cooling of ions

Resolved sideband spectroscopy

Temperature measurement techniques
- Sideband Rabi oscillations
- Red / blue sideband ratio
- Carrier Rabi oscillations

Resolved sideband cooling
- Quadrupole transition
- Optimizing the cooling rate
- Raman transition

Heating rate
Coherence of vibrational superposition states

Cooling in multi-level systems
- Dark resonances
- EIT cooling

Cold Ions and their Applications for Quantum Computing and Frequency Standards

- Trapping Ions
- Cooling Ions
- **Superposition and Entanglement**
- **Quantum computer: basics, gates, algorithms, future challenges**
- **Ion clocks: from Ramsey spectroscopy to quantum techniques**

Ferdinand Schmidt-Kaler
Institute for Quantum Information Processing
www.quantenbit.de

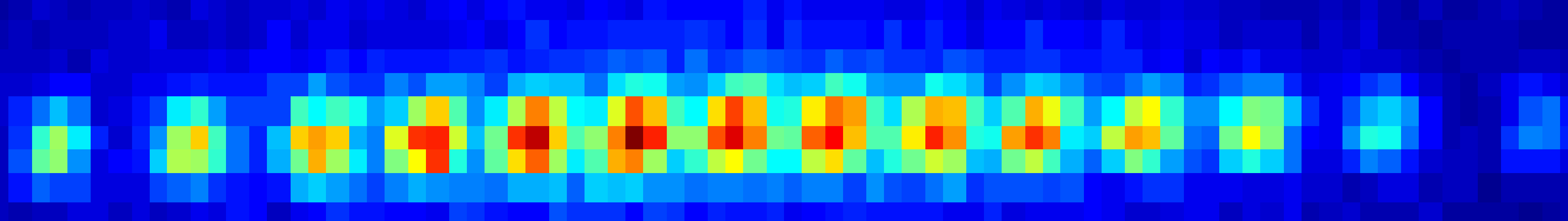

Ulm, Germany: $^{40}Ca^{+}$